DISSERTATION

HOPF BIFURCATION IN ANISOTROPIC REACTION DIFFUSION SYSTEMS POSED IN LARGE RECTANGLES

Submitted by

Travis A. Olson

Department of Mathematics

In partial fulfillment of the requirements

For the Degree of Doctor of Philosophy

Colorado State University

Fort Collins, Colorado

Summer 2010

COLORADO STATE UNIVERSITY

May 13, 2010

WE HEREBY RECOMMEND THAT THE DISSERTATION PREPARED UNDER OUR SUPERVISION BY TRAVIS A. OLSON ENTITLED HOPF BIFURCATION IN ANISOTROPIC REACTION DIFFUSION SYSTEMS POSED IN LARGE RECTANGLES BE ACCEPTED AS FULFILLING IN PART REQUIREMENTS FOR THE DEGREE OF DOCTOR OF PHILOSOPHY.

Committee on Graduate Work

Richard Eykholt

Michael Kirby

Iuliana Oprea

Advisor: Gerhard Dangelmayr

Department Head: Gerhard Dangelmayr

ABSTRACT OF DISSERTATION

HOPF BIFURCATION IN ANISOTROPIC REACTION DIFFUSION SYSTEMS POSED IN LARGE RECTANGLES

The oscillatory instability (Hopf bifurcation) for anisotropic reaction diffusion equations posed in large (but finite) rectangles is investigated. The work pursued in this dissertation extends previous studies for infinitely extended 2D systems to include finite-size effects. For the case considered, the solution of the reaction diffusion system is represented in terms of slowly modulated complex amplitudes of four wave-trains propagating in four oblique directions. While for the infinitely extended system the modulating amplitudes are independent dynamical variables, the finite size of the domain leads to relations between them induced by wave reflections at the boundaries. This leads to a single amplitude equation for a doubly periodic function that captures all four envelopes in different regions of its fundamental domain. The amplitude equation is derived by matching an asymptotic bulk solution to an asymptotic boundary layer solution. While for the corresponding infinitely extended system no further parameters generically remain in the amplitude (envelope) equations above the onset value of the control parameter, the finite-size amplitude equation retains a dependence on a rescaled version of this parameter. Numerical simulations show that the dynamics of the bounded system shows different behavior at onset in comparison to

the unbounded system, and the complexity of the solutions significantly increases when the rescaled control parameter is increased. As an application of the technique developed, an anisotropic Activator-Inhibitor model with higher order diffusion is studied, and parameter values of the amplitude equations are calculated for several parameter sets of the model equations.

Travis A. Olson
Department of Mathematics
Colorado State University
Fort Collins, CO 80523
Summer 2010

Contents

1 Introduction

There are two generic mechanisms through which a uniform equilibrium state of a physical system may lose stability due to variation of an external control parameter: It can undergo a stationary instability (steady state bifurcation), or an oscillatory instability (Hopf bifurcation). In this thesis we will consider reaction diffusion systems posed in two-dimensional, large but finite, domains that undergo a Hopf bifurcation. By large domain we mean that the characteristic wavelength of the marginally stable modes at the onset of the instability is much smaller than the size of the domain in the two main directions.

This problem is part of the general area of pattern formation in extended systems, which has grown into a major branch of physics and applied mathematics during the past decades, with strong impact on fields as diverse as ecology, chemistry, engineering, as well as new technologies and processes.

1.1 Mathematical Approaches to Pattern Formation

Since the seminal paper of Turing appeared in 1952 [58], it is well known that pattern formation is intimately connected with instabilities encountered in systems of nonlinear partial differential equations (PDE's), and spontaneously broken symmetries arising in their attracting solutions. Schematically, the PDE-systems considered in pattern formation can be written in the form

$$\frac{\partial u}{\partial t} = \mathcal{L}(\nabla, R)u + \mathcal{N}(\nabla, u, R), \tag{1.1}$$

where t is time, $\mathcal{L}$ is a linear operator, R is an external control parameter, and ∇ is the gradient with respect to the unbounded variables x (usually one or two) on which the solution-vector u dpends. Further, bounded variables such as the vertical coordinate in a 2D, infinitely extended layer, are taken into consideration by viewing the solutions $u(x,t)$ as elements of an appropriate function space (Hilbert ot Banach space). The second term $\mathcal{N}$ has to be understood symbolically, it stands for nonlinear terms that are at least quadratic in u and its derivatives. The system (1.1) has $u = 0$ as a distinct solution corresponding to

a spatiotemporally uniform state (the basic state) of the underlying physical system, for example the heat conduction state in Rayleigh-Bènard convection. The typical scenario is that the basic state becomes unstable when R, usually a measure of energy flow, exceeds a critical value R_c. At the critical (onset or threshold) value the linearized operator $\mathcal{L}$ has eigenvalues on the imaginary axis. The associated non-decaying solutions of the linearized system at onset, $u_t = \mathcal{L}u$, are referred to as marginally stable modes. A generic zero eigenvalue gives rise to a stationary instability (the marginally stable modes are time-independent) and a generic imaginary eigenvalue to an oscillatory instability or Hopf bifurcation (temporally oscillating marginally stable modes). Since (1.1) is translation invariant in time and space, the marginally stable modes are spatial or spatiotemporal Fourier modes associated with certain critical wave numbers. At leading order in terms of a small parameter $\epsilon \sim R - R_c$, measuring the distance of the control parameter from its critical value, the solutions are then represented as a superposition of the marginally stable modes. While the basic state has general time and space translation invariance, the solutions above the onset usually have lower symmetry invariance, which is referred to as spontaneous symmetry breaking.

Equivariant bifurcation theory The connection between spontaneous symmetry breaking and pattern formation has led to the development of equivariant bifurcation theory, initiated by Sattinger in the 1970's [50], and established as a branch of mathematics by Golubistky and Stewart in the 1980's, see [32]. In equivariant bifurcation theory the patterns studied in unbounded systems are spatially or spatiotemporally periodic, in two and higher dimensions the spatial periodicity is usually imposed by choosing a lattice. This restriction enables one to reduce the PDE's to a finite dimensional system of ordinary differential equations (ODE's), called 'normal form' or 'amplitude equations,' for the amplitudes of those marginally stable modes that satisfy the chosen periodicity constraints. The application of equivariant bifurcation theorems then allows prediction of the spatially periodic patterns that can be expected above the instability threshold, and to study their stability against perturbations satisfying the same periodicity constraints, but not against non-periodic perturbations or perturbations that are periodic with respect to another lat-

tice. For example, in 2D isotropic systems one often considers both hexagonal and square lattices for the same system, but the stability of a hexagonal pattern against perturbations in the form of square or rhombic patterns cannot be determined. Nevertheless, the importance of this approach relies on the fact that the structure of a normal form follows solely from the symmetries of the PDE's, the critical eigenvalue, and the marginally stable modes taken into account, whereas the details of the particular system studied are revealed in the specific values of the coefficients of the normal form.

Ginzburg Landau formalism The modulation or envelope approach, also referred to as 'Ginzburg Landau (GL) formalism,' takes both temporal and spatial modulations of the marginally stable modes into account. Accordingly, the amplitudes of these modes are treated as slowly varying in time and space, and their evolution is governed by time and space dependent amplitude or envelope equations. This approach was initiated by Newell and Whitehead [45] and Segel [51] in the late 1960's in the context of fluid mechanics. In the case of several marginally stable modes, the equations for their envelopes are coupled canonical PDE's of the Ginzburg Landau type. In the case of a generic stationary instability in 1D, the envelope equation is the real Ginzburg Landau equation (RGLE) for a single, complex envelope as described below. For 2D isotropic systems the derivation of GL-type equations is problematic in the case of nonzero critical wave vectors, because then there exists a continuum (circle) of critical wave vectors due to the rotation invariance of the PDE's. In this case one may choose again a lattice, and take only those marginally stable modes into account that are periodic with respect to that lattice. Since the amplitudes of these modes are still allowed to vary slowly in space, the class of solutions considered contains spatially periodic as well as aperiodic functions, in contrast to the approach used in equivariant bifurcation theory. Generally, the normal forms used in equivariant bifurcation theory follow from the GL-systems when spatial variations are neglected, in which case the GL-PDE's reduce to ODE's. However, a rigorous derivation of GL-systems in dimensions two or higher, in the sense that all possible extended solutions are captured, is strictly possible only for anisotropic systems, which exhibit only a finite number of linearly independent

marginally stable modes. A more in depth discussion of these techniques can be found in [34, 42, 19].

Complex Ginzburg Landau equation The general 'building block' for Ginzburg Landau systems is the complex Ginzburg Landau equation (CGLE). In 1D the general (non-rescaled) form of this equation is

$$\Big(\frac{\partial}{\partial T} - c\frac{\partial}{\partial X}\Big)A = \Big(\mu + d\frac{\partial^2}{\partial X^2} - a|A|^2\Big)A, \tag{1.2}$$

where A is a complex amplitude, T and X are (slow) time and space variables, c is real, and μ, d, and a are complex coefficients. If reflection invariance $X \to -X$ is required, one has to set $c = 0$. For 2D isotropic systems, $\frac{\partial^2}{\partial X^2}$ is replaced by the Laplacean, and for 2D anisotropic systems by a general complex second order differential operator. The RGLE is recovered when $c = 0$ and μ, d, and a are real. In this limit the equation is purely relaxative and can be written as $\frac{\partial A}{\partial T} = -\frac{\delta \mathcal{F}}{\delta \overline{A}}$ [19, 1], where $\mathcal{F}$ is a functional of $(A, \overline{A})$ expressed in terms of an integral, and $\delta/\delta\overline{A}$ denotes a functional derivative. The RGLE resembles the equation derived by Ginzburg and Landau [30], see, also [54], in their phenomenological theory of superconductivity. There are in fact a number of analogies between this theory and the modulational theory of pattern forming systems, see [19]. The other limiting case arises when $c = 0$ and μ, d, and a are purely imaginary, in which case (1.2) becomes the conservative nonlinear Schrödinger equation. The convective term $-c\frac{\partial}{\partial X}$ can be formally eliminated by setting $B(X, T) = A(X - cT, T)$, which means that the solutions are drifting when $c \neq 0$.

The CGLE (1.2) is one of the most extensively studied equations in physics. It has a huge variety of solutions and transitions between them when the parameters are varied, see [1] for a review. The most prominent features of the solutions are phase turbulence, a weak form of "space-time turbulence", and hole-mediated turbulence which is dominated by the appearance of zeros of the complex amplitude A [1, 41]. The role of (1.2) as envelope equation near instabilities is, however, limited to generic instabilities with nonzero critical

wave numbers in 1D translation invariant systems *without reflection symmetry*. In such systems instabilities generically exhibit an imaginary eigenvalue and the separation between stationary and oscillatory instabilities disappears. All finite wave number instabilities are described by a single CGLE with a convective term (group velocity $c \neq 0$). By contrast, in systems with a reflection symmetry there is a clear separation between stationary and oscillatory instabilities. In 1D, stationary instabilities lead to the RGLE, whereas for oscillatory instabilities the marginally stable modes consist of a pair of counterpropagating travelling waves, which means that two envelopes and accordingly a system of two coupled CGLE's are needed to describe this instability. In [38] it is shown that the two CGLE's have to be globally coupled to each other (see Section 2).

Weakly nonlinear analysis The main technique used for reducing a nonlinear PDE-system to a GL-system near an instability is a weakly nonlinear analysis [45, 51]. In this technique the method of multiple scales, see [37, 61], is combined with an expansion of the solutions in terms of a small parameter $\epsilon \sim R - R_c$, measuring the deviation of the control parameter from the onset value. The envelopes are assumed to be small and slowly varying. Specifically, since the envelopes are assumed to be $O(\epsilon)$, the leading terms in the expansion of the PDE's are the linear terms and are $O(\epsilon)$ as well, whereas the nonlinear terms are $O(\epsilon^k)$ with $k > 1$. The slow variation of the envelopes is captured by assuming that they depend on slow space and time variables, for example $T = \epsilon^p t$, $X = \epsilon^q x$, with integers $p, q \geq 1$. The appropriate values for p, q are found by balancing certain terms in the expansion, depending on the particular type of instability. For example, $T = \epsilon^2 t$, $X = \epsilon x$ in the case of a stationary instability in 1D. For oscillatory instabilities one has to use two different slow scales, see Section 2. The solutions are then expanded in an asymptotic series in powers of ϵ, with the leading term consisting of a superposition of the marginally stable modes multiplied by their envelopes. Substitution of the expansion into the PDE's then leads to a hierarchy of linear equations for the higher order terms. These terms are distinguished in 'resonant terms' and 'non-resonant terms.' The equations for the non-resonant terms admit unique solutions, whereas the equations for the resonant

terms (which are of the same form as the marginally stable modes) are singular and require the invoking of solvability conditions related to a Fredholm alternative. The solvability conditions finally lead to the system of GL-equations for the envelopes. In most cases of interest, nonresonant terms occur already at $O(\epsilon^2)$, and resonant terms at $O(\epsilon^3)$. The method has some resemblance to the averaging method widely used in Dynamical Systems [2, 59], where zero averages are required to guarantee that certain equations have periodic (and hence bounded) solutions.

If the envelopes are assumed to depend only on a slow time but not on space, the weakly nonlinear analysis yields an ODE-normal form common in equivariant bifurcation theory. Another approach to find this normal is a process called center manifold reduction and normal form transformation, which does not utilize multiple time scales. The advantage of the weakly nonlinear analysis is that the normal form is determined directly, without the necessity of a subsequent near identity normal form transformation after the reduction to the center manifold. Another reduction method used in equivariant bifurcation theory is the so called Lyapunov Schmidt reduction, see [7]. This reduction yields a system of reduced *algebraic equations* for amplitudes of specific (usually spatially or spatiotemporally periodic) solutions.

Finite size effects In most papers on pattern formation it is assumed that there are one or two unbounded space variables, and the GL formalism captures patterns of infinite extent with respect to these variables. Infinitely extended systems are, however, idealized, since any mesoscopic or macroscopic system in which pattern formation is observed is bounded. The infinite extent idealization is often justified by arguing that the system is large compared to the intrinsic wavelengths of the patterns emerging from instabilities [19], hence the effect of distant sidewalls should be weak. Studies of sidewall effects have been pursued in the 1970's and 1980's for 1D stationary instabilities in the context of Rayleigh-Bènard convection [12, 13, 24, 25, 29]. In this case the sidewalls mainly induce a selection mechanism in that special "phase winding solutions" are selected, which are still contained within the solutions set of the RGLE. Sidewalls have, however, a strong effect on propagating pat-

terns that are created in oscillatory instabilities. With broken spatial translation invariance, ideal travelling waves cannot exist, since any wave propagating through a bounded domain eventually encounters reflection at the boundary, as has been observed in convection experiments on binary mixtures [40] (see Subsection 1.2). To include finite size effects in the GL-description for oscillatory instabilities, Cross [10, 11] has phenomenologically (without rigorous derivation) introduced a system of two locally coupled CGLE's on a finite interval with Robin boundary conditions containing a parameter that is interpreted as a reflection coefficient. Another approach has been used in [17] by introducing imperfection terms breaking the spatial translation invariance in the normal form for a Hopf bifurcation for systems with periodic boundary conditions. These imperfection terms give rise to solutions that are reminiscent of the so called blinking state observed experimentally [40]. In [18] the normal form with these imperfection terms was derived from the system of Cross [10, 11] via center manifold reduction, and in [22] a numerical bifurcation study of the full system of Cross has been pursued showing a variety of complex wave states, including a period doubling cascade to chaos, see, also [16].

A rigorous weakly nonlinear analysis of the effect of sidewalls on the GL description of oscillatory instabilities in 1D systems with reflection symmetry has been performed by Martel and Vega for the case of reaction diffusion equations [43]. The starting point of their analysis is the globally coupled system of CGLE's of [38]. Martel and Vega have shown that the appropriate GL-equation for this type of instability is an evolution equation for a single spatially periodic function with global nonlinear terms, which incorporates the envelopes of the two counterpropagating waves in two parts of its fundamental domain, see Section 2. The method used in this analysis is the method of matched asymptotic expansions [37, 36], where a boundary layer expansion is matched to the bulk expansion. This paper plays a key role for the analysis pursued in this thesis.

1.2 Oscillatory Instabilities in Physical Systems

The Hopf bifurcation is one of the basic mechanisms that leads to temporal oscillations in parameter-dependent dynamical systems. It has been observed experimentally in a variety of biological, chemical, and physical systems. A classical example is the Belusov-Zhabotinsky reaction [3, 62], in which for the first time the possibility of concentration oscillations in chemical reactions has been demonstrated (in this reaction the oscillations are visible by alternating colors), as well as the possibility of concentration wave propagation if the reaction takes place in an extended container allowing diffusion of the substances involved in the reaction.

In systems with few effective degrees of freedom, including spatiotemporal systems of small spatial extent, the Hopf bifurcation leads to sustained limit-cycle oscillations. More complicated dynamics has been observed in spatially extended systems. Experiments with fluids, in particular convection experiments, have shown that a large variety of complex spatiotemporal patterns can appear already slightly above the onset of an oscillatory instability [53, 4, 40, 35, 49].

Thermal double diffusive convection Thermal convection systems, where a fluid layer is heated from below, may encounter a Hopf bifurcation at the onset of convection when there is an additional restraint that acts stabilizing on the heat conduction state, and operates on a slower time scale than the thermal expansion. In most experiments performed, the restraint has the form of a second diffusion process [40, 35, 49]; convection in such fluids is referred to as 'double diffusive' convection. Prototype examples are thermohaline convection (diffusion of salt), convection in binary mixtures (concentration diffusion), and magnetoconvection of an electrically conducting fluid in the presence of an external, vertical magnetic field (diffusion of magnetic flux) [39]. In each of these fluids, the destabilizing buoyancy is opposed by a stabilizing effect, for example, a salt gradient in thermohaline convection, where the fluid is saltier on the bottom than on the top.

In order that in double diffusive systems the onset of convection is a Hopf bifurcation,

the second diffusion process has to be slower than the heat diffusion [9, 39]. In this case the conduction state loses stability to overstable disturbances. Consider for example a fluid parcel in a saltwater heated from below and containing a stabilizing salt gradient. If the parcel is placed upwards through some disturbance, it rapidly gives up heat to the ambient medium while maintaining its salt content. This makes it overdense relative to the ambient medium, and the fluid parcel descends faster than it moved upwards, overshooting on its downward excursion. In this way growing oscillations result. For small, 2D fluid layers that undergo a Hopf bifurcation, linear theory predicts convection rolls which alternate in the orientation of the fluid circulation (corresponding to standing waves). In large containers one observes convection rolls propagating through the container (traveing waves), until they are reflected at the boundary and propagate in the opposite direction resulting in 'blinking state' solutions [40].

Electroconvection in Nematic Liquid Crystals Nematic liquid crystals are charge-carrying fluids composed of long macro-molecules. They differ from ordinary liquids in that their molecules are on average locally oriented along a preferred direction, called the director. For electroconvection, the nematic is sandwiched between two parallel glass plates, treated to produce planar (parallel to the plates) alignment of the director, and an ac-voltage is applied across the electrode plates. Above a critical value of the applied voltage, an electrohydrodynamic instability occurs that leads to various types of convection patterns.

The instability mechanism is that a bending of the director leads to charge accumulation which in turn induces an electric volume force driving the fluid motion. In the original theoretical description (the so-called 'standard model' [5, 33]), the resistivity is assumed Ohmic, with the result that only the destabilizing mechanism is included. As a consequence, the standard model does not show a Hopf bifurcation in contrast to experimental observations [26, 27, 28]. It was later noticed that the ionization-recombination process of the charge carriers acts stabilizing on the basic state, since the electric volume force tends to recombine the charged particles and hence to lower the volume force. In a macroscopic description, this process is incorporated through a non-Ohmic resistivity, in which the conductivity becomes

a further field variable, similarly like the salt concentration in thermohaline convection. The standard model extended by this additional field variable is referred to as 'weak electrolyte model' [55, 56, 57]. The weak electrolyte model shows a Hopf bifurcation if the relaxation time of the conductivity is larger than the relaxation time of the director-variable.

Electroconvection experiments have shown a variety of patterns above the onset, including zig-zag stationary patterns, localized worm-like patterns, and alternating waves [26, 27, 28]. Nematic liquid crystals provide one of the few convection systems where extended spatiotemporal chaos [6] has been observed directly at the onset of convection [55, 28, 15]. The Ginzburg Landau formalism for the Hopf bifurcation in systems posed in infinitely extended domains has been applied to the weak electrolyte model in [56, 57, 20, 46].

1.3 Oscillatory Instabilities in 2D Anisotropic Systems

The subject of this thesis are oscillatory instabilities in 2D anisotropic systems. Our model of the physical system assumes that we can describe the quantities of interest in terms of two space variables and time, $u = u(x, y, t)$. Even if the system is a three dimensional system, for example a thin film, we assume that it is large in two of the dimensions and the pattern formation can be sufficiently described by the extended directions. To keep the problem as simple as possible, we consider systems of reaction diffusion equations posed in a large rectangle with sizes L_p and L_q in the x and y directions respectively, with $L_p \gg 1$ and $L_q \gg 1$, while the aspect ratio of the system is of order one ($L_p/L_q = \mathcal{O}(1)$). Although this is a restricted class of equations, the resulting envelope equation is canonical and holds for any anisotropic system of PDE's posed in a rectangle that encounters the instability considered.

This large domain assumption is necessary to allow us to consider the behavior of the large, but finite, domain separated into two regions, one near the edges where the boundary conditions dominate, and the other in the bulk where the external control parameter dictates the dynamics. The derivation of the bulk solution proceeds by considering the system as infinitely extended in both spatial directions, with the only restriction that the solutions

of the system remain bounded at infinity. For the instability type considered in this work the marginally stable modes of the infinitely extended bulk solution at onset consist of four spatiotemporally periodic Fourier modes corresponding to two pairs of counterpropagating travelling waves. In order for this type of instability to be generic, the system must be anisotropic.

A weakly nonlinear analysis of the infinite size case problem is performed in which the solutions slightly above onset are represented as an asymptotic series in terms of a small parameter ϵ. The leading term of this series is a modulation of the marginally stable modes by slowly varying (in time and space) amplitudes or envelopes. Solvability conditions at higher orders lead to an evolution equation in the form of a set of four globally coupled partial differential equations of the Ginzburg Landau type. These equations have been derived for general systems by using symmetry arguments in [23], and parameter calculations for reaction diffusion systems have been done in [21]. The physical meaning of the global coupling is that the group velocities are finite (rather than asymptotically small) which indicates fast energy transport that causes wave interactions to occur on average rather than locally.

For the finite size problem, the asymptotic solution series of the infinite size case is used to represent the solution in the bulk of the domain. A boundary layer solution is then constructed at each of the four edges of the rectangle such that the solution decays exponentially with increasing distance from each edge. The bulk solution and edge solutions are then matched in an intermediate range between the bulk and the edges. The matching conditions impose relations between the envelopes of the bulk solution which correspond to wave reflections of the travelling waves modulated by the envelopes. The final result is a globally coupled evolution equation for a single, doubly periodic function that captures all four amplitudes in different regions of its fundamental domain.

The derivation of the reduced envelope equation is the main theoretical result of this thesis. While propagation and interaction of the waves in the bulk are adequately described by the equations of [21] for infinitely extended systems, these equations fail when the waves

approach the boundary. Since every real system is confined, the equations of [21] can be considered as valid only over a time range in which no wave reflections and interactions take place at the boundary. For longer times any travelling wave created in an oscillatory instability reaches the boundary, where finite size effects become dominant, and will lead to states such as the so called 'blinking state' where the bulk solution alternates between travelling waves in opposing directions as observed experimentally in convection experiments [40]. The boundary interactions are particularly important when there is energy absorption or injection at the boundary. In the approach used in this work, the effect of the boundary conditions are incorporated into the evolution equations through dependence on two reflection coefficients which incorporate the details of the boundary conditions.

1.4 Overview

In Section 2, previous work on oscillatory instabilities in extended systems, which is related to this thesis, is reviewed. We first discuss in some detail Hopf instabilities in 1D reaction diffusion systems, and outline the derivation of the globally coupled amplitude equations of Knobloch and DeLuca [38]. In addition we present the modification of these equations due to effects of a finite size domain by Martel and Vega [43]. Next we review the 2D infinite size case where the system of globally coupled equations for the envelopes of the four travelling waves is adapted from [23].

In Section 3 we describe the asymptotic analysis leading to the amplitude equations for the Hopf instability in large rectangles. The main difference between the 2D and the 1D cases is the subtle resonances that occur in the 2D case if a certain ratio of L_p, L_q, the group velocities, and the real parts of the diffusion parameters is rational. Explicit equations are given for the generic irrational case as well as the case of a (1,1)-resonance. The work in this section is related to [21, 23] for the 2D case in the same manner as Martel's and Vega's work in [43] is related to [38] for the 1D case. In Section 4 we introduce a Neural Activator-Inhibitor reaction diffusion model adapted from a book by Murray [44] that shows how the theoretical work in Section 3 can be extended to systems that include higher order diffusion

terms. Section 5 discusses results of numerical simulations of the amplitude equations from the bounded case and compares the resulting patterns with simulations of the infinite extent case in [21]. Finally, Section 6 summarizes the results and discusses possible extensions of this work.

2 Hopf Bifurcation in Extended Systems

In this section previous work on Hopf instabilities in 1D and 2D systems that is related to this thesis is reviewed in the context of reaction diffusion equations. The discussion of the 1D case in Section 2.1 also serves to introduce the basic ideas from pattern formation.

2.1 Hopf Bifurcation in 1D Reaction Diffusion Equations

Consider the system of reaction diffusion equations

$$\frac{\partial u}{\partial t} = D_p \frac{\partial^2 u}{\partial x^2} + f(u, R), \tag{2.1}$$

where $u = (u_1, ...u_N)^T$ is a vector of concentrations measured as deviations from equilibrium, D_p is a $N \times N$ diagonal matrix with positive entries, f describes the reaction kinetics and satisfies $f(0, R) = 0$, and R is an external control parameter, for example, temperature or catalyst concentration. For all values of R, (2.1) admits the trivial $u = 0$ solution corresponding to the spatially and temporally uniform equilibrium state. We begin by discussing the idealized situation of an unbounded domain, where $-\infty < x < \infty$, and u is required to remain bounded when $|x| \to \infty$.

2.1.1 Unbounded Domain

Let

$$M(R) = f_u(0, R)$$

be the Jacobian of f at $u = 0$. The stability of the equilibrium $u = 0$ is determined by the linearized system,

$$\frac{\partial u}{\partial t} = D_p \frac{\partial^2 u}{\partial x^2} + M(R)u. \tag{2.2}$$

The trivial solution of (2.1) is (linearly) stable if all solutions of (2.2) decay exponentially in time. Since (2.2) does not depend explicitly on t or x, we look for solutions that are superpositions of the form $e^{\sigma t} e^{ipx} U$, with $U \in \mathbb{C}^N$. This excludes solutions in the form of

diffusing Gaussians which may be important in other contexts. Substituting this into (2.2) yields the eigenvalue problem

$$\sigma U = K(p^2, R)U, \tag{2.3}$$

where

$$K(p^2, R) = -D_p p^2 + M(R). \tag{2.4}$$

Thus, for a given value of R, $u = 0$ is stable if for all p the matrix K has only eigenvalues with negative real parts. The modes $e^{\sigma t}e^{ipx}U$ are called marginally, or neutrally, stable if U is an eigenvector of K with eigenvalue σ and $\mathrm{Re}(\sigma) = 0$. Marginally stable modes with $\sigma = 0$ are called stationary and marginally stable modes with $\sigma = i\Omega$ ($\Omega \in \mathbb{R}$) are called oscillatory. Assuming that the condition for the stationary marginally stable modes with a zero eigenvalue,

$$\det K(p^2, R) = 0,$$

can be solved for $R = R_s(p^2)$ this leads to a curve in the (p, R)-plane, which is referred to as a stationary neutral stability curve [14]. Analogously, assuming that a condition for the oscillatory instability with a purely imaginary eigenvalue can be solved for $R = R_o(p^2)$, the associated curve in the (p, R)-plane is called an oscillatory neutral stability curve. For example, for $N = 3$, the characteristic equation for an eigenvalue σ of K is

$$\sigma^3 + k_2\sigma^2 + k_1\sigma + k_0 = 0,$$

where the real coefficients k_j depend on (p^2, R), $k_j = k_j(p^2, R)$. Then the condition for an imaginary eigenvalue $\sigma = i\Omega$ leads to the equations $\Omega^2 = k_1$ and $-k_2\Omega^2 + k_0 = 0$, giving

$$k_0(p^2, R) - k_2(p^2, R)k_1(p^2, R) = 0$$

as an equation for $R_o(p^2)$, with the constraint $k_1(p^2, R) > 0$. For general N, the equation for (p^2, R) is the resultant of two polynomial equations in Ω^2 found by substituting $\sigma = i\Omega$ into the characteristic equation.

Typically, the curves $R_s(p^2)$ and $R_o(p^2)$ both have minima R_{sc} and R_{oc} and for

$$R < R_c = \min\{R_{sc}, R_{oc}\}$$

the eigenvalues of K are either negative or have negative real parts for all p. The transition to instability occurs when R is increased from below and exceeds R_c. If $R_c = R_{sc}$, the system encounters a stationary instability, and if $R_c = R_{oc}$ the system undergoes an oscillatory instability or Hopf bifurcation. The value p_c for which the minimum is attained, $R_c = R_{sc}(p_c^2)$ or $R_c = R_{oc}(p_c^2)$, is called the critical wavenumber and the corresponding marginally stable modes are called the critical modes.

In the case of a Hopf bifurcation, the critical modes are of the form

$$u(x,t) = U_0 e^{i\omega t} e^{\pm i p_c x}, \tag{2.5}$$

where $\sigma_c = i\omega$ is the critical eigenvalue and U_0 is the associated eigenvector of $K(p_c^2, R_c)$ with respect to σ_c. The neutral stability curves for this case are sketched in Figure 1(a). Note that the neutral stability curves are symmetric about $p = 0$ due to the reflection symmetry $x \to -x$ of (2.2). For $R = R_c$ this linear system has the non-decaying modes (2.5) as solutions, all other solutions decay exponentially. For R slightly above R_c, $R = R_c + \Delta R$, the modes associated with wave numbers in certain intervals around $\pm p_c$ of width $\sim \sqrt{\Delta R}$ are exponentially increasing and $u = 0$ is unstable against perturbations in the form of these modes. The underlying wave numbers are called unstable wave numbers (see Figure 1 (b)).

For small $\Delta R > 0$, solutions of (2.1) are represented in terms of small and slowly varying complex amplitudes or envelopes $A_1(x,t)$ and $A_2(x,t)$ in the form

$$u(x,t) = (A_1(x,t)e^{ip_c x} + A_2(x,t)e^{-ip_c x})U_0 e^{i\omega t} + cc + HOT, \tag{2.6}$$

where cc refers to the complex conjugate expression and HOT refers to higher order terms

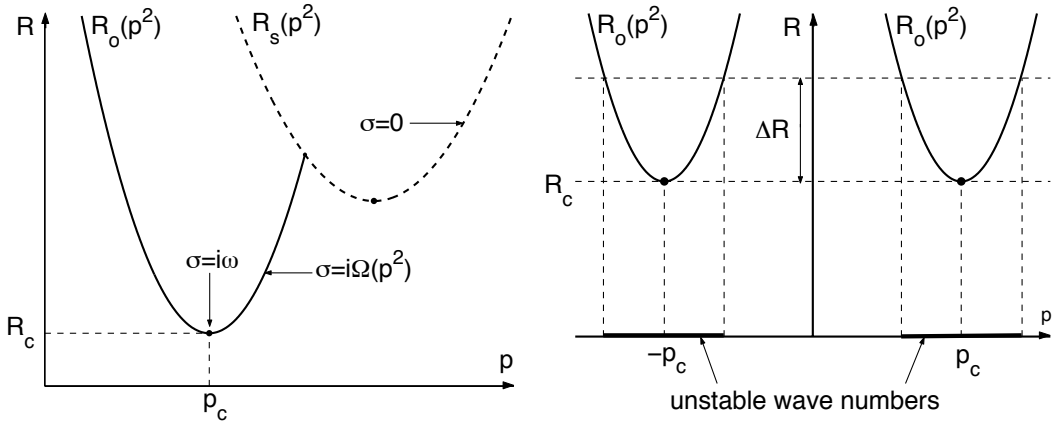

Figure 1: (a) Neutral stability curves $R_s(p^2)$ and $R_o(p^2)$ with the lower minimum on $R_o(p^2)$. (b) Bands of unstable wave numbers for $R = R_c + \Delta R$.

defined as follows. The assumption on the envelopes are that

$$\left|\frac{\partial A_j}{\partial t}\right| \ll |A_j| \ll 1, \quad \left|\frac{\partial^2 A_j}{\partial x^2}\right| \ll \left|\frac{\partial A_j}{\partial x}\right| \ll |A_j|,$$

and in addition it is assumed that $\Delta R \ll 1$. The HOT in (2.6) are terms of higher order than A_1 and A_2 in this sense. According to (2.6), the envelopes A_1 and A_2 modulate the left and right travelling waves, respectively.

We briefly describe the derivation of the evolution equations for A_1 and A_2, and the globally coupled equations resulting from them, following [38]. Fourier transformation of the linear system (2.2) yields $i\Omega\widetilde{u} = K\widetilde{u}$ where $\widetilde{u}$ is the Fourier transform of u with respect to the Fourier variables (Ω, p). Substituting the Fourier transform of the modulated left travelling wave, $A_1 e^{ip_c x + i\omega t} U_0$, into this equation and projecting with the adjoint eigenvector leads to

$$i\Delta\Omega \widetilde{A}_1(\Delta\Omega, \Delta p) = (\sigma(p^2, R) - i\omega)\widetilde{A}_1(\Delta\Omega, \Delta p), \tag{2.7}$$

where $\widetilde{A}_1$ is the Fourier transform of A_1, which is centered around (0,0) because A_1 is slowly varying, and $\Delta\Omega = \Omega - \omega$, $\Delta p = p - p_c$. The eigenvalue σ can be expanded about this

critical value as

$$\sigma(p^2, R) = i\omega + a_0 \Delta R + i v_p \Delta p - d_{pp} \Delta p^2 + \cdots , \tag{2.8}$$

with complex coefficients a_0 and d_{pp}, and the 'critical group velocity'

$$v_p = \frac{\partial}{\partial p} \mathrm{Im}\sigma(p^2, R_c)|_{p_c}.$$

Fourier inversion of (2.7) yields

$$\frac{\partial A_1}{\partial t} - v_p \frac{\partial A_1}{\partial x} = \Big(a_0 \Delta R + d_{pp} \frac{\partial^2}{\partial x^2} \Big) A_1 + HOT,$$

and analogously one obtains

$$\frac{\partial A_2}{\partial t} + v_p \frac{\partial A_2}{\partial x} = \Big(a_0 \Delta R + d_{pp} \frac{\partial^2}{\partial x^2} \Big) A_2 + HOT.$$

These equations are not complete, since nonlinear terms and, in particular, coupling terms are missing. The form of nonlinear terms can be inferred from symmetry considerations. The original system (2.1) is invariant under spatial translations $x \to x + x_0$, the reflection $x \to -x$ and time translations $t \to t + t_0$. Applying these symmetry operations to the modulated left and right travelling waves induces symmetry operations on the envelopes (A_1, A_2),

$$\begin{aligned} t \to t + t_0\text{:} \quad & (A_1, A_2) \quad \to \quad e^{i\omega t_0}(A_1, A_2) \\ x \to x + x_0\text{:} \quad & (A_1, A_2) \quad \to \quad (e^{ip_c x_0} A_1, e^{-ip_c x_0} A_2) \\ x \to -x\text{:} \quad & (A_1, A_2) \quad \to \quad (A_2, A_1). \end{aligned}$$

The evolution equations for (A_1, A_2) have to be invariant under these operations. The only nonlinear terms up to third order that satisfy that invariance are $(|A_1|^2 A_1, |A_2|^2 A_2)$ and

$(|A_2|^2 A_1, |A_1|^2 A_2)$. Adding these generic nonlinear terms to the linear equations gives

$$\frac{\partial A_1}{\partial t} - v_p \frac{\partial A_1}{\partial x} = \big(a_0 \Delta R + d_{pp} \frac{\partial^2}{\partial x^2} + e_1 |A_1|^2 + e_2 |A_2|^2\big) A_1 + HOT, \tag{2.9}$$

$$\frac{\partial A_2}{\partial t} + v_p \frac{\partial A_2}{\partial x} = \big(a_0 \Delta R + d_{pp} \frac{\partial^2}{\partial x^2} + e_1 |A_2|^2 + e_2 |A_1|^2\big) A_2 + HOT, \tag{2.10}$$

where the parameters e_1 and e_2 are complex coefficients computable from the nonlinear terms in (2.1)

A complication of the system (2.9), (2.10) is that, assuming the generic case that v_p is $\mathcal{O}(1)$, $\partial A_j/\partial x$ is of lower order than $\partial^2 A_j/\partial x^2$. To deal with this, one introduces wave variables to eliminate the first order wave operators on the left hand sides of (2.9) and (2.10). Setting $\Delta R = \epsilon^2$ and introducing the slow variables $X_\pm$ and the 'super-slow' time τ,

$$X_\pm = \epsilon(x \pm v_p t), \quad \tau = \epsilon^2 t,$$

and expanding

$$\begin{aligned} A_1 &= \epsilon B_1(X_+, \tau) + \epsilon^2 B_1^{(2)}(X_+, X_-, \tau) + \mathcal{O}(\epsilon^3) \\ A_2 &= \epsilon B_2(X_-, \tau) + \epsilon^2 B_2^{(2)}(X_+, X_-, \tau) + \mathcal{O}(\epsilon^3), \end{aligned}$$

the equation (2.9) is satisfied at $\mathcal{O}(\epsilon^2)$, and at $\mathcal{O}(\epsilon^3)$ it becomes

$$-2 v_p \frac{\partial B_1^{(2)}}{\partial X_-} = \big(- \frac{\partial}{\partial \tau} + a_0 + d_{pp} \frac{\partial^2}{\partial X_+^2} + e_1 |B_1|^2 + e_2 |B_2|^2\big) B_1.$$

In order for this equation to have a bounded solution $B_1^{(2)}$, the average with respect to X_- must vanish. This condition leads to an evolution equation for B_1,

$$\frac{\partial B_1}{\partial \tau} = \big(a_0 + d_{pp} \frac{\partial^2}{\partial X_+^2} + e_1 |B_1|^2 + e_2 < |B_2|^2 > \big) B_1, \tag{2.11}$$

where

$$< |B_2|^2 > = \lim_{L \to \infty} \frac{1}{2L} \int_{-L}^{L} |B_2(X_-, \tau)|^2 \, dX_-$$

denotes the average of $|B_2|^2$ with respect to X_-. Analogously one finds

$$\frac{\partial B_2}{\partial \tau} = \big(a_0 + d_{pp}\frac{\partial^2}{\partial X_-^2} + e_1|B_2|^2 + e_2 < |B_1|^2 > \big)B_2, \tag{2.12}$$

where $< |B_1|^2 >$ is the average of $|B_1|^2$ with respect to X_+. The averaged terms are then the direct result of the $\mathcal{O}(1)$ group velocity, v_p. One can think of this as a wavefront of the left travelling wave interacting with an infinite number of wavefronts of the right travelling wave in terms of the super-slow time, and thus the left travelling wave cannot react with any particular right travelling wavefront individually but can only interact on average with the incident wavefronts leading to global coupling with the incident wave amplitude. The system of globally coupled equations (2.11) and (2.12) has been first derived by Knobloch and DeLuca [38], and has been applied to reaction diffusion systems and edge waves in [43] and [48], respectively.

As a first approximation spatial variations are ignored leading to (2.11) and (2.12) reducing to the ODE-system

$$\frac{dB_1}{d\tau} = (a_0 + e_1|B_1|^2 + e_2|B_2|^2)B_1, \tag{2.13}$$

$$\frac{dB_2}{d\tau} = (a_0 + e_1|B_2|^2 + e_2|B_1|^2)B_2, \tag{2.14}$$

which is known as the normal form for a Hopf bifurcation with $\mathcal{O}(2)$-symmetry [31]. The system (2.13), (2.14) describes solutions of (2.1) slightly above R_c when periodic boundary conditions with period $2\pi/p_c$ are imposed. For generic values of e_1, e_2, the only non-transient solutions (up to symmetry operations) of (2.13), (2.14) are of the form $(B_1, B_2) = (re^{i\Omega t}, 0)$ corresponding to ideal travelling waves, and $(B_1, B_2) = (re^{i\Omega t}, re^{i\Omega t})$ corresponding to ideal standing waves, with different amplitudes r and frequencies Ω for the two wave types. The travelling waves are stable if $e_{2r} < e_{1r} < 0$, and the standing waves are stable if $e_{1r} < 0$ and $e_{2r}^2 < e_{1r}^2$ (subscripts r and i are used to denote real and imaginary parts, respectively). If none of these conditions are satisfied, both the standing and travelling waves are unstable.

2.1.2 Bounded Domain

The case of a Hopf bifurcation of (2.1) posed in a large, but bounded, domain with generic boundary conditions has been studied by Martel and Vega [43]. In this paper, (2.1) is posed in a domain $-L_p/2 < x < L_p/2$ where $L_p \gg 1$, $\Delta R = \mu \sim L_p^{-2}$, and $|A_1| \sim |A_2| \sim L_p^{-1}$. The solution in the bulk is represented as in Section 2.1.1. Near the boundaries the solution is represented by boundary layer solutions that decay exponentially with increasing distance from the end points, and ensure the boundary conditions are satisfied. The bulk solution is then matched to the boundary layer solution in certain transition regions. As a consequence of this matching, A_1 and A_2 are no longer independent, but become related to each other by translations in the wave variables. After several transformations and rescalings, and utilizing a reflection principle, Martel and Vega arrive at the following globally coupled equation,

$$\frac{\partial W}{\partial \tau} = b''_{1p}\frac{\partial W}{\partial X} + d'_{pp}\frac{\partial^2 W}{\partial X^2} + \left[\lambda + e'_1|W|^2 + e'_2\int_{-1/2}^{1/2}\phi(z)|W(X-2z-1,\tau)|^2\,dz\right]W. \quad (2.15)$$

The function $W(X,\tau)$ is periodic in X with period 2, where d'_{pp}, e'_1, and e'_2 are rescaled versions of d_{pp}, e_1 and e_2. The coefficient $b''_{1p} \in \mathbb{C}$ comes from higher order terms in the expansion of σ, and $\lambda \in \mathbb{R}$ plays the role of the rescaled bifurcation parameter due to choosing the small parameter as $\epsilon = 1/L_p$. The variable X is a modified version of the slow characteristic variable X_+, and the function $\phi(z)$ is given by

$$\phi(z) = \begin{cases} (2\log\rho_p)\rho_p^{1-2z}/(\rho_p^2-1) & \text{if} \quad \rho_p \neq 1, \\ 1 & \text{if} \quad \rho_p = 1, \end{cases}$$

where $r_p = \rho_p e^{i\alpha_p}$, $0 < \rho_p < \infty$, is a reflection coefficient derived from the boundary conditions. Scaled and transformed versions of the envelopes A_1 and A_2 are contained in W in the regions $-3/2 < X < -1/2$ and $-1/2 < X < 1/2$, respectively.

An important consequence of the addition of boundaries is that the spatial translation invariance $x \to x + x_0$ is broken. Accordingly, the equation for W possesses only the phase

shift invariance $W \to e^{i\phi}W$ resulting from temporal translations. The reflection symmetry $x \to -x$ is revealed in the invariance of the equation under

$$W(X,\tau) \to W(-1-X-c\tau,\tau)e^{-i(kX+\nu\tau)},$$

where $k = b''_{1pi}/d'_{ppr}$, $\nu = (b''_{1pi}/d'^2_{ppr})\mathrm{Re}(d'_{pp}\overline{b''_{1p}})$, and $c = (2/d'_{ppr})\mathrm{Re}(d'_{pp}\overline{b''_{1p}})$.

2.2 Hopf Bifurcation in 2D Reaction Diffusion Systems in an Unbounded Domain

For this thesis we are concerned with the 2D extension of (2.1),

$$\frac{\partial u}{\partial t} = D_p\frac{\partial^2 u}{\partial x^2} + D_q\frac{\partial^2 u}{\partial y^2} + f(u,R), \quad f(0,R) = 0, \tag{2.16}$$

where D_p and D_q are diagonal matrices with positive entries, and $D_p \neq D_q$ making the diffusion anisotropic. The meaning of u, R and f is as in Section 2.1. The stability of the trivial solution $u = 0$ is determined by the linearized system

$$\frac{\partial u}{\partial t} = D_p\frac{\partial^2 u}{\partial x^2} + D_q\frac{\partial^2 u}{\partial y^2} + M(R)u, \quad M(R) = f_u(0,R), \tag{2.17}$$

and substitution of $u = e^{\sigma t}e^{ipx+iqy}U$, $U \in \mathbb{C}^N$, yields the eigenvalue problem

$$\sigma U = K(p^2,q^2,R)U, \tag{2.18}$$

with

$$K(p^2,q^2,R) = -D_p p^2 - D_q q^2 + M(R). \tag{2.19}$$

The eigenvalue problem (2.18) now involves two wave numbers $\mathbf{p} = (p,q) \in \mathbb{R}^2$, and the neutral stability curves for the 1D case become neutral stability surfaces $R_s(p^2,q^2)$ and $R_o(p^2,q^2)$ in the 2D case. Note that in isotropic systems K only depends on $|\mathbf{p}|^2$, and the 1D discussion of the neutral stability minima can be directly carried over into the 2D case

by identifying p^2 with $|\mathbf{p}|^2$. However, a minimum of the neutral stability curve $R_s(|\mathbf{p}|^2)$ or $R_o(|\mathbf{p}|^2)$ with $|\mathbf{p}|^2 > 0$ will now give a full circle of critical wave numbers due to the rotational invariance. This is a high degeneracy for which, to the author's knowledge, no satisfactory Ginzburg Landau formalism that captures all non-transient solutions slightly above criticality is available.

With the assumption of an anisotropic system, the minima of the neutral stability surfaces generically occur at isolated wave numbers. Since the system has two reflection symmetries, one of three cases will be present, a single minimum will occur at the origin, or two minima will exist on a reflection axis (referred to as the 'normal case'), or four minima off both reflection axes (referred to as the 'oblique case'). We assume that the critical value of the control parameter R_c occurs on the oscillatory neutral stability surface at four critical wave numbers $(\pm p_c, \pm q_c)$ with $p_c > 0$, $q_c > 0$. This leads to critical modes of the form

$$u(x, y, t) = U_0 e^{i\omega \pm i p_c x \pm i q_c y} \tag{2.20}$$

where $\sigma_c = i\omega$ is the imaginary eigenvalue of (2.18) at $(p_c, q_c, 0)$, and U_0 is the corresponding eigenvector. At $R = R_c$ these four modes are the only non-decaying modes as solutions. For $\Delta R = R - R_c$ slightly above 0, the modes in the roughly elliptical areas around $(\pm p_c, \pm q_c)$ with average diameter $\sim \sqrt{\Delta R}$ will increase exponentially and the $u = 0$ state is unstable with respect to perturbations in those modes. The corresponding wave number pairs (p, q) are called unstable. Globally coupled envelope equations for this 'oblique Hopf bifurcation' in unbounded domains have been set up in [23], and are studied to some extent in [21, 46, 47]. In the following we briefly describe the derivation of these equations.

For small $\Delta R > 0$, solutions to (2.16) are represented as a superposition of four modulated oblique travelling waves in the form

$$u(x, y, t) = (A_1 e^{i(p_c x + q_c y)} + A_2 e^{i(-p_c x + q_c y)} + A_3 e^{i(-p_c x - q_c y)} + A_4 e^{i(p_c x - q_c y)}) U_0 e^{i\omega t} + cc + HOT, \tag{2.21}$$

where $A_j(x, y, t)$ are small and slowly varying envelopes. As in the 1D case the linear terms

in the evolution equations can be inferred from the expansion of the critical eigenvalue,

$$\sigma(p^2, q^2, R) = i\omega + a_0\mu + iv_p\Delta p + iv_q\Delta q - d_{pp}\Delta p^2 - 2d_{pq}\Delta p\Delta q - d_{qq}\Delta q^2 + \cdots,$$

where $\Delta p = p - p_c$, $\Delta q = q - q_c$, and a_0, d_{pp}, d_{pq}, d_{qq} are complex coefficients with d_{ppr}, d_{pqr}, d_{qqr} forming a positive definite quadratic form (assuming a non-degenerate minimum of $R_o(p^2, q^2)$ at (p_c^2, q_c^2)). The coefficients $v_p \in \mathbb{R}$ and $v_q \in \mathbb{R}$ are the critical group velocities,

$$v_p = \frac{\partial}{\partial p}\mathrm{Im}\sigma(p^2, q_c^2, R_c)|_{p_c}, \quad v_q = \frac{\partial}{\partial q}\mathrm{Im}\sigma(p_c^2, q^2, R_c)|_{q_c}.$$

The leading nonlinear terms in the equations for the A_j are derived again by symmetry considerations. The system (2.16) is invariant under time translations $t \to t + t_0$, two spatial translations $x \to x + x_0$ and $y \to y + y_0$, and two reflections $x \to -x$ and $y \to -y$. Applying these operations to the representation (2.21) of u induces the following symmetry operations on the envelopes,

$$\begin{aligned}
t \to t + t_0\text{:} \quad & (A_1, A_2, A_3, A_4) \quad \to \quad e^{i\omega t_0}(A_1, A_2, A_3, A_4) \\
x \to x + x_0\text{:} \quad & (A_1, A_2, A_3, A_4) \quad \to \quad (e^{ip_c x_0}A_1, e^{-ip_c x_0}A_2, e^{-ip_c x_0}A_3, e^{ip_c x_0}A_4) \\
y \to y + y_0\text{:} \quad & (A_1, A_2, A_3, A_4) \quad \to \quad (e^{ip_c y_0}A_1, e^{ip_c y_0}A_2, e^{-ip_c y_0}A_3, e^{-ip_c y_0}A_4) \\
x \to -x\text{:} \quad & (A_1, A_2, A_3, A_4) \quad \to \quad (A_2, A_1, A_4, A_3) \\
y \to -y\text{:} \quad & (A_1, A_2, A_3, A_4) \quad \to \quad (A_4, A_3, A_2, A_1),
\end{aligned}$$

and the evolution equations for A_1, A_2, A_3 and A_4 are invariant under these operations. Up to cubic order there are five nonlinear terms that respect these symmetries for each equation. With linear terms taken from σ and the nonlinear terms multiplied by generic coefficients $e_1, \cdots, e_5$, the evolution equation for A_1 can be written as

$$\frac{\partial A_1}{\partial t} - v_p\frac{\partial A_1}{\partial x} - v_q\frac{\partial A_1}{\partial y} = \Big(a_0\mu + \widetilde{\mathcal{D}}(\partial_x, \partial_y) + \sum_{j=1}^{4} e_j|A_j|^2\Big)A_1 + e_5 A_2\overline{A}_3 A_4 + HOT, \quad (2.22)$$

where

$$\widetilde{\mathcal{D}}(\partial_x, \partial_y) = d_{pp}\partial_x^2 + 2d_{pq}\partial_x\partial_y + d_{qq}\partial_y^2.$$

The equations for A_2 and A_4 follow from (2.22) by applying the $x-$ and $y-$reflections, respectively, and the equation for A_3 by applying the combined reflection

$$(x, y, A_1, A_2, A_3, A_4) \to (-x, -y, A_3, A_4, A_1, A_2).$$

The problem of the lower order first derivative terms is again dealt with by utilizing characteristic wave variables. In [21] the following variables are used

$$X_\pm = \epsilon(t \pm x/v_p), \;\; Y_\pm = \epsilon(t \pm y/v_q), \;\; \tau = \epsilon^2 t, \;\; \mu = \epsilon^2,$$

and the A_j are expanded as $A_j = \epsilon B_j + \epsilon^2 B_j^{(2)} + \mathcal{O}(\epsilon^3)$, with

$$B_1 = B_1(X_+, Y_+, \tau), \;\; B_2 = B_2(X_-, Y_+, \tau), \;\; B_3 = B_3(X_-, Y_-, \tau), \;\; B_4 = B_4(X_+, Y_-, \tau),$$

which ensures that the $\mathcal{O}(\epsilon^2)$-terms in the equations for the A_j cancel out. The wave variables are no longer independent because of the relation

$$X_+ + X_- = Y_+ + Y_- = 2\epsilon t$$

Accordingly, the second order envelopes $B_j^{(2)}$ depend on three wave variables which can be chosen arbitrarily from $X_\pm$, $Y_\pm$. In [21] $B_1^{(2)}$ is considered a function of (X_+, Y_+, X_-, τ). With the above expansion, the equation (2.22) becomes up to $\mathcal{O}(\epsilon^3)$

$$-2v_p\frac{\partial B_1^{(2)}}{\partial X_-} = -\frac{\partial B_1}{\partial \tau} + \Big(a_0 + \hat{\mathcal{D}}(\partial_{X_+}, \partial_{Y_+}) + \sum_{j=1}^{4} e_j|B_j|^2\Big)B_1 + e_5 B_2\overline{B}_3 B_4,$$

where $\hat{\mathcal{D}}(\partial_{X_+}, \partial_{Y_+}) = \widetilde{\mathcal{D}}(\partial_{X_+}/v_p, \partial_{Y_+}/v_q)$. In order for this equation to have a bounded solution $B_1^{(2)}$, the average of the right hand side with respect to X_- must vanish, which

leads, after some manipulations, to the following equation for B_1 with global couplings to B_2, B_3, B_4,

$$\begin{aligned}\frac{\partial B_1}{\partial \tau} &= \big(a_0 + \hat{\mathcal{D}}(\partial_X, \partial_Y) + e_1|B_1|^2 \\ &\quad + e_2 < |B_2(z, Y, \tau)|^2 > + e_3 < |B_3(z - X, z - Y, \tau)|^2 > + e_4 < |B_4(X, z, \tau)|^2 > \big) B_1 \\ &\quad + e_5 < B_2(z - X, Y, \tau)\overline{B_3}(z - X, z - Y, \tau) B_4(X, z - Y, \tau) >, \end{aligned} \tag{2.23}$$

where the subscript '+' has been dropped, and the brackets denote averages over z. Analogous equations follow for B_2, B_3, and B_4.

If spatial variations are ignored, the globally coupled system for $B_1, \ldots, B_4$ reduces to the ODE-system,

$$\begin{aligned}\tfrac{dB_1}{d\tau} &= \big(a_0 + e_1|B_1|^2 + e_2|B_2|^2 + e_3|B_3|^2 + e_4|B_4|^2\big) B_1 + e_5 B_2 \overline{B}_3 B_4, \\ \tfrac{dB_2}{d\tau} &= \big(a_0 + e_1|B_2|^2 + e_2|B_1|^2 + e_3|B_4|^2 + e_4|B_3|^2\big) B_2 + e_5 B_1 \overline{B}_4 B_3, \\ \tfrac{dB_3}{d\tau} &= \big(a_0 + e_1|B_3|^2 + e_2|B_4|^2 + e_3|B_1|^2 + e_4|B_2|^2\big) B_3 + e_5 B_4 \overline{B}_1 B_2, \\ \tfrac{dB_4}{d\tau} &= \big(a_0 + e_1|B_4|^2 + e_2|B_3|^2 + e_3|B_2|^2 + e_4|B_1|^2\big) B_4 + e_5 B_3 \overline{B}_2 B_1. \end{aligned} \tag{2.24}$$

This is the normal form for a Hopf bifurcation with $O(2) \times O(2)$ symmetry, and it follows directly from (2.16) when periodic boundary conditions on (x, y) with periods $(2\pi/p_c, 2\pi/q_c)$ are imposed. This case has been introduced and studied in [52] and [60]. The basic periodic solutions correspond to the following wave types (amplitudes r and frequencies Ω are different for different wave types):

$$\begin{aligned} \text{Travelling waves:} &\quad B_1 = re^{i\Omega\tau}, \;\; B_2 = B_3 = B_4 = 0, \\ \text{Standing waves:} &\quad B_1 = B_3 = re^{i\Omega\tau}, \;\; B_2 = B_4 = 0, \\ \text{Travelling rectangles in the } x\text{-direction:} &\quad B_1 = B_2 = re^{i\Omega\tau}, \;\; B_3 = B_4 = 0, \\ \text{Travelling recangles in the } y\text{-direction:} &\quad B_1 = B_4 = re^{i\Omega\tau}, \;\; B_2 = B_3 = 0, \\ \text{Standing rectangles:} &\quad B_1 = B_2 = B_3 = B_4 = re^{i\Omega\tau}, \\ \text{Alternating waves:} &\quad B_1 = iB_2 = B_3 = iB_4 = re^{i\Omega\tau}. \end{aligned}$$

The alternating waves are waves oscillating between the two oblique stripe patterns in the directions $(\pm p_c, q_c)$. Beyond the basic wave solutions, (2.24) admits more complex solutions such as structurally stable heteroclinic cycles [52, 60], and recently a period doubling route to chaos has been found numerically in a certain parameter regime [46].

3 Reaction Diffusion System Posed in a 'Large' Rectangle

In this section we describe the derivation of the amplitude equations for a Hopf bifurcation with four critical wavenumbers in the reaction diffusion system (2.16), when the PDEs are posed in a large rectangle. An extension that includes higher order diffusion terms is given in Section 4.

The problem for $u = (u_1, \ldots, u_N)^T$ is the following (derivatives are denoted here by subscripts):

$$u_t = (D_p \partial_x^2 + D_q \partial_y^2)u + f(u, \mu), \tag{3.1}$$

in

$$-L_p/2 < x < L_p/2, \quad -L_q/2 < x < L_q/2, \tag{3.2}$$

subject to the boundary conditions,

$$C_p u \pm E_p u_x = 0 \quad \text{at} \quad x = \pm L_p/2, \tag{3.3}$$

$$C_q u \pm E_q u_y = 0 \quad \text{at} \quad y = \pm L_q/2. \tag{3.4}$$

The parameter μ is the reduced bifurcation parameter, $\mu = R - R_c$, and C_p, C_q, E_p, E_q are constant $N \times N$-matrices. The assumptions on f are:

(1) $f(0, \mu) = 0$.

(2) Let $f_u(0, \mu)$ be the Jacobian of f at $u = 0$, and let

$$K(p^2, q^2, \mu) = -D_p p^2 - D_q q^2 + f_u(0, \mu).$$

Then $K_c = K(p_c^2, q_c^2, 0)$ has a simple pair of imaginary eigenvalues $\pm i\omega$, with eigenvector $K_c U_0 = i\omega U_0$, for fixed wave numbers $(\pm p_c, \pm q_c)$ with $p_c > 0$, $q_c > 0$. All other eigenvalues of K_c have negative real parts.

(3) For all $(p^2, q^2) \neq (p_c^2, q_c^2)$, the eigenvalues of $K(p^2, q^2, 0)$ have negative real parts.

(4) Let $F_2 = f_{u\mu}(0,0)$, and let U_0^* be the adjoint eigenvector of K_c for $i\omega$, $K_c^T U_0^* = -i\omega U_0^*$, with the normalization $\overline{U}_0^{*T} U_0 = 1$. Let $a_0 = \overline{U}_0^{*T} F_1 U_0$. Then $a_{0r} > 0$.

Assumption (1) means that $u = 0$ is a uniform steady state for all μ. This assumption can actually be relaxed as in [43], where nonhomogeneous boundary conditions are admitted, giving rise to a steady boundary layer solution that decays exponentially in the bulk. Since this generalization does not alter the *form* of the resulting amplitude equations, we consider here the simpler case of homogeneous boundary conditions with basic solution $u = 0$. Another possible generalization would be allowing the matrices C_p, C_q, E_p, E_q depend on the variables along the corresponding edges in a reflection symmetric manner, $C_p = C_p(y)$ with $C_p(-y) = C_p(y)$ etc. Also this generalization would not alter the form of the amplitude equations, and we assume constant boundary-matrices for simplicity.

Assumptions (2) and (3) are the conditions for a generic Hopf bifurcation, and assumption (4) guarantees that the instability occurs when μ crosses 0 from below. Assumption (4) is the standard transversality condition common in bifurcation theory. Two further genericity assumptions on the linearized problem concern the first and second order terms with respect to (p, q), and will be introduced below.

In the weakly nonlinear analysis of (3.1)-(3.4), f is expanded as

$$f(u,\mu) = (F_1 + F_2\mu + F_3\mu^2)u + \mathcal{B}(u,u) + \mathcal{C}(u,u,u) + \mathcal{O}(|u|^3 + |u\mu| + |\mu|^3)|u|,$$

where $F_1 = f_u(0,0)$, $F_2 = f_{u\mu}(0,0)$, $F_3 = f_{u\mu\mu}(0,0)/2$ are $N \times N$-matrices, and $\mathcal{B} = f_{uu}(0,0)/2$ and $\mathcal{C} = f_{uuu}(0,0)/6$ are bilinear and trilinear operators corresponding to the second and third order terms in the Taylor expansion of $f(u,0)$, respectively.

3.1 Linearized Equation

For $\mu = 0$, the linearization of (3.1) about $u = 0$ has the plane wave solution $e^{i\omega t} e^{i(p_c x + q_c y)} U_0$. This solution is extended to a solution $e^{\sigma t} e^{i(px+qy)} U$ by expanding the critical eigenvalue σ about $i\omega$, and the corresponding eigenvector U about U_0, in terms of $(\Delta p, \Delta q) =$

$(p - p_c, q - q_c)$ and μ. Substituting the expansions

$$\begin{aligned}
\sigma &= i\omega + i(v_p + \mu b_{1p})\Delta p + i(v_q + \mu b_{1q})\Delta q \\
&\quad + d_{pp}\Delta p^2 - 2d_{pq}\Delta p\Delta q - d_{qq}\Delta q^2 + (a_0 + a_1\mu)\mu + \cdots \qquad (3.5) \\
U &= U_0 + \Delta p U_{1p} + \Delta q U_{1q} + \Delta p^2 U_{2pp} + 2\Delta p\Delta q U_{2pq} + \Delta q^2 U_{2qq} \\
&\quad + \mu U_3 + \mu(\Delta p U_{4p} + \Delta q U_{4q}) + \mu^2 U_5 + \cdots \qquad (3.6)
\end{aligned}$$

into the eigenvalue equation $[K(p^2, q^2, \mu) - \sigma I]U = 0$, where I is the identity matrix, yields a hierarchy of linear equations for the expansion vectors in U

$$\begin{aligned}
T(p_c^2, q_c^2, \omega)U_0 &= 0 \\
T(p_c^2, q_c^2, \omega)U_{1p} &= (2p_c D_p + iv_p I)U_0 \\
T(p_c^2, q_c^2, \omega)U_{1q} &= (2q_c D_q + iv_q I)U_0 \\
T(p_c^2, q_c^2, \omega)U_{2pp} &= (2p_c D_p + iv_p I)U_{1p} + (D_p - d_{pp}I)U_0 \\
T(p_c^2, q_c^2, \omega)U_{2pq} &= (2p_c D_p + iv_p I)U_{1q}/2 + (2q_c D_q + iv_q I)U_{1p}/2 + d_{pq}U_0 \\
T(p_c^2, q_c^2, \omega)U_{2qq} &= (2q_c D_q + iv_q I)U_{1q} + (D_q - d_{qq}I)U_0 \\
T(p_c^2, q_c^2, \omega)U_3 &= (a_0 I - F_2)U_0 \\
T(p_c^2, q_c^2, \omega)U_{4p} &= (2p_c D_p + iv_p I)U_3 + (a_0 I - F_2)U_{1p} + ib_{1p}U_0 \\
T(p_c^2, q_c^2, \omega)U_{4q} &= (2q_c D_q + iv_q I)U_3 + (a_0 I - F_2)U_{1q} + ib_{1q}U_0 \\
T(p_c^2, q_c^2, \omega)U_5 &= (a_1 I - F_3)U_0 + (a_0 I - F_2)U_3
\end{aligned}$$

where $T(p^2, q^2, \Omega) = (F_1 - p^2 D_p - q^2 D_q - i\Omega I)$ is a singular matrix when $(p^2, q^2, \Omega) = (p_c^2, q_c^2, \omega)$. Note that these equations are all of the form

$$T(p_c^2, q_c^2, \omega)U_e = V_e + \sigma_e U_0,$$

where U_e is an expansion vector in U, σ_e the expansion coefficient for the same term in σ (e.g. $U_e = U_{2pp}$, $\sigma_e = -d_{pp}$), and the vector V_e depends on expansion vectors and

coefficients of lower order. The solvability condition for U_e is that $V_e + \sigma_e U_0$ be orthogonal to U_0^*. This gives $\sigma_e = -\overline{U}_0^{*T} V_e$, and leads to a unique solution for U_e if it is required that $\overline{U}_0^{*T} U_e = 0$. Applying the orthogonality condition leads to the following equations for the coefficients occurring in (3.5),

$$\begin{aligned}
v_p &= 2ip_c \overline{U_0}^{*T} D_p U_0 \\
v_q &= 2iq_c \overline{U_0}^{*T} D_q U_0 \\
d_{pp} &= \overline{U}_0^{*T}(2p_c D_p + ib_{1p} I)U_{1p} + \overline{U}_0^{*T} D_p U_0 \\
d_{pq} &= \overline{U}_0^{*T}(2p_c D_p + iv_p I)U_{1q} + \overline{U}_0^{*T}(2q_c D_q + iv_q I)U_{1p} \\
d_{qq} &= \overline{U}_0^{*T}(2q_c D_q + ib_{1q} I)U_{1q} + \overline{U}_0^{*T} D_q U_0 \\
a_0 &= \overline{U}_0^{*T} F_2 U_0 \\
b_{1p} &= \overline{U}_0^{*T}(2ip_c D_p - b_{1p} I)U_3 + \overline{U}_0^{*T}(ia_0 I - iF_2)U_{1p} \\
b_{1q} &= \overline{U}_0^{*T}(2iq_c D_q - b_{1q} I)U_3 + \overline{U}_0^{*T}(ia_0 I - iF_2)U_{1q} \\
a_1 &= \overline{U}_0^{*T} F_3 U_0 + \overline{U}_0^{*T}(F_2 - a_0 I)U_0.
\end{aligned}$$

Note that these include the terms $\mu\Delta p$, $\mu\Delta q$, μ^2, which are not taken into account in the weakly nonlinear analysis of the unbounded problem. In the bounded case they have to be included because the stability threshold is shifted from $\mu = 0$ to a small nonzero value of μ.

The additional genericity assumptions concerning the linearized system are

(5) $v_p \neq 0$ and $v_q \neq 0$.

(6) $d_{ppr} > 0$ and $d_{ppr} d_{qqr} - d_{pqr}^2 > 0$.

Assumption (5) is our basic assumption of nonzero critical group velocities, giving rise to global coupling terms. Assumption (6) states that the minimum of the oscillatory neutral stability surface is non-degenerated, and leads to a non-degenerated diffusion term in the amplitude equations.

3.2 Bulk Solution

In the weakly nonlinear analysis of (3.1) without boundary constraints, one seeks a solution of the form

$$u = \sum_{m,n,k} U_{mnk}(x, y, t, \mu) e^{i(mp_c x + nq_c y + k\omega t)}, \tag{3.7}$$

with small and slowly varying coefficient functions $U_{mnk} = \overline{U}_{-m,-n,-k}$. Setting

$$E_1 = e^{i(p_c x + q_c y + \omega t)}, \;\; E_2 = e^{i(-p_c x + q_c y + \omega t)}, \;\; E_3 = e^{i(-p_c x - q_c y + \omega t)}, \;\; E_4 = e^{i(p_c x - q_c y + \omega t)},$$

to simplify the notation, the leading terms in (3.7) are the basic travelling waves,

$$u = \sum_{j=1}^{4} A_j(t, x, y) E_j U_0 + cc + HOT,$$

where the A_j are the small and slowly varying envelopes introduced in Section 2.2. The coefficient functions U_{mnk} are represented as formal power series in

$$(\partial_t, \partial_x, \partial_y, A_1, \ldots, A_4, \overline{A}_1, \ldots, \overline{A}_4, \mu),$$

with each term in the power series multiplied by a vector to be determined. A hierarchy of equations for these vectors follows by substituting the series into (3.1).

In the Fourier series one distinguishes resonant Fourier terms, which are the basic waves E_j and $\overline{E}_j$ $(m, n, k = \pm 1)$, and non-resonant terms. A power series coefficient vector U_e in a non-resonant Fourier term with labels (m, n, k) satisfies an equation of the form

$$T(m^2 p_c^2, n^2 q_c^2, k\omega) U_e = V_e,$$

where V_e depends only on lower order terms. Since $(m^2, n^2, k^2) \neq (1, 1, 1)$ in the non-resonant case, the matrix on the left hand side of this equation is nonsingular and yields a unique solution U_e. For the resonant terms this does not work, because the relevant matrix ($T(p_c^2, q_c^2, \omega)$ if $k = 1$) is singular. To handle the resonant terms, one supplements

the procedure by evolution equations for the A_j as described in Section 2.2, with initially undetermined coefficients, up to the same order as the terms that are kept in the resonant harmonics, and replaces A_{jt} by the right hand sides of these evolution equations. In this way undetermined coefficients c_e are introduced, and the equations for the coefficient vectors get the form (for $k = 1$)

$$T(p_c^2, q_c^2, \omega)U_e = V_e + c_e U_0.$$

As for the linear problem, this fixes the coefficients c_e in the evolution equations for the envelopes by projecting with U_0^*, and yields unique coefficient vectors U_e recursively at each order that is taken into account.

The resonant terms needed in the expansion of u up to a prescribed order are the same as the terms kept in the equations for the A_j. We expand the equation for A_1 as

$$\begin{aligned} A_{1t} \;=\; & (v_p + b_{1p}\mu)A_{1x} + (v_q + b_{1q}\mu)A_{1y} + d_{pp}A_{1xx} + 2d_{pq}A_{1xy} + d_{qq}A_{1yy} \\ & + \big(a_0\mu + a_1\mu^2 + e_1|A_1|^2 + e_2|A_2|^2 + e_3|A_3|^2 + e_4|A_4|^2\big)A_1 + e_5 A_2\overline{A}_3 A_4 \\ & + HOT, \end{aligned} \tag{3.8}$$

i.e., the expansion is carried out up to third order (one order higher in the linear terms than in Section 2.2). The linear terms in this expansion do not involve non-resonant terms, and coincide with the expansion terms of the critical eigenvalue. Nonlinear non-resonant terms are created from the leading terms in u by the nonlinear terms in f. For example, the term $|A_1|^2 A_1$ is created through

$$\mathcal{C}(A_1U_0E_1, A_1U_0E_1, \overline{A}_1\overline{U}_0\overline{E}_1) = |A_1|^2 A_1 \mathcal{C}(U_0, U_0, \overline{U}_0)E_1,$$

as well as from

$$\begin{aligned} \mathcal{B}(A_1U_0E_1, |A_1|^2U_7) &= |A_1|^2 A_1 \mathcal{B}(U_0, U_7)E_1, \\ \mathcal{B}(\overline{A}_1\overline{U}_0\overline{E}_1, A_1^2U_6E_1^2) &= |A_1|^2 A_1 \mathcal{B}(\overline{U}_0, U_6)E_1, \end{aligned}$$

which requires the determination of the vectors U_7 and U_6 (notation from Appendix A.1) associated with $|A_1|^2$ and A_1^2 in the non-resonant $T(0,0,0)$ and $T(4p_c^2, 4q_c^2, 2\omega)$ Fourier terms, respectively. In turn, the terms $|A_1|^2$ and A_1^2 in these Fourier terms are created from the leading terms by pairing $A_1E_1U_0$ with $\overline{A}_1\overline{E}_1\overline{U}_0$ and $A_1E_1U_0$ in $\mathcal{B}$, respectively, thus U_7 and U_6 are the unique solutions of

$$\begin{aligned} T(0,0,0)U_7 &= -2\mathcal{B}(U_0, \overline{U}_0), \\ T(4p_c^2, 4q_c^2, 2\omega)U_6 &= -\mathcal{B}(U_0, U_0). \end{aligned}$$

The resulting resonant term in u is $|A_1|^2A_1U_8E_1$, where U_8 satisfies $T(p_c^2, q_c^2, \omega)U_8 = V_8 + e_1U_0$, with

$$V_8 = -2\mathcal{B}(U_0, U_7) - 2\mathcal{B}(\overline{U}_0, U_6) - 3\mathcal{C}(U_0, U_0, \overline{U}_0),$$

which determines e_1 and U_8. The other cubic resonant terms follow similarly, the details are summarized in Appendix A.1.

The non-resonant terms needed to determine all cubic resonant terms involve products $A_jA_kE_jE_k$, $A_j\overline{A}_kE_j\overline{E}_k$ and their complex conjugates, which arise in the Fourier terms with labels $m, n, k = 0$ or ± 2. Several of these vectors are related by symmetries, reducing the total number of vectors at second (non-resonant) orders to seven (vectors U_6, U_7, W_{11}, W_{1j}, W_{j1}, $j = 2, 3$ in Appendix A.1). The resonant expansion vectors associated with the coefficients $e_1, \ldots, e_5$ are denoted by $U_8, \ldots, U_{12}$ in Appendix A.1.

3.3 Boundary Layer Expansion

Near the edge $y = -L_q/2$, the solution of (3.1)-(3.4) cannot be represented by envelopes varying slowly in y. We set $\tilde{y} = y + L_q/2$ and consider the problem

$$u_t = D_p u_{xx} + D_q u_{\tilde{y}\tilde{y}} + f(u, \mu), \tag{3.9}$$

$$C_q u - E_q u_{\tilde{y}} = 0 \text{ at } \tilde{y} = 0, \tag{3.10}$$

$$u \to u_{\text{bulk}} \text{ for } \tilde{y} \to \infty, \tag{3.11}$$

where u_{bulk} is the bulk solution, and the approach in (3.11) is on an exponential rate. The starting point is again the solution of the linearized problem for $\mu = 0$, for which we seek a solution in the form

$$\mathcal{U}^0_\pm(x, \tilde{y}, t) = \mathcal{U}^0(\tilde{y}) e^{\pm i p_c x} e^{i\omega t} + cc,$$

that satisfies (3.10) and (3.11). Substituting this into the linearized equation of (3.9) yields

$$D_q \mathcal{U}^0_{\tilde{y}\tilde{y}} + (-p_c^2 D_p + F_1 - i\omega I)\mathcal{U}^0 = 0. \tag{3.12}$$

This equation has the fundamental solutions $U_0 e^{\pm i q_c \tilde{y}}$ and $2(N-1)$ solutions of the form $V^k_\pm(\tilde{y}) = W^k_\pm(\tilde{y}) e^{\pm \lambda_k \tilde{y}}$, $2 \le k \le N$, where $\text{Re}\lambda_k > 0$ and the $W^k_\pm(\tilde{y})$ increase at most algebraically as $\tilde{y} \to \infty$ (generically they are constant). The λ_k are the $N-1$ remaining roots of the characteristic equation,

$$\det\left[\lambda^2 D_q - p_c^2 D_p + F_1 - i\omega I\right] = 0,$$

and $\lambda_1^2 = -q_c^2$. The superposition

$$\mathcal{U}^0(\tilde{y}) = U_0(e^{i q_c \tilde{y}} + r_q e^{-i q_c \tilde{y}}) + \sum_{k=2}^{N} \alpha_k V^k_-(\tilde{y}) \tag{3.13}$$

takes the form of the basic waves when $\tilde{y} \to \infty$, and substitution into (3.10) gives a non-homogeneous system of N linear equations for $(r_q, \alpha_2, \ldots, \alpha_N)$, which we assume to have a unique solution with $r_q \neq 0$. The coefficient r_q plays the role of a reflection coefficient.

The solutions $\mathcal{U}^0_\pm$ are then extended to solutions of the nonlinear problem (3.9)-(3.11) through a weakly nonlinear analysis in a similar manner as the bulk solution was derived, except that the $\tilde{y}$-dependence is solved exactly. The solution is sought in the form of a modulated Fourier series,

$$u = \sum_{m,k} \mathcal{U}^{(m,k)}(x, t, \mu; \tilde{y}) e^{i(m p_c x + k\omega t)},$$

with small coefficient functions $\mathcal{U}^{(m,k)}$ that vary slowly in (x,t) and are power series in μ. The leading terms are modulations in (x,t) of the 'edge waves' $\mathcal{U}^0_\pm$,

$$u = \Big(M(x,t)\mathcal{U}^0(\tilde{y})e^{ip_c x} + N(x,t)\mathcal{U}^0(\tilde{y})e^{-ip_c x}\Big)e^{i\omega t} + cc + HOT, \tag{3.14}$$

where $M(x,t)$ and $N(x,t)$ are again small and slowly varying envelopes. Each Fourier coefficient is expanded in a formal power series in $(\partial_t, \partial_x, M, N, \overline{M}, \overline{N}, \mu)$ with $\tilde{y}$-dependent coefficients taking care of the boundary conditions at $\tilde{y} = 0$. This leads to a hierarchy of nonhomogeneous boundary value problems for the expansion functions $\mathcal{U}^{(e)}(\tilde{y})$ of the form

$$\begin{aligned} D_q\mathcal{U}^{(e)}_{\tilde{y}\tilde{y}} - \big(m^2p_c^2D_p + ik\omega I\big)\mathcal{U}^{(e)} &= \mathcal{V}^{(e)}, \\ C_q\mathcal{U}^{(e)} - E_q\mathcal{U}^{(e)}_{\tilde{y}} &= 0 \text{ at } \tilde{y} = 0, \end{aligned}$$

and $\mathcal{U}^{(e)}(\tilde{y})$ has to remain bounded when $\tilde{y} \to \infty$. For matching purposes only the asymptotic behavior of these functions for $\tilde{y} \to \infty$ is needed. The details are summarized in Appendix A.2. The expansion at $y = L_q/2$ is found by applying the reflection $y \to -y$. The solutions near the edges $x = \pm L_p/2$ are obtained in the same manner as the solutions near $y = \pm L_q/2$, and lead to another reflection coefficient r_p.

3.4 Matching Boundary Layer Solutions and Bulk Solution

The boundary conditions for the bulk-envelopes $A_1, \ldots, A_4$ follow from matching the bulk solution to the boundary layer solutions. Considering again the edge $y = -L_q/2$, the variable $\tilde{y} = y + L_q/2$ is treated as $\mathcal{O}(1)$-variable in the boundary layer. For the matching, we consider the limit $1 \ll \tilde{y} \ll s$, where $s \gg 1$ is the space scale in the bulk such that $s|A_{jy}| = \mathcal{O}(|A_j|)$. In this limit, the leading terms in the bulk solution can be expanded as

$$\begin{aligned} u &= \Big\{\big[(A_{10} + A_{1y0}\tilde{y})e^{i(p_cx+q_c\tilde{y})} + (A_{20} + A_{2y0}\tilde{y})e^{i(-p_cx+q_c\tilde{y})}\big]e^{-iq_cL_q/2} \\ &\quad \big[(A_{30} + A_{3y0}\tilde{y})e^{i(-p_cx-q_c\tilde{y})} + (A_{40} + A_{4y0}\tilde{y})e^{i(p_cx-q_c\tilde{y})}\big]e^{iq_cL_q/2}\Big\}U_0e^{i\omega t} + cc + HOT, \end{aligned}$$

where $A_{j0}(x,t) = A_j(x,-L_q/2,t)$, $A_{jy0}(x,t) = A_{jy}(x,-L_q/2,t)$, and in the higher order terms the A_j and their derivatives are evaluated at $(x,-L_q/2,t)$. Comparing the resulting bulk expansion and the boundary layer expansion from Appendices A.1 and A.2, and requiring that they coincide up to the orders taken into account, leads to eight matching conditions relating the A_{j0} and A_{jy0} to expressions involving the boundary envelopes M, N and their derivatives, which are summarized in Appendix A.3. Eliminating the (M,N)-terms from these matching conditions gives the following four boundary conditions for the A_j at $y = -L_q/2$,

$$e^{iq_cL_q}A_4 = r_qA_1 + HOT, \tag{3.15}$$

$$v_q(e^{iq_cL_q}A_{4y} + r_qA_{1y}) = r_q(|r_q|^2-1)[(e_1-e_4)|A_1|^2 + (e_2-e_3-e_5)|A_2|^2]A_1 + HOT, \tag{3.16}$$

$$e^{iq_cL_q}A_3 = r_qA_2 + HOT, \tag{3.17}$$

$$v_q(e^{iq_cL_q}A_{3y} + r_qA_{2y}) = r_q(|r_q|^2-1)[(e_1-e_4)|A_2|^2 + (e_2-e_3-e_5)|A_1|^2]A_2 + HOT. \tag{3.18}$$

With these boundary conditions, the matching conditions also provide evolution equations for the edge-envelopes $M(x,t)$, $N(x,t)$. Boundary conditions for M, N at $x = \pm L_p/2$ may be found by matching the edge solution to a corner solution valid in some neighborhood of the corners $(x,y) = (\pm L_p/2, -L_q/2)$, but we don't pursue this since our main interest in this paper is the equations for the bulk-envelopes.

A similar matching procedure leads to the following boundary conditions at $x = -L_p/2$,

$$e^{ip_cL_p}A_2 = r_pA_1 + HOT, \tag{3.19}$$

$$v_p(e^{ip_cL_p}A_{2x} + r_pA_{1x}) = r_p(|r_p|^2-1)[(e_1-e_2)|A_1|^2 + (e_4-e_3-e_5)|A_4|^2]A_1 + HOT, \tag{3.20}$$

$$e^{ip_cL_p}A_3 = r_pA_4 + HOT, \tag{3.21}$$

$$v_p(e^{ip_cL_p}A_{3x} + r_pA_{4x}) = r_p(|r_p|^2-1)[(e_1-e_2)|A_4|^2 + (e_4-e_3-e_5)|A_1|^2]A_4 + HOT.$$

(3.22)

which involves the second reflection coefficient r_p. Note that at the $-L_p/2$ boundary the e_4 and e_2 exchange places when compared to the $-L_q/2$ boundary. The boundary conditions at the other two edges follow from (3.15)-(3.18) and (3.19)-(3.22) via reflection $y \to -y$ and $x \to -x$.

3.5 Rescaled Coefficients

We first apply some transformations to the envelopes A_j that simplify the coefficients in (3.8). The transformation $A_j = A'_j e^{i(a_{0i}\mu + a_{1i}\mu^2)t}$ removes the imaginary parts of a_0 and a_1. We then rescale t, x, y (and accordingly L_p, L_q), μ and the A'_j according to

$$t = \frac{d_{ppr}}{v_p^2} t', \quad x = \frac{d_{ppr}}{v_p} x', \quad y = \frac{\sqrt{d_{ppr} d_{qqr}}}{v_p} y', \quad \mu = \frac{v_p^2}{a_{0r} d_{ppr}} \mu', \quad A'_j = \frac{v_p}{\sqrt{|e_{1r}| d_{ppr}}} A''_j.$$

Denoting the coefficients in the resulting transformed equation for A''_1 by primes, these coefficients are related to the original coefficients by

$$\begin{gathered} v'_p = 1, \quad v'_q = \sqrt{\tfrac{d_{ppr}}{d_{qqr}}} \tfrac{v_q}{v_p}, \quad d'_{pp} = \tfrac{d_{pp}}{d_{ppr}}, \quad d'_{qq} = \tfrac{d_{qq}}{d_{qqr}}, \quad d'_{pq} = \tfrac{d_{pq}}{\sqrt{d_{ppr} d_{qqr}}}, \\ b'_{1p} = \tfrac{v_p b_{1p}}{a_{0r} d_{ppr}}, \quad b'_{1q} = \tfrac{v_p b_{1q}}{a_{0r} \sqrt{d_{ppr} d_{qqr}}}, \quad a'_0 = 1, \quad a'_1 = \tfrac{v_p^2 a_{1r}}{a_{0r}^2 d_{ppr}}, \quad e'_j = \tfrac{e_j}{|e_{1r}|}. \end{gathered}$$

Omitting the primes, we then rewrite the equation for A_1 as

$$\begin{aligned} A_{1t} \;=\; & (1 + b_{1p}\mu) A_{1x} + (v_r + b_{1q}\mu) A_{1y} + d_{pp} A_{1xx} + 2 d_{pq} A_{1xy} + d + d_{qq} A_{1yy} \\ & + \big(\mu + a_1 \mu^2 + \sum_{j=1}^{4} e_j |A_j|^2\big) A_1 + e_5 A_2 \overline{A}_3 A_4, \end{aligned} \tag{3.23}$$

where $d_{ppr} = d_{qqr} = 1$, $e_{1r} = -1$ (assuming the supercriticality condition $e_{1r} < 0$ before the rescaling), and $v_r, a_1 \in \mathbb{R}$ ($v_r = v'_q$). Using polar forms for the reflection coefficients,

$$r_q e^{-i q_c L_q} = \rho_q e^{i\alpha_q}, \quad r_p e^{-i p_c L_p} = \rho_p e^{i\alpha_p},$$

the boundary conditions at $y = -L_q/2$ are written in the form

$$A_4 = \rho_q e^{i\alpha_q} A_1 + HOT, \tag{3.24}$$

$$v_r(A_{4y} + \rho_q e^{i\alpha_q} A_{1y}) = \rho_q e^{i\alpha_q}(\rho_q^2 - 1)[(e_1 - e_4)|A_1|^2 + (e_2 - e_3 - e_5)|A_2|^2]A_1 + HOT, \tag{3.25}$$

$$A_3 = \rho_q e^{i\alpha_q} A_2 + HOT, \tag{3.26}$$

$$v_r(A_{3y} + \rho_q e^{i\alpha_q} A_{2y}) = \rho_q e^{i\alpha_q}(\rho_q^2 - 1)[(e_1 - e_4)|A_2|^2 + (e_2 - e_3 - e_5)|A_1|^2]A_2 + HOT. \tag{3.27}$$

3.6 Slow Variables and $\mathcal{O}(1)$-Amplitudes

We consider the case where L_p and L_q are large and of the same order, and write $L_q = lL_p$, with the aspect ratio $l = L_q/L_p$ of the rectangle of order one. The boundary conditions shift the instability threshold to a nonzero value

$$\mu_c = -L_p^{-1} \log(\rho_q^{lv_r} \rho_p) + \mathcal{O}(L_p^{-2} + (L_p L_q)^{-1} + L_q^{-2}), \tag{3.28}$$

that is, the trivial solution $A_j = 0$ becomes unstable for $\mu > \mu_c > 0$ when $\rho_q^{lv_r} \rho_p < 1$. We introduce a small parameter ϵ, an $\mathcal{O}(1)$-control parameter λ so that the instability occurs at $\lambda = 0$, and slow space and time variables (ξ, η, T) by setting

$$\epsilon = L_p^{-1}, \quad \rho = \rho_q^{lv_r} \rho_p, \quad \mu = -\epsilon \log(\rho) + \epsilon^2(\lambda + b), \quad (\xi, \eta, T) = \epsilon(x, ly, t).$$

In the slow space variables (ξ, η), the rectangle is rescaled to the square $-1/2 \le \xi, \eta \le 1/2$. The variables (ξ, η, T) are considered as new variables for the envelopes. The derivatives then scale with ϵ, $\partial_t = \epsilon \partial_T$, $\partial_x = \epsilon \partial_\xi$ and $\partial_y = l\epsilon \partial_\eta$.

We next express the A_j in terms of $\mathcal{O}(1)$-amplitudes Y_j,

$$A_1 = \epsilon \rho_p^{\xi + 1/2} \rho_q^{\eta + 1/2} Y_1 \exp\big[i\alpha_p(\xi + T + 1/2) + i\alpha_q(\eta + v_r T + 1/2) + i\epsilon a T\big], \tag{3.29}$$

$$A_2 = \epsilon \rho_p^{-\xi+\frac{1}{2}} \rho_q^{\eta+1/2} Y_2 \exp\big[i\alpha_p(-\xi + T + 1/2) + i\alpha_q(\eta + v_r T + 1/2) + i\epsilon a T\big], \quad (3.30)$$

$$A_3 = \epsilon \rho_p^{-\xi+\frac{1}{2}} \rho_q^{-\eta+1/2} Y_3 \exp\big[i\alpha_p(-\xi + T + 1/2) + i\alpha_q(-\eta + v_r T + 1/2) + i\epsilon a T\big], \quad (3.31)$$

$$A_4 = \epsilon \rho_p^{\xi+1/2} \rho_q^{-\eta+1/2} Y_4 \exp\big[i\alpha_p(\xi + T + \frac{1}{2}) + i\alpha_q(-\eta + v_r T + 1/2) + i\epsilon a T\big], \quad (3.32)$$

where the parameters a and b are chosen so that the extra Y_j terms introduced when taking derivatives of the A_j are eliminated,

$$\begin{aligned} -b + ia \;=\; & -\log(\rho) b_{1p} (\log(\rho_p) + i\alpha_p) - l \log(\rho) b_{1q} (\log(\rho_q) + i\alpha_q) + d_{pp} (\log(\rho_p) + i\alpha_p)^2 \\ & + l^2 (\log(\rho_q) + i\alpha_q)^2 + 2l d_{pq} (\log(\rho_p) + i\alpha_p)(\log(\rho_q) + i\alpha_q). \end{aligned} \quad (3.33)$$

The evolution equation for Y_1 in the interior of the square, $-1/2 < \xi, \eta < 1/2$, follows from (3.23) as

$$\begin{aligned} Y_{1T} \;=\; & (1 + \epsilon b''_{1p}) Y_{1\xi} + l(v_r + \epsilon b''_{1q}) Y_{1\eta} + \epsilon d_{pp} Y_{1\xi\xi} + l^2 \epsilon d_{qq} Y_{1\eta\eta} + 2l\epsilon d_{pq} Y_{1\xi\eta} \\ & + \epsilon[\lambda + e_1 \rho_p^{2\xi+1} \rho_q^{2\eta+1} |Y_1|^2 + e_2 \rho_p^{-2\xi+1} \rho_q^{2\eta+1} |Y_2|^2 \\ & \quad + e_3 \rho_p^{-2\xi+1} \rho_q^{-2\eta+1} |Y_3|^2 + e_4 \rho_p^{2\xi+1} \rho_q^{-2\eta+1} |Y_4|^2] Y_1 \\ & + \epsilon e_5 \rho_p^{-2\xi+1} \rho_q^{-2\eta+1} Y_2 \overline{Y_3} Y_4 + \mathcal{O}(\epsilon^2), \end{aligned} \quad (3.34)$$

where b''_{1p} and b''_{1q} are given by

$$b''_{1p} = -\log(\rho) b_{1p} + 2 d_{pp} (\log(\rho_p) + i\alpha_p) + 2 l d_{pq} (\log(\rho_q) + i\alpha_q), \quad (3.35)$$

$$b''_{1q} = -l \log(\rho) b_{1q} + 2 l^2 d_{pp} (\log(\rho_q) + i\alpha_q) + 2 l d_{pq} (\log(\rho_p) + i\alpha_p). \quad (3.36)$$

Note that when $\rho_p = \rho_q = 1$ and $\alpha_p = \alpha_q = 0$ we have $b''_{1p} = b''_{1q} = 0$. The equations for Y_2, Y_3, Y_4 are obtained by applying the reflections

$$\begin{aligned} (\xi, \eta, Y_1, Y_2, Y_3, Y_4) \;&\to\; (-\xi, \eta, Y_2, Y_1, Y_4, Y_3), \\ (\xi, \eta, Y_1, Y_2, Y_3, Y_4) \;&\to\; (-\xi, -\eta, Y_3, Y_4, Y_1, Y_2), \end{aligned} \quad (3.37)$$

$$(\xi, \eta, Y_1, Y_2, Y_3, Y_4) \quad \rightarrow \quad (-\xi, \eta, Y_4, Y_3, Y_2, Y_1).$$

to (3.34). The boundary conditions at $\eta = \mp 1/2$ follow from (3.24)-(3.27) as

$$Y_4 \;=\; Y_1 + \mathcal{O}(\epsilon^2), \tag{3.38}$$

$$Y_3 \;=\; Y_2 + \mathcal{O}(\epsilon^2), \tag{3.39}$$

$$lv_r(Y_{4\eta} + Y_{1\eta}) \;=\; \pm\epsilon\rho_p(\rho_q^2 - 1)[(e_1 - e_4))\rho_p^{2\xi}|Y_1|^2 + (e_2 - e_3 - e_5)\rho_p^{-2\xi}|Y_2|^2]Y_1 + \mathcal{O}(\epsilon^2), \tag{3.40}$$

$$lv_r(Y_{3\eta} + Y_{2\eta}) \;=\; \pm\epsilon\rho_p(\rho_q^2 - 1)[(e_1 - e_4))\rho_p^{-2\xi}|Y_2|^2 + (e_2 - e_3 - e_5)\rho_p^{2\xi}|Y_1|^2]Y_2 + \mathcal{O}(\epsilon^2), \tag{3.41}$$

and analogously we find the following boundary conditions at $\xi = \mp 1/2$,

$$Y_2 = Y_1 + \mathcal{O}(\epsilon^2), \tag{3.42}$$

$$Y_3 = Y_4 + \mathcal{O}(\epsilon^2), \tag{3.43}$$

$$Y_{2\xi} + Y_{1\xi} = \pm\epsilon\rho_q(\rho_p^2 - 1)[(e_1 - e_2)\rho_q^{2\eta}|Y_1|^2 + (e_4 - e_3 - e_5)\rho_q^{-2\eta}|Y_4|^2]Y_1 + \mathcal{O}(\epsilon^2), \tag{3.44}$$

$$Y_{3\xi} + Y_{4\xi} = \pm\epsilon\rho_q(\rho_p^2 - 1)[(e_1 - e_2)\rho_q^{-2\eta}|Y_4|^2 + (e_4 - e_3 - e_5)\rho_p^{2\xi}|Y_1|^2]Y_4 + \mathcal{O}(\epsilon^2). \tag{3.45}$$

We now expand the amplitudes Y_j in powers of ϵ and introduce a 'super-slow' time scale τ,

$$Y_j(\xi, \eta, T, \tau) = Y_{j0}(\xi, \eta, T, \tau) + \epsilon Y_{j1}(\xi, \eta, T, \tau), \quad \tau = \epsilon T, \tag{3.46}$$

and expand the evolution equations for the Y_j and the boundary conditions up to $\mathcal{O}(\epsilon)$. At $\mathcal{O}(1)$ equation (3.34) reduces to the first order wave equation,

$$Y_{10T} - Y_{10\xi} - lv_r Y_{10\eta} = 0, \tag{3.47}$$

and at $\mathcal{O}(\epsilon)$ we find

$$\begin{aligned} Y_{11T} - Y_{11\xi} - lv_r Y_{11\eta} \;=\; & -Y_{10\tau} + b''_{1p} Y_{10\xi} + lb''_{1q} Y_{10\eta} + d_{pp} Y_{10\xi\xi} + l^2 d_{qq} Y_{10\eta\eta} + 2l d_{pq} Y_{10\xi\eta} \\ & + [\lambda + e_1 \rho_p^{2\xi+1} \rho_q^{2\eta+1} |Y_{10}|^2 + e_2 \rho_p^{-2\xi+1} \rho_q^{2\eta+1} |Y_{20}|^2 \\ & \quad + e_3 \rho_p^{-2\xi+1} \rho_q^{-2\eta+1} |Y_{30}|^2 + e_4 \rho_p^{2\xi+1} \rho_q^{-2\eta+1} |Y_{40}|^2] Y_{10} \\ & + e_5 \rho_p^{-2\xi+1} \rho_q^{-2\eta+1} Y_{20} \overline{Y_{30}} Y_{40}. \end{aligned} \tag{3.48}$$

The equations for Y_{j0} and Y_{j1} for $j = 2, 3, 4$ are obtained by applying the operations (3.37) to (3.48). These equations are valid in the interior of the square $-1/2 < \xi, \eta < 1/2$. Substituting (3.46) into (3.38)-(3.41) and (3.42)-(3.45) leads to the following boundary conditions

$$Y_{10} - Y_{40} = Y_{20} - Y_{30} = 0 = Y_{11} - Y_{41} = Y_{21} - Y_{31}, \tag{3.49}$$

$$Y_{10\eta} + Y_{40\eta} = Y_{20\eta} + Y_{30\eta} = 0, \tag{3.50}$$

$$lv_r(Y_{11\eta} + Y_{41\eta}) = \mp \rho_p(\rho_q^2 - 1)[(e_1 - e_4))\rho_p^{2\xi} |Y_{10}|^2 + (e_2 - e_3 - e_5)\rho_p^{-2\xi} |Y_{20}|^2] Y_{10}, \tag{3.51}$$

$$lv_r(Y_{21\eta} + Y_{31\eta}) = \mp \rho_p(\rho_q^2 - 1)[(e_1 - e_4))\rho_p^{-2\xi} |Y_{20}|^2 + (e_2 - e_3 - e_5)\rho_p^{2\xi} |Y_{30}|^2] Y_{20}, \tag{3.52}$$

at $\eta = \pm 1/2$, and

$$Y_{10} - Y_{20} = Y_{40} - Y_{30} = 0 = Y_{11} - Y_{21} = Y_{41} - Y_{31}, \tag{3.53}$$

$$Y_{10\xi} + Y_{20\xi} = Y_{40\xi} + Y_{30\xi} = 0, \tag{3.54}$$

$$Y_{11\xi} + Y_{21\xi} \;=\; \mp \rho_p(\rho_q^2 - 1)[(e_1 - e_2)\rho_p^{2\xi} |Y_{10}|^2 + (e_4 - e_3 - e_5)\rho_p^{-2\xi} |Y_{40}|^2] Y_{10}, \tag{3.55}$$

$$Y_{31\xi} + Y_{41\xi} \;=\; \mp \rho_p(\rho_q^2 - 1)[(e_1 - e_2)\rho_p^{-2\xi} |Y_{40}|^2 + (e_4 - e_3 - e_5)\rho_p^{2\xi} |Y_{10}|^2] Y_{40}, \tag{3.56}$$

at $\xi = \pm 1/2$.

Since the functions Y_{j0} satisfy homogeneous first order wave equations with respect to the $\mathcal{O}(\epsilon)$-variables (ξ, η, T), they depend on these variables through characteristic wave variables

$$X_\pm = T \pm \xi, ; \quad Y_\pm = T \pm \frac{\eta}{l v_r}, \tag{3.57}$$

as

$$\begin{aligned} Y_{10}(\xi, \eta, T, \tau) &= Z_{10}(X_+, Y_+, \tau), \\ Y_{20}(\xi, \eta, T, \tau) &= Z_{20}(X_-, Y_+, \tau), \\ Y_{30}(\xi, \eta, T, \tau) &= Z_{30}(X_-, Y_-, \tau), \\ Y_{40}(\xi, \eta, T, \tau) &= Z_{40}(X_+, Y_-, \tau). \end{aligned} \tag{3.58}$$

This can be used to rewrite (3.48) in the form

$$\begin{aligned} \mathcal{D}Y_{11} \;=\; & -Z_{10\tau} + b''_{1p} Z_{10X_+} + v_r^{-1} b''_{1q} Z_{10Y_+} + d_{pp} Z_{10X_+X_+} + v_r^{-2} d_{qq} Z_{10Y_+Y_+} \\ & + 2 v_r^{-1} d_{pq} Z_{10X_+Y_+} \\ & + [\lambda + e_1 \rho_p^{2\xi+1} \rho_q^{2\eta+1} |Z_{10}(X_+, Y_+, \tau)|^2 + e_2 \rho_p^{-2\xi+1} \rho_q^{2\eta+1} |Z_{20}(X_-, Y_+, \tau)|^2 \\ & \quad + e_3 \rho_p^{-2\xi+1} \rho_q^{-2\eta+1} |Z_{30}(X_-, Y_-, \tau)|^2 + e_4 \rho_p^{2\xi+1} \rho_q^{-2\eta+1} |Z_{40}(X_+, Y_-, \tau)|^2] Z_{10} \\ & + e_5 \rho_p^{-2\xi+1} \rho_q^{-2\eta+1} Z_{20}(X_-, Y_+, \tau) \overline{Z}_{30}(X_-, Y_-, \tau) Z_{40}(X_+, Y_-, \tau), \end{aligned} \tag{3.59}$$

where $\mathcal{D}$ is the first order wave operator

$$\mathcal{D} = \partial_T - \partial_\xi - l v_r \partial_\eta.$$

An important consequence of the boundary conditions is that the leading order envelopes are no longer independent. The boundary conditions (3.49) and (3.50) imply the relations

$$Z_{10}(X_+, Y_+, \tau) = Z_{20}(X_+ + 1, Y_+, \tau) = Z_{10}(X_+ + 2, Y_+, \tau), \tag{3.60}$$

$$Z_{40}(X_+, Y_-, \tau) = Z_{30}(X_+ + 1, Y_-, \tau) = Z_{40}(X_+ + 2, Y_-, \tau), \tag{3.61}$$

and from (3.53) and (3.54) it follows that

$$Z_{10}(X_+, Y, \tau) = Z_{40}(X_+, Y + 1/(lv_r), \tau) = Z_{10}(X_+, Y + 2/(lv_r), \tau), \tag{3.62}$$

$$Z_{20}(X_-, Y, \tau) = Z_{30}(X_-, Y + 1/(lv_r), \tau) = Z_{20}(X_-, Y + 2/(lv_r), \tau). \tag{3.63}$$

We conclude that the leading order envelopes Z_{j0} are periodic of period 2 in the X-variable, and of period $2/(lv_r)$ in the Y-variable. Moreover, they are related to each other by shifts of half a period in one or both of these variables.

3.7 Application of a Reflection Principle

The continuity of the boundary conditions enables us to apply a reflection principle to extend the four coupled equations over $-1/2 \le \xi, \eta \le 1/2$ to a single equation valid in $-\infty \le \xi, \eta \le \infty$. This is done by first reflecting at the boundaries,

$$\begin{aligned}
w_j(\xi,\eta,T,\tau) &= Y_{1j}(\xi,\eta,T,\tau) && \text{if} \quad -1/2 \le \xi \le 1/2, && -1/2 \le \eta \le 1/2,\\
w_j(\xi,\eta,T,\tau) &= Y_{2j}(-1-\xi,\eta,T,\tau) && \text{if} \quad -3/2 \le \xi \le -1/2, && -1/2 \le \eta \le 1/2,\\
w_j(\xi,\eta,T,\tau) &= Y_{3j}(-1-\xi,-1-\eta,T,\tau) && \text{if} \quad -3/2 \le \xi \le -1/2, && -3/2 \le \eta \le -1/2,\\
w_j(\xi,\eta,T,\tau) &= Y_{4j}(\xi,-1-\eta,T,\tau) && \text{if} \quad -1/2 \le \xi \le 1/2, && -3/2 \le \eta \le -1/2,
\end{aligned} \tag{3.64}$$

and then extending periodically over $\mathbb{R}^2$,

$$w_j(\xi+2,\eta,T,\tau) = w_j(\xi,\eta+2,T,\tau) = w_j(\xi+2,\eta+2,T,\tau) = w_j(\xi,\eta,T,\tau). \tag{3.65}$$

In this way the four equations for Y_{j0} and for Y_{j1} combine to single equations for the periodic functions w_0 and w_1. With the wave operator $\mathcal{D}$, these equations can be written as

$$\mathcal{D}w_0 = 0, \tag{3.66}$$

$$\mathcal{D}w_1 \;=\; -w_{0\tau} + b''_{1p}w_{0\xi} + lb''_{1q}w_{0\eta} + d_{pp}w_{0\xi\xi} + l^2 d_{qq}w_{0\eta\eta} + 2ld_{pq}w_{0\xi\eta}$$

$$
\begin{aligned}
&+[\lambda + e_1\phi(\xi,\eta)|w_0(\xi,\eta,T,\tau)|^2 + e_2\phi(-\xi,\eta)|w_0(-1-\xi,\eta,T,\tau)|^2 \\
&\quad + e_3\phi(-\xi,-\eta)|w_0(-1-\xi,-1-\eta,T,\tau)|^2 \\
&\quad + e_4\phi(\xi,-\eta)|w_0(\xi,-1-\eta,T,\tau)|^2]w_0 \\
&+e_5\phi(-\xi,-\eta)w_0(-1-\xi,\eta,T,\tau)\overline{w_0}(-1-\xi,-1-\eta,T,\tau)w_0(\xi,-1-\eta,T,\tau),
\end{aligned}
\tag{3.67}
$$

where $\phi(\xi,\eta)$ is given by

$$
\phi(\xi,\eta) = \rho_p^{2\xi+1}\rho_q^{2\eta+1} \ \text{ in } \ -1/2 \le \xi,\eta \le 1/2,
$$

and extended periodically with periods 1 in ξ and η over $\mathbb{R}^2$.

The equation (3.66) implies that w_0 depends on (ξ,η,T) through the wave variables $X \equiv X_+$ and $Y \equiv Y_+$. Thus we write

$$
\begin{aligned}
w_0(\xi,\eta,T,\tau) &= W(X,Y,\tau), \\
w_1(\xi,\eta,T,\tau) &= W_1(X,Y,T,\tau).
\end{aligned}
\tag{3.68}
$$

The function W is periodic in X and Y with periods 2 and $2P$, respectively, where $P = 1/(lv_r)$. The equation for W_1 follows from (3.67) and is given by

$$
\begin{aligned}
W_{1T} \ = \ & -W_\tau + b_{1p}''W_X + v_r^{-1}b_{1q}''W_Y + d_{pp}W_{XX} + v_r^{-2}d_{qq}W_{YY} + 2v_r^{-1}d_{pq}W_{XY} \\
&+\big[\lambda + e_1\phi(\xi,\eta)|W(X,Y,\tau)|^2 \\
&\quad + e_2\phi(-\xi,\eta)|W(2T-X-1,Y,\tau)|^2 \\
&\quad + e_3\phi(-\xi,-\eta)|W(2T-X-1,2T-Y-P,\tau)|^2 \\
&\quad + e_4\phi(\xi,-\eta)|W(X,2T-Y-P,\tau)|^2\big]W \\
&+e_5\phi(-\xi,-\eta)W(2T-X-1,Y,\tau) \\
&\quad \times \overline{W}(2T-X-1,2T-Y-P,\tau)W(X,2T-Y-P,\tau),
\end{aligned}
\tag{3.69}
$$

where in the periodic function ϕ, ξ and η are replaced by $\xi = X - T$ and $\eta = (Y-T)/P$.

In order that this equation admits a bounded solution as $T \to \infty$, the average with respect to T must vanish. This condition leads to the following evolution equation for W,

$$\begin{aligned} W_\tau \;=\; & b''_{1p} W_X + v_r^{-1} b''_{1q} W_Y + d_{pp} W_{XX} + v_r^{-2} d_{qq} W_{YY} + 2 v_r^{-1} d_{pq} W_{XY} \\ & + \big[\lambda + e_1 < \phi(\xi,\eta) > |W(X,Y,\tau)|^2 \\ & \quad + e_2 < \phi(-\xi,\eta) |W(2T - X - 1, Y, \tau)|^2 > \\ & \quad + e_3 < \phi(-\xi,-\eta) |W(2T - X - 1, 2T - Y - P, \tau)|^2 > \\ & \quad + e_4 < \phi(\xi,-\eta) |W(X, 2T - Y - P, \tau)|^2 > \big] W \\ & + e_5 < \phi(-\xi,-\eta) W(2T - X - 1, Y, \tau) \\ & \quad \times \overline{W}(2T - X - 1, 2T - Y - P, \tau) W(X, 2T - Y - P, \tau) >, \end{aligned} \tag{3.70}$$

with $\xi = X - T$ and $\eta = (Y - T)/P$ substituted in ϕ. In (3.70), the brackets denote an average over T,

$$< f(T) > = \lim_{T \to \infty} \frac{1}{T} \int_0^T f(T')\, dT'.$$

This equation, and the more explicit versions given below, are the main theoretical result of this thesis.

Equation (3.70) is a nonlinear evolution equation for W with four global coupling terms in the form of T-averages. These averages can be understood as follows. In the 'short' time scale, when $T = \epsilon t \sim 1$, the four wave-trains exhibit only linear propagation and reflections at the walls. The propagation velocity is large (of the order ϵ^{-1}) in the slower time scale $\tau = \epsilon^2 t \sim 1$. Thus, in the slower time scale each wave-train 'sees' the other travelling waves very fast in the other oblique directions, and reflecting many times at the walls, meaning that only a weighted, averaged effect is felt in this time scale. The weights are revealed in the function ϕ and arise from the fact that the wave-trains are amplified if $\rho_k < 1$ ($k = p$ or q) or reduced if $\rho_k > 1$ as they travel, in order to compensate the instantaneous reduction (if $\rho_k < 1$) or amplification (if $\rho_k > 1$) at the walls.

For given (X, Y), $(\xi, \eta) = (X - T, (Y - T)/P)$ defines a trajectory in the (ξ, η)-plane.

Since W, viewed as function of (ξ, η, T), is periodic of periods 2 in both ξ and η, this trajectory can be considered as trajectory on a 2-torus. When $P = 1/(lv_r)$ is irrational, a single trajectory fills the torus densely, and the average becomes simply an average over the fundamental domain. In this case the equation for W can be written more explicitly as

$$\begin{aligned}
W_\tau \;=\; & b''_{1p} W_X + v_r^{-1} b''_{1q} W_Y + d_{pp} W_{XX} + v_r^{-2} d_{qq} W_{YY} + 2 v_r^{-1} d_{pq} W_{XY} \\
& + \Big[\lambda + e'_1 |W|^2 + e'_2 \int_{-1/2}^{1/2} \rho_p^{-2\xi'+1} |W(X - 2\xi' - 1, Y, \tau)|^2 \, \mathrm{d}\xi' \\
& \quad + e_3 \int_{-1/2}^{1/2} \int_{-1/2}^{1/2} \rho_p^{-2\xi'+1} \rho_q^{-2\eta'+1} |W(X - 2\xi' - 1, Y - 2\eta' P - 1, \tau)|^2 \, \mathrm{d}\xi' \mathrm{d}\eta' \\
& \quad + e'_4 \int_{-1/2}^{1/2} \rho_q^{-2\eta'+1} |W(X, Y - 2\eta' P - 1, \tau)|^2 \, \mathrm{d}\eta' \Big] W \\
& + e_5 \int_{-1/2}^{1/2} \int_{-1/2}^{1/2} \rho_p^{-2\xi'+1} \rho_q^{-2\eta'+1} W(X - 2\xi' - 1, Y, \tau) \\
& \quad \times \overline{W}(X - 2\xi' - 1, Y - 2\eta' P - 1, \tau) W(X, Y - 2\eta' P - 1, \tau) \, \mathrm{d}\xi' \mathrm{d}\eta', \qquad (3.71)
\end{aligned}$$

where

$$e'_1 = e_1 \frac{(\rho_p^2 - 1)(\rho_q^2 - 1)}{4 \log \rho_p \log \rho_q}, \quad e'_2 = e_2 \frac{(\rho_q^2 - 1)}{2 \log \rho_q}, \quad e'_4 = e_4 \frac{(\rho_p^2 - 1)}{2 \log \rho_p}.$$

Regarding the rational cases, we consider only the case of a $1:1$-resonance, $lv_r = 1$, in some detail. Trajectories in this case will traverse all four primary sub-boxes B_j (B_j denotes the box in which Y_{j0} is placed) and then close up. If we let $\theta = X - Y$, then if $-1 < \theta \bmod 2 < 0$, a trajectory will traverse the boxes in the order $B_1 \to B_2 \to B_3 \to B_4$. If $-2 < \theta \bmod 2 < -1$ it will traverse the boxes in the order $B_2 \to B_1 \to B_4 \to B_3$. In either case, the equation for $W(X, Y, \tau)$ is as follows,

$$\begin{aligned}
W_\tau \;=\; & b''_{1p} W_X + v_r^{-1} b''_{1q} W_Y + d_{pp} W_{XX} + v_r^{-2} d_{qq} W_{YY} + 2 v_r^{-1} d_{pq} W_{XY} + \lambda W \\
& + \frac{1}{2} \int_{-\frac{3}{2}}^{\frac{1}{2}} \Big\{ \big[e_1 \phi(z, z - \theta) |W|^2 + e_2 \phi(-z, z - \theta) |W(X - 2z - 1, Y, \tau)|^2 \\
& \quad + e_3 \phi(-z, -z + \theta) |W(X - 2z - 1, -Y + 2X - 2z - 1, \tau)|^2 \\
& \quad + e_4 \phi(z, -z + \theta) |W(X, -Y + 2X - 2z - 1, \tau)|^2 \big] W \qquad (3.72) \\
& \quad + e_5 \phi(-z, -z + \theta) W(X - 2z - 1, Y, \tau)
\end{aligned}$$

$$\times \overline{W}(X-2z-1,-Y+2X-2z-1,\tau)W(X,-Y+2X-2z-1,\tau)\Big\}\,\mathrm{d}z,$$

but the function ϕ has to be evaluated differently for the two cases.

4 Neural Activation-Inhibition Model

In this section we apply the methods of Section 3 to a reaction-diffusion model that has been introduced and studied by Dangelmayr and Oprea [21] and extends a neural Activation-Inhibition model introduced by Murray [44]. The model of [21] contains fourth order diffusion terms which require an extension of some of the formulae defined in Section 3.

The original model given by Murray is used to describe the light and dark patterns in mollusk shells which emerge through intermittent deposition. It is assumed that the color of secretion is determined by activation via sensing the coloring of the existing color at the deposition edge and accumulation of inhibitory material existing in the secretory cell. The difference between the activation and inhibition inputs from surrounding cells determines the net neural stimulation for that cell. Hence, the pattern evolves based on the existing pattern and additional chemical conditions in the mollusk.

We briefly describe Murray's model which is given by the following equations,

$$\begin{aligned} \frac{\partial P}{\partial t} &= S(M_0 P) - P - Q - d_0 \frac{\partial^2 P}{\partial x^2} - d_1 \frac{\partial^4 P}{\partial x^4}, \\ \frac{\partial Q}{\partial t} &= dP - eQ, \end{aligned}$$

where $P(x,t)$ and $Q(x,t)$ are amounts of activation and inhibition substances provided by 1D arrays of cells (cell position x), and $d, e > 0$. The neural activation mechanism is described by a sigmoid function $S(M_0 P)$ that depends on a parameter M_0 controlling its steepness. Lateral activation and inhibition are described by the two diffusion terms in the P-equation. Since both coefficients, d_0 and d_1, are assumed positive, the first diffusion term is destabilizing and the second is stabilizing.

The sigmoid form assumed for $S(M_0 P)$ implies that the equations for P, Q have a unique spatially and temporally uniform solution (P^*, Q^*), given by $Q^* = dP^*/e$ and $S(M_0 P^*) = (1 + d/e)P^*$. Using incremental variables $P = P^* + u_1$, $Q = Q^* + u_2$, expanding $S(M_0 P)$

in a Taylor series about P^*, and truncating the series at third order gives

$$\begin{aligned}\frac{\partial u_1}{\partial t} &= Ru_1 - u_2 + bu_1^2 - cu_1^3 - d_0 u_{1xx} - d_1 u_{1xxxx}, \\ \frac{\partial u_2}{\partial t} &= du_1 - eu_2,\end{aligned}$$

with coefficients $R, b, c > 0$ depending on S and its derivatives. The parameter R is related to the steepness of the sigmoid function and is treated as the main bifurcation parameter.

In [21] the following 2D extension of the $u = (u_1, u_2)^T$ system has been introduced,

$$\partial_t u = \begin{bmatrix} Ru_1 - u_2 + bu_1^2 - cu_1^3 - u_{1xx} - u_{1yy} - \frac{1}{2}d_1 u_{1xxxx} - d_2 u_{1xxyy} - \frac{1}{2}d_3 u_{1yyyy} \\ du_1 - eu_2 - (c_1 - 1)u_{2xx} - (c_2 - 1)u_{2yy} \end{bmatrix}, \tag{4.1}$$

which includes fourth order diffusion terms in u_1 and second order diffusion terms in u_2, with a scaling of (x, y) such that the second order diffusion terms of u_1 are scaled to unity. To have a globally stable situation the d_j must satisfy $d_1 > 0$ and $d_1 d_3 - d_2^2 > 0$. The diffusion terms in u_2 are allowed to be stabilizing ($c_j < 1$) or destabilizing ($c_j > 1$).

A generalized form of (4.1) posed in our rectangle is

$$\frac{\partial u}{\partial t} = D(-\partial_x^2, -\partial_y^2)u + f(u, R) \text{ in } -L_p/2 < x < L_p/2, -L_q/2 < y < L_q/2, \tag{4.2}$$

with the diffusion operator

$$D(-\partial_x^2, -\partial_y^2) = -D_p\partial_x^2 - D_q\partial_y^2 - \frac{1}{2}D_{2p}\partial_x^4 - D_{pq}\partial_x^2\partial_y^2 - \frac{1}{2}D_{2q}\partial_y^4, \tag{4.3}$$

where D_p, D_q, D_{2p}, D_{pq} and D_{2q} are diagonal matrices. The fourth order terms in (4.2) require us to impose two sets of boundary conditions at each edge,

$$C_{p1}u \pm E_{p1}u_x = 0 \quad \text{at} \quad \pm L_p/2 \tag{4.4}$$

$$C_{p2}u_{xx} \pm E_{p2}u_{xxx} = 0 \quad \text{at} \quad \pm L_p/2 \tag{4.5}$$

$$C_{q1}u \pm E_{q1}u_y = 0 \quad \text{at} \quad \pm L_q/2 \tag{4.6}$$

$$C_{q2}u_{yy} \pm E_{q2}u_{yyy} = 0 \quad \text{at} \quad \pm L_q/2. \tag{4.7}$$

Note that for the model (4.1), the boundary conditions (4.5) and (4.7) must not involve u_2, that is, only the (1,1) components of C_{p2}, E_{p2}, C_{q2} and E_{q2} are allowed to be nonzero. For the specific model (4.1), f and the diffusion matrices are given by

$$f(u,R) = \begin{bmatrix} Ru_1 - u_2 + bu_1^2 - cu_1^3 \\ du_1 - eu_2 \end{bmatrix}, \tag{4.8}$$

$$D_p = \begin{bmatrix} 1 & 0 \\ 0 & (c_1 - 1) \end{bmatrix}, \quad D_q = \begin{bmatrix} 1 & 0 \\ 0 & (c_2 - 1) \end{bmatrix},$$

$$D_{2p} = \begin{bmatrix} d_1 & 0 \\ 0 & 0 \end{bmatrix}, \quad D_{pq} = \begin{bmatrix} d_2 & 0 \\ 0 & 0 \end{bmatrix}, \quad D_{2q} = \begin{bmatrix} d_3 & 0 \\ 0 & 0 \end{bmatrix}.$$

The stability of $u = 0$ is determined by considering the linearized system

$$[F(R) - D_p\partial_x^2 - D_q\partial_y^2 - \frac{1}{2}D_{2p}\partial_x^4 - D_{pq}\partial_x^2\partial_y^2 - \frac{1}{2}D_{2q}\partial_y^4]u = u_t. \tag{4.9}$$

with

$$F(R) = f_u(0,R) = \begin{bmatrix} R & -1 \\ d & -e \end{bmatrix}$$

for (4.1). Using the usual ansatz $u = U\exp(ipx+iqy+\sigma t)$ and solving the related eigenvalue problem for the minimum R to produce a purely imaginary σ gives the values at the Hopf bifurcation. The general eigenvalue problem is

$$[F(R) + p^2D_p + q^2D_q - \frac{p^4}{2}D_{2p} - p^2q^2D_{pq} - \frac{q^4}{2}D_{2q}]U = \sigma U. \tag{4.10}$$

which in the case of (4.1) becomes

$$\begin{bmatrix} Ru_1 - u_2 + p^2u_1 + q^2u_1 - d_1\frac{p^4}{2}u_1 - d_2p^2q^2u_1 - d_3\frac{q^4}{2}u_1 \\ du_1 - eu_2 + (c_1-1)p^2u_2 + (c_2-1)q^2u_2 \end{bmatrix} = \sigma u. \tag{4.11}$$

To find (p_c^2, q_c^2, R_c) from (4.11) we consider the matrix

$$K(p^2,q^2,R) = \begin{bmatrix} R + p^2 + q^2 - d_1\frac{p^4}{2} - d_2p^2q^2 - d_3\frac{q^4}{2} & -1 \\ d & -e + (c_1-1)p^2 + (c_2-1)q^2 \end{bmatrix}. \tag{4.12}$$

The matrix K has an imaginary eigenvalue if $\mathrm{Tr}K = 0$ and $\det K > 0$. The condition $\mathrm{Tr}K = 0$ can be solved for R leading to

$$R_c(p^2,q^2) = e - c_1p^2 - c_2q^2 + \frac{1}{2}d_1p^4 + d_2p^2q^2 + \frac{1}{2}d_3q^4.$$

It is easy to see that if $d_3c_1 - d_2c_2 > 0$ and $d_1c_2 - d_2c_1 > 0$, the surface $R_c(p^2,q^2)$ has a unique minimum R_c at (p_c^2, q_c^2), given by [21]

$$(p_c^2, q_c^2) = \frac{1}{d_1d_3 - d_2^2}(d_3c_1 - d_2c_2, d_1c_2 - d_2c_1) \tag{4.13}$$

$$R_c = e - \frac{d_1c_2^2 + d_3c_1^2 - 2d_2c_1c_2}{2(d_1d_3 - d_2^2)}. \tag{4.14}$$

Letting

$$E = e - \frac{(c_1-1)(d_3c_1 - d_2c_2) + (c_2-1)(d_1c_2 - d_2c_1)}{d_1d_3 - d_2^2} \text{ and } \omega^2 = d - E^2$$

and assuming $d > E^2$, the matrix $K(p_c, q_c, R_c)$ simplifies to

$$K(p_c^2, q_c^2, R_c) = \begin{bmatrix} E & -1 \\ E^2 + \omega^2 & -E \end{bmatrix} \tag{4.15}$$

and has eigenvalues $\pm i\omega$ and left and right eigenvectors

$$U_0 = \begin{pmatrix} 1 \\ E - i\omega \end{pmatrix}, \quad \overline{U}_0^{*T} = \frac{1}{2\omega}(\omega - iE, i).$$

Exploiting the fact that $K(p^2, q^2, R)$ is a 2×2 matrix we have σ_r =TrK and σ_i =(det$K$ − (TrK)^2/4)$^{1/2}$. This allows us to find the critical wave velocities from the $p - p_c$ and $q - q_c$ coefficients of σ_i, and the diffusion terms from the second order coefficients of σ,

$$\begin{aligned}
v_p &= 2p_c E(c_1 - 1)/\omega, \\
v_q &= 2q_c E(c_2 - 1)/\omega, \\
d_{pp} &= d_1 p_c^2 + \frac{i}{\omega}[\frac{2dp_c^2(c_1 - 1)^2}{\omega^2} - E(d_1 p_c^2 + c_1 - 1)], \\
d_{pq} &= d_2 p_c q_c + \frac{ip_c q_c}{\omega}[\frac{2d(c_1 - 1)(c_2 - 1)}{\omega^2} - Ed_2], \\
d_{qq} &= d_3 q_c^2 + \frac{i}{\omega}[\frac{2dq_c^2(c_2 - 1)^2}{\omega^2} - E(d_3 q_c^2 + c_2 - 1)].
\end{aligned}$$

We next consider the bulk solution for the general system (4.1). The expansion is the same as in Section 3, and the expansion vectors satisfy the same hierarchy of linear equations, except that the matrix T is now

$$T(p^2, q^2, \Omega) = F_1 + p^2 D_p + q^2 D_q - p^4 \frac{1}{2} D_{2p} - p^2 q^2 D_{pq} - q^4 \frac{1}{2} D_{2q} - i\Omega I,$$

and the vectors on the right hand sides involving the diffusion matrices have to be extended by the additional diffusion matrices. We list only those equations that have been modified, which are

$$\begin{aligned}
T(p_c^2, q_c^2, \omega)U_{1p} &= (-2p_c D_p + 2p_c^3 D_{2p} + 2p_c q_c^2 D_{pq} + iv_p I)U_0 \\
T(p_c^2, q_c^2, \omega)U_{1q} &= (-2q_c D_q + 2p_c^2 q_c D_{pq} + 2q_c^3 D_{2q} + iv_q I)U_0 \\
T(p_c^2, q_c^2, \omega)U_{2pp} &= (-2p_c D_p + 2p_c^3 D_{2p} + 2p_c q_c^2 D_{pq} + iv_p I)U_{1p} \\
&\quad +(-D_p + 3p_c^2 D_{2p} + q_c^2 D_{pq} - d_{pp} I)U_0
\end{aligned}$$

$$
\begin{aligned}
T(p_c^2, q_c^2, \omega)U_{2pq} &= (-2p_cD_p + 2p_c^3D_{2p} + 2p_cq_c^2D_{pq} + iv_pI)U_{1q}/2 \\
&\quad +(-2q_cD_q + 2p_c^2q_cD_{pq} + 2q_c^3D_{2q} + iv_qI)U_{1p}/2 \\
&\quad +(2p_cq_cD_{pq} - d_{pq}I)U_0 \\
T(p_c^2, q_c^2, \omega)U_{2qq} &= (-2q_cD_q + 2p_c^2q_cD_{pq} + 2q_c^3D_{2q} + iv_qI)U_{1q} \\
&\quad +(-D_q + p_c^2D_{pq} + 3q_c^2D_{2q} - d_{qq}I)U_0 \\
T(p_c^2, q_c^2, \omega)U_{4p} &= (-2p_cD_p + 2p_c^3D_{2p} + 2p_cq_c^2D_{pq} + iv_pI)U_3 + (a_0I - F_2)U_{1p} + ib_{1p}U_0 \\
T(p_c^2, q_c^2, \omega)U_{4q} &= (-2q_cD_q + 2p_c^2q_cD_{pq} + 2q_c^3D_{2q} + iv_qI)U_3 + (a_0I - F_2)U_{1q} + ib_{1q}U_0.
\end{aligned}
$$

For (4.1) the operators occurring in the hierarchy have the simple forms

$$
F_1 = \begin{bmatrix} R_c & -1 \\ d & -e \end{bmatrix}, \quad F_2 = \begin{bmatrix} 1 & 0 \\ 0 & 0 \end{bmatrix}, \quad F_3 = 0,
$$

$$
\mathcal{B}(u_j, u_k) = \begin{bmatrix} bu_{1j}u_{1k} \\ 0 \end{bmatrix}, \quad \mathcal{C}(u_j, u_k, u_l) = \begin{bmatrix} -cu_{1j}u_{1k}u_{1l} \\ 0 \end{bmatrix}.
$$

The coefficients for the Ginzburg Landau equations also have the same form as in Section 3, except for modifications coming from the additional diffusion terms. We again list only those coefficients which are modified,

$$
\begin{aligned}
v_p &= i\overline{U_0}^{*T}(-2p_cD_p + 2p_c^3D_{2p} + 2p_cq_c^2D_{pq})U_0 \\
d_{pp} &= \overline{U}_0^{*T}(-2p_cD_p + 2p_c^3D_{2p} + 2p_cq_c^2D_{pq} + iv_pI)U_{1p} + \overline{U}_0^{*T}(-D_p + 3p_c^2D_{2p} + q_c^2D_{pq})U_0 \\
d_{pq} &= \overline{U}_0^{*T}(-2p_cD_p + 2p_c^3D_{2p} + 2p_cq_c^2D_{pq} + iv_pI)U_{1q}/2 \\
&\quad +\overline{U}_0^{*T}(-2q_cD_q + 2p_c^2q_cD_{pq} + 2q_c^3D_{2q} + iv_qI)U_{1p}/2 + 2p_cq_c\overline{U}_0^{*T}D_{pq}U_0 \\
b_{1p} &= i\overline{U}_0^{*T}(-2p_cD_p + 2p_c^3D_{2p} + 2p_cq_c^2D_{pq} + iv_pI)U_3 + i\overline{U}_0^{*T}(a_0I - F_2)U_{1p}
\end{aligned}
$$

The parameters v_q, d_{qq} and b_{1q} can be found through the symmetry operation $p \leftrightarrow q$.

It is straightforward to find explicit expressions for the coefficients in the A_j equations for the model system (4.1). The linear coefficients have already been computed from the

eigenvalue σ. To obtain the nonlinear coefficients we need to find U_6, U_7, $W_{11} - W_{13}$ and $W_{21} - W_{23}$. Since

$$\mathcal{B}(U_0, U_0) = \mathcal{B}(U_0, \overline{U}_0) = \begin{bmatrix} b \\ 0 \end{bmatrix}, \mathcal{C}(U_0, U_0, \overline{U}_0) = \begin{bmatrix} -c \\ 0 \end{bmatrix},$$

these are all of the form

$$W_k = \frac{-2b}{\det\, T(p^2, q^2, \Omega)} \begin{pmatrix} T_{22}(p^2, q^2, \Omega) \\ d \end{pmatrix},$$

where $T_{22}(p^2, q^2, \Omega)$ is the (2,2) entry in the $T(p^2, q^2, \Omega)$ matrix. Using these vectors, U_0 and U_0^* in the general formulae for $e_1 - e_5$ we get

$$\begin{aligned}
e_1 &= (1 - \frac{iE}{\omega})(\frac{2eb^2}{d - eR_c} - \frac{b^2 T_{22}(4p_c^2, 4q_c^2, 2\omega)}{\det\, T(4p_c^2, 4q_c^2, 2\omega)} - \frac{3}{2}c) \\
e_2 &= (1 - \frac{iE}{\omega})(\frac{2eb^2}{d - eR_c} - \frac{2b^2 T_{22}(4p_c^2, 0, 0)}{\det\, T(4p_c^2, 0, 0)} - \frac{2b^2 T_{22}(0, 4q_c^2, 2\omega)}{\det\, T(0, 4q_c^2, 2\omega)} - 3c) \\
e_3 &= (1 - \frac{iE}{\omega})(\frac{2eb^2}{d - eR_c} - \frac{2b^2 T_{22}(4p_c^2, 4q_c^2, 0)}{\det\, T(4p_c^2, 4q_c^2, 0)} - \frac{2b^2 T_{22}(0, 0, 2\omega)}{\det\, T(0, 0, 2\omega)} - 3c) \\
e_4 &= (1 - \frac{iE}{\omega})(\frac{2eb^2}{d - eR_c} - \frac{2b^2 T_{22}(0, 4q_c^2, 0)}{\det\, T(0, 4q_c^2, 0)} - \frac{2b^2 T_{22}(4p_c^2, 0, 2\omega)}{\det\, T(4p_c^2, 0, 2\omega)} - 3c) \\
e_5 &= (1 - \frac{iE}{\omega})(-\frac{2b^2 T_{22}(4p_c^2, 0, 0)}{\det\, T(4p_c^2, 0, 0)} - \frac{2b^2 T_{22}(0, 4q_c^2, 0)}{\det\, T(0, 4q_c^2, 0)} - \frac{2b^2 T_{22}(0, 0, 2\omega)}{\det\, T(0, 0, 2\omega)} - 3c).
\end{aligned}$$

For the specific values of the fourth order diffusion parameters

$$d_1 = 22.3862, \quad d_2 = 13.0021, \quad d_3 = 20.6642,$$

and $c = 1$ and $e = 1.5$, and varying the parameters b, d, c_1 and c_2 as below we obtain numerical values for the corresponding Ginzburg Landau coefficients in Table 1. Note that the parameter set L_3 has $c_1, c_2 < 1$ as stabilizing parameters which implies $v_p, v_q < 0$.

We now consider the boundary layer expansion for the general problem (4.2), (4.4)-(4.7)

	L_1	L_2	L_3	L_4
b	0.1729	0.1500	0.1650	0.2
d	2.4144	2.4	2.3	2.6
c_1	1.2	1.5	0.8	1.5
c_2	1.3	1.1	0.6	1.5
R_c	1.4540	1.4477	1.4850	1.4347
p_c	0.1640	0.2385	0.1725	0.1979
q_c	0.2145	0.1321	0.1016	0.2190
ω	0.4707	0.4895	0.1402	0.6919
v_p	0.2064	0.7160	-0.7428	0.4165
v_q	0.4048	0.0793	-0.8752	0.4609
d_{pp}	0.6020-2.4734i	1.2731-4.7422i	0.6658-3.0314i	0.8765-2.7438i
d_{pq}	0.4573-1.3408i	.4096-1.1653i	0.2278-.1153i	0.5634-1.0158i
d_{qq}	0.9503-3.8484i	.3605-1.2043i	0.2133+2.6990i	0.9909-2.9501i
e_1	-1.2875+3.1314i	-1.2632+3.3814i	-2.4793-2.4121i	-1.3598+2.4312i
e_2	-3.2190+7.5421i	-2.9067+8.1088i	-5.1571+23.9691i	-2.9103+5.4716i
e_3	-2.9585+8.2732i	-2.9377+8.1548i	-93.5446+90.5574i	-2.9124+5.6948i
e_4	-2.9356+8.0792i	-3.0271+6.6482i	-2.9140+7.8088i	-2.9009+5.5444i
e_5	-2.9761+8.3283i	-2.8958+8.0288i	-2.9064+8.1372i	-2.9573+5.7893i

Table 1: Calculated amplitude equation parameters for the Activator-Inhibitor model

at $y \sim -L_q/2$,

$$\begin{aligned} u_t &= (-D_p\partial_x^2 - D_q\partial_{\tilde{y}}^2 - \tfrac{1}{2}D_{2p}\partial_x^4 - D_{pq}\partial_x^2\partial_{\tilde{y}}^2 - \tfrac{1}{2}D_{2q}\partial_{\tilde{y}}^4)u + f(u,\mu), \\ C_{q1}u - E_{q1}u_{\tilde{y}} &= 0 \text{ at } \tilde{y} = 0, \\ C_{q2}u_{\tilde{y}\tilde{y}} - E_{q2}u_{\tilde{y}\tilde{y}\tilde{y}} &= 0 \text{ at } \tilde{y} = 0, \\ u &\to u_{\text{bulk}} \text{ for } \tilde{y} \to \infty. \end{aligned} \tag{4.16}$$

Using the edge ansatz from Section 3 we get the following ODE for $\mathcal{U}^0$,

$$(-D_q + p_c^2 D_{pq})\mathcal{U}^0_{\tilde{y}\tilde{y}} - \frac{1}{2}D_{2q}\mathcal{U}^0_{\tilde{y}\tilde{y}\tilde{y}\tilde{y}} + (p_c^2 D_p - \frac{p_c^4}{2}D_{2p} + F_1 - i\omega I)\mathcal{U}^0 = 0. \tag{4.17}$$

The roots of the characteristic polynomial are found from

$$\det[(-D_q + p_c^2 D_{pq})\lambda^2 - \frac{1}{2}D_{2q}\lambda^4 + (p_c^2 D_p - \frac{p_c^4}{2}D_{2p} + F_1 - i\omega I)] = 0. \tag{4.18}$$

If D_{2q} is of full rank there will be $4N$ roots of this polynomial. In the case of (4.1), D_{2q} has only a single nonzero entry in the (1,1) entry leaving 6 roots coming in three pairs, one pair will be $\pm iq_c$ and the two other pairs, $\pm\lambda_{q1}, \pm\lambda_{q2}$, have $\mathrm{Re}\lambda_{qj} > 0$, thus only the roots with the negative sign can be used leaving

$$\mathcal{U}^0(\tilde{y}) = U_0(e^{iq_c\tilde{y}} + r_q e^{-iq_c\tilde{y}}) + r_{q1}V_{q1}^0 e^{-\lambda_{q1}\tilde{y}} + r_{q2}V_{q2}^0 e^{-\lambda_{q2}\tilde{y}}, \tag{4.19}$$

where V_{q1}^0 and V_{q2}^0 are the eigenvectors corresponding to the eigenvalues $-\lambda_{q1}$ and $-\lambda_{q2}$.

We then apply the boundary conditions to solve for the boundary parameter r_q. Letting

$$C_q = I_2, \quad C_{q2} = \begin{bmatrix} 1 & 0 \\ 0 & 0 \end{bmatrix}, \quad E_q = \begin{bmatrix} \beta_1 & 0 \\ 0 & \beta_2 \end{bmatrix}, \quad E_{q2} = \begin{bmatrix} \beta_3 & 0 \\ 0 & 0 \end{bmatrix},$$

gives us three equations for r_q, r_{q1} and r_{q2}. Denoting the eigenvectors by $V_{q1} = [v_1, w_1]^T$, $V_{q2} = [v_2, w_2]^T$ the equations to be solved are

$$\begin{aligned}
(1 - \beta_1 iq_c + r_q(1 + \beta_1 iq_c))u_{1c} + (1 + \beta_1\lambda_{q1})r_{q1}v_1 + (1 + \beta_1\lambda_{q2})r_{q2}v_2 &= 0 \\
(1 - \beta_2 iq_c + r_q(1 + \beta_2 iq_c))u_{2c} + (1 + \beta_2\lambda_{q1})r_{q1}w_1 + (1 + \beta_2\lambda_{q2})r_{q2}w_2 &= 0 \\
-q_c^2(1 - \beta_3 iq_c + r_q(1 + \beta_3 iq_c))u_{1c} + \lambda_{q1}^2(1 + \beta_3\lambda_{q1})r_{q1}v_1 + \lambda_{q2}^2(1 + \beta_3\lambda_{q2})r_{q2}v_2 &= 0
\end{aligned}$$

In the general case, if D_{2q} is of full rank, this system becomes a system of $4N$ equations.

Considering the parameter set L_4 above, the three eigenvalue and eigenvector pairs are

$$\pm q_c i = \pm 0.2190i, \quad U_0 = \begin{bmatrix} 1 \\ 1.4564 - 0.6919i \end{bmatrix},$$

$$-\lambda_{q1} = -1.9883 + 0.0912i, \quad V_{q1} = \begin{bmatrix} 1 \\ 1.4448 - 0.6507i \end{bmatrix},$$

β_1	1	1	-0.5	0.25
β_2	1	-1	-1.3	5.3
β_3	1	1	-1.1	4.83
r_q	-0.9085+0.4179i	-0.5701-0.3743i	-0.8824+0.4807i	0.0594+0.9943i

Table 2: Values of r_q using parameter set L_4 for four values of β_j

$$-\lambda_{q2} = -0.3805 + 1.7710i, \quad V_{q2} = \begin{bmatrix} 1 \\ -70.7820 - 83.3390i \end{bmatrix}.$$

For the case of $\beta_1 = \beta_2 = \beta_3 = 0$ the reflection coefficient is $r_q = -1$. Some values of r_q for L_4 have been calculated for various values $\beta_j \neq 0$ and are given in Table 2.

The hierarchy of differential equations for the functions $\mathcal{U}^j(\tilde{y})$ in the general case coincides with the equations from Section 3, except that the differential operator is now

$$\tilde{T}(p^2, \Omega) = F_1 + p^2 D_p - D_q \partial_{\tilde{y}}^2 - p^4 \frac{1}{2} D_{2p} + p^2 D_{pq} \partial_{\tilde{y}}^2 - \frac{1}{2} D_{2q} \partial_{\tilde{y}}^4 - i\Omega I$$

and the right hand sides involving diffusion matrices have to be extended again. We list only the modified equations, which are

$$\begin{aligned}
\tilde{T}(p_c^2, \omega)\mathcal{U}^1 &= (-2p_c D_p - 2p_c D_{pq} \partial_{\tilde{y}}^2 + 4\frac{p_c^3}{2} D_{2p})\mathcal{U}^0 \\
\tilde{T}(p_c^2, \omega)\mathcal{U}^2 &= (-2p_c D_p - 2p_c D_{pq} \partial_{\tilde{y}}^2 + 4\frac{p_c^3}{2} D_{2p})\mathcal{U}^1 + (-D_p - D_{pq} \partial_{\tilde{y}}^2 + 6\frac{p_c^2}{2} D_{2p})\mathcal{U}^0 \\
\tilde{T}(p_c^2, \omega)\mathcal{U}^4 &= (-2p_c D_p - 2p_c D_{pq} \partial_{\tilde{y}}^2 + 4\frac{p_c^3}{2} D_{2p})\mathcal{U}^3 - F_2 \mathcal{U}^1.
\end{aligned}$$

This leads to the persistent parts of the edge expansion as stated in the general case with lower order diffusion, and the analysis can proceed as described in that section leading to the boundary conditions for the envelopes.

5 Simulations

To demonstrate the pattern dynamics provided by the non-local evolution equation for the doubly periodic function $W(X, Y, \tau)$, we construct visualizations of the patterns resulting form the simulation for the generic irrational case of $lv_r \notin \mathbb{Q}$. For practical reasons we also require that L_p, L_q, p_c and q_c are such that the basic wavelength is at least two grid lengths in each direction and that $\alpha_p = \alpha_q = 0$. In addition we consider $b''_{1p} = b''_{1q} = 0$ and for the visualization we assume $a = 0$ in the rescaling of A_j to Y_j.

The method used to simulate the equation is based on the pseudo-spectral method, where one exploits the one-to-one nature of the function values at a finite number of grid points and a finite Fourier series. This correspondence allows us to calculate the derivatives in Fourier space, while calculating the local and averaged terms in wave-variable, (X, Y), space through the use of fast Fourier transforms. The solutions are calculated in Fourier space using Matlab's routine ODE45, a fourth order Runge-Kutta method with variable step size.

The use of a spectral method is warranted by the fact that the function to be computed is two-periodic, and spatial derivatives are turned into scalar multiplication of the Fourier coefficients. If M^2 Fourier modes are used, we start by introducing an $M \times M$ random, complex matrix as initial condition in wave-variable space for the system. Since ODE45 works on vectors, we must convert the grid point values into Fourier modes through a two-dimensional FFT, and then vectorize the matrix before we input it into the Matlab solver. This is done by taking each column and adjoining it to the bottom of a growing column vector $V((k-1)M + 1 : kM) = u(:, k)$ (using Matlab notation). The intermediate calculations for each step are done by reconstituting the $M \times M$ matrix. The input Fourier mode matrix is used to calculate the derivatives via scalar multiplication. The computation of the local terms and the averaging terms is done in physical space by taking the Fourier mode matrix and calculating a two-dimensional inverse fast Fourier transform. In (X, Y) space the local term is simply a scalar multiplication at the grid points, while the averaged terms are sums over the appropriate dimensions of the matrix divided by the total lengths.

The average over the X-dimension is a sum across the rows, and the average over the Y-dimension is a sum across the columns, with each of them divided by $M/2$. These vectors are then turned back into $M \times M$ matrices by adjoining each vector with itself in the appropriate way, and then using scalar multiplication to create the corresponding matrix in (X, Y) space. The overall average term is the sum of the entire matrix divided by $M^2/4$, and consists of a single number which multiplies the matrix values. The final average can be turned into matrix multiplication as $u * \overline{u}^T u/(M^2/4)$ which simplifies the calculation. These terms in (X, Y) space are then summed and transformed back into Fourier space and added to the derivative terms, vectorized, and then fed into the ODE45 solver for the next step. A final two-dimensional inverse Fourier transform captures the solution at the grid points in wave-variable space for visualization. To build the visualization we translate our solution in wave-variable space to the solution in the slow space variables, $W(X, Y, \tau) \to w_0(\xi, \eta, T, \tau)$, and then split w_0 into the four $\mathcal{O}(1)$ envelopes Y_{j0} which are then scaled to the approximate A_j and thus reconstruct the resultant pattern.

In the first subsection we focus our simulations on comparing the bounded case with the infinite extent case, so we begin by simulating parameter regimes that have been explored in the infinite case to compare the resulting solutions. We assume perfectly reflecting boundary conditions, $\rho_p = \rho_q = 1$, for these simulations and consider no phase change at the boundary, $\alpha_j = 0$, representing a reflection off of a free boundary.

In the next subsection we explore the effects of $\rho_k \neq 1$ which represent energy injection or absorption at the boundary. We explore several sets of parameter values and allow the reflection parameter to vary between $0.1 \leq \rho_k \leq 2$ and observe the changes in the resulting pattern.

For all simulations in this paper we set

$$L_p = 57, \quad L_q = 53, \quad p_c = 0.75, \quad q_c = 0.8, \quad \omega = 1.1, \quad M = 32.$$

5.1 Effects of the Bounded Domain: $\rho_p = \rho_q = 1$

We begin by considering the case of perfect reflection at the boundaries. Perfectly reflecting boundaries cause the critical value of the control parameter to be unchanged. For all explored parameter values the basic pattern is a standing (pulsating) rectangle (SR) pattern that is stable at the stability threshold. This pattern has $|W|$ constant in time and space and a Fourier spectrum consisting of a dominant constant mode (mode number (17,17) in our Fourier mode plots). As λ increases, SR becomes unstable and the resulting patterns are determined by the specific parameters for the Ginzburg-Landau equation. The Fourier modes are listed as (Y-mode,X-mode).

First, a set of parameters is studied for which the differential equations for the A_j, obtained by ignoring spatial variations in the envelope equations (the 'normal form'), shows a period doubling sequence to chaos [21],

$$(e_1, e_2, \mathrm{Im}(e_3), e_4, e_5) =$$

$$(-1 - 1.1806i, -0.923 - 0.5538i, 1.3613, -0.2223 - 3.3025i, -0.4647 - 0.2472i),$$

$$(d_{pp}, d_{pq}, d_{qq}, v_r) = (1 + 0.0108i, 0.4364 + 0.0149i, 1 + 0.0276i, 1.13),$$

and $\mathrm{Re}(e_3)$ is varied. The period doubling route to chaos in the normal form occurs as $\mathrm{Re}(e_3)$ goes from -0.641 to -0.644. For the W-equation, a period doubling route to chaos was not specifically observed in the simulations run for this thesis. This may be because the proper values of λ have not been found, or the nature of the coupling at the boundaries has precluded the period doubling sequence from occurring. However, for this set of parameters and $\mathrm{Re}(e_3) = -0.6422$ (referred to as PD) the system is sensitive to the values in the initial random matrix. While all patterns described below occurred in all simulations of PD, the transition from the TR-crash to the V-stripe pattern (described below), and the loss of stability of the V-stripe pattern occur at different values of λ depending on the specific run. This may constitute chaotic solutions predicted by the infinite extent case with a shift in

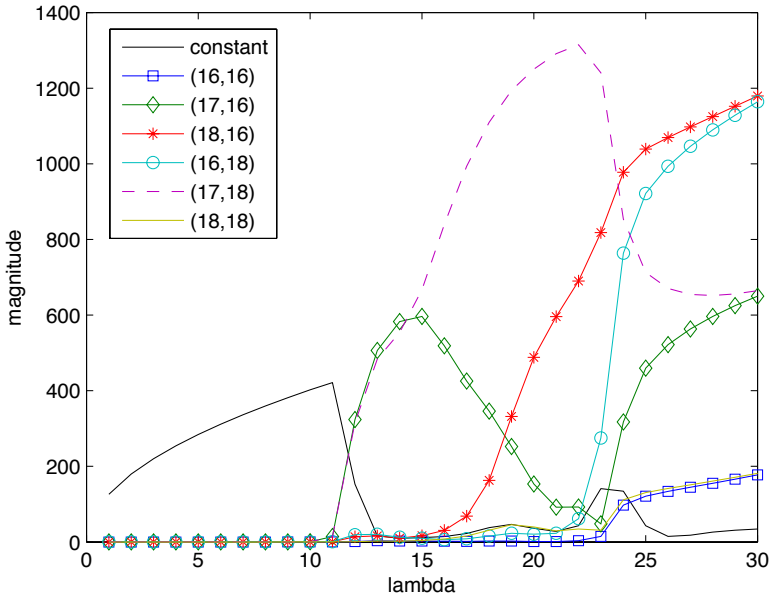

Figure 2: Plot of main modes of PD (averaged over $7 \leq \tau \leq 8$) for $1 \leq \lambda \leq 30$

parameter values due to the finite domain, or may be some other, not yet discovered, cause. This is an avenue for further study, but is beyond the scope of this thesis. One random matrix was used to generate the wave-pattern graphs in this subsection (labeled PD*) and another was used to generate Figure 2 and form the basis of the discussions.

The SR pattern is stable up to $\lambda = 10$. For all values of the rescaled driving parameter $\lambda \leq 10$, $|W|$ and $|A_j|$ are constant in space and time. This can be seen in the Fourier spectrum of the W solution at $\lambda = 10$, which has nearly all of its energy in the constant mode as can be seen in Figure 2.

The first instability of the SR pattern occurs at $\lambda = 11$ and leads to a cycle in which the standing rectangle develops a 'wobble' that grows until a short period of a horizontal travelling rectangle (TR) pattern is observed. This then decays through the wobble state back to the standing rectangle as seen in Figure 3. The wobble is created when the amplitudes have their minima at alternating sides of the cell, and the travelling rectangle is caused by (A_2, A_3) having minima at locations where (A_1, A_4) have maxima and vice versa.

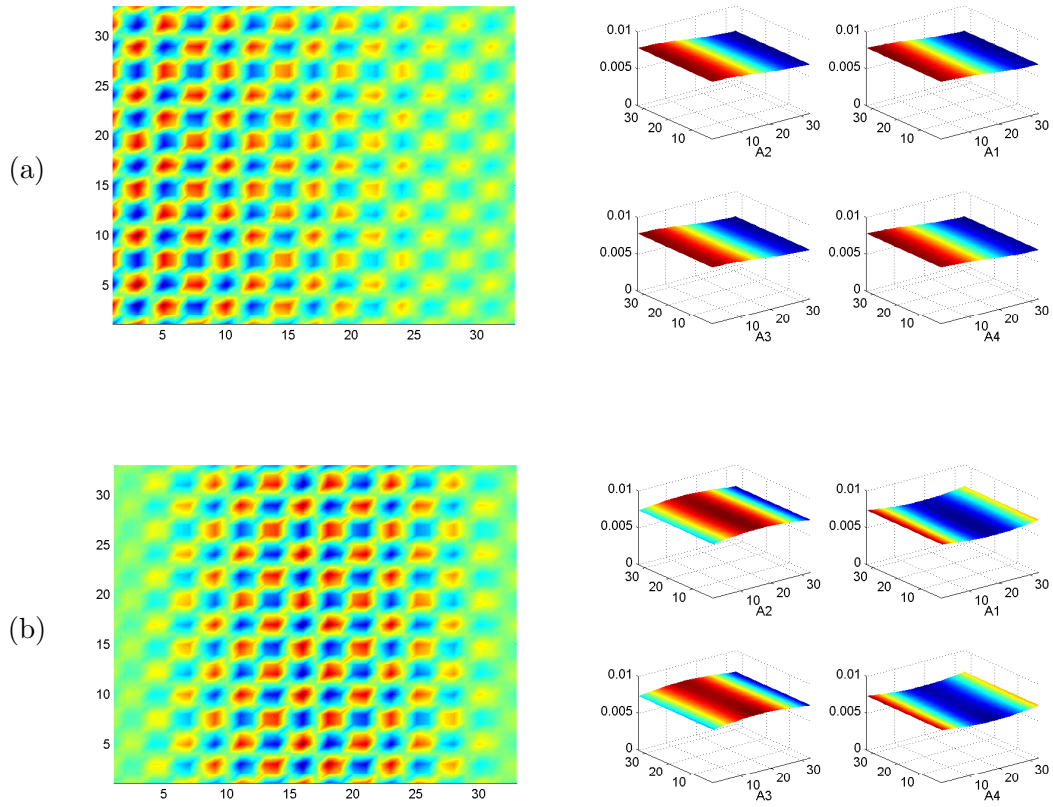

Figure 3: Wobble-TR pattern (left) and $|A_j|$ (right) for PD* with $\lambda = 11$ at (a) $\tau = 3.5219$ and (b) $\tau = 3.5296$

Then the variations of the amplitudes decay until they are nearly identical leading back to the standing rectangles. The directions of the horizontal travelling wave state do not show a pattern from one cycle to the next but waves travelling in both directions are observed. The $|W|$ solution is uniform in the Y-direction, however in the X-direction it shows a time varying oscillation around the average value of 0.41. In this oscillation, minima occur in the center when the maxima are at the boundaries and vice versa, and oscillate between values of 0.39 to 0.43 with a period of $\tau = 1.44$. The Fourier spectrum of this case still has most of its energy in the constant mode, but the (17,16) and (17,18) modes begin to show slight gains in energy as can be seen in Figure 2.

For $12 \leq \lambda \leq 15$ the pattern shows a splitting of the domain into left and right parts.

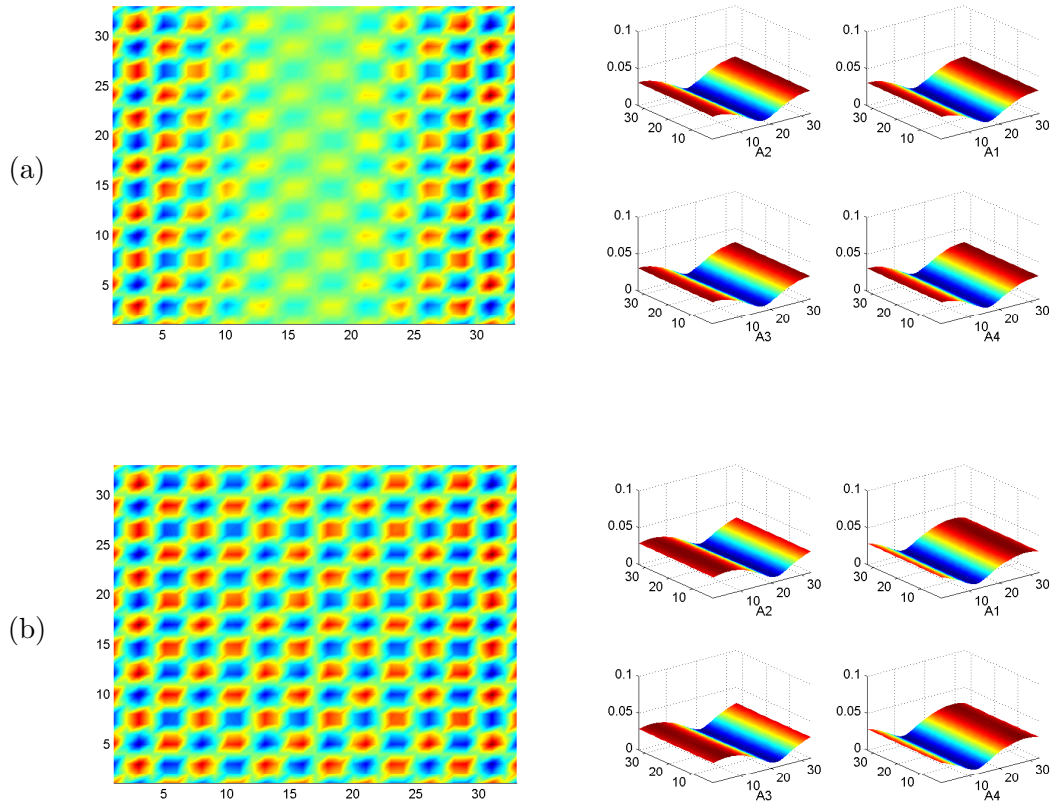

Figure 4: TR-crash pattern (left) and $|A_j|$ (right) for PD* at $\lambda = 12$ for (a) $\tau = 3.302$ and (b) $\tau = 3.304$.

In each, opposing travelling rectangle patterns occur that alternate directions, first moving towards the vertical center axis, and then away from it (referred to as TR-crash) as seen in Figure 4. There are periods where all four amplitudes have minima in the middle and maxima near the boundaries leading to standing rectangles that simply decay, spatially, towards the y-axis in the center. At other points in the cycle, (A_2, A_3) have maxima when (A_1, A_4) have minima on one side leading to right travelling rectangles on that side while the situation is reversed on the other side leading to left travelling waves on that side. In these periods one observes, alternatively, travelling rectangles colliding in the center of the cell or travelling rectangles emerging from the center of the cell. The $|W|$ solution is, again, uniform in the Y direction, however, it presents a travelling sine wave in the X direction

with two spatial periods over the domain. The spectrum for the W solution of PD on the range of $12 \leq \lambda \leq 15$ has most of its energy in the (17,16) and (17,18) modes at equivalent magnitudes. In this region the constant mode rapidly decreases as seen in Figure 2.

For $16 \leq \lambda \leq 18$ the (17,16) mode decreases while the (18,16) mode increases leading to a pattern that is a slight variation of SR, where there is some motion of the rectangles around the cell during minima-maxima exchanges of the standing rectangles. It is during this transition that the $|W|$ solution changes from being uniform in the Y-direction to having oblique rolls, creating the next pattern.

For $19 \leq \lambda \leq 24$ the pattern shows symmetry across the y-axis but begins to show motion in the vertical direction leading to alternating V-stripe patterns of diagonal waves in each half plane as seen in Figure 5. These are interspersed with brief phases where the SR pattern can be observed. The V-stripe can be seen when maxima for (A_1, A_3) coincide with minima for (A_2, A_4) leading to a region of oblique standing waves. The corresponding oblique standing waves can be seen when (A_2, A_4) have maxima in the same region where minima for (A_1, A_3) occur. The solution $|W|$ has a slow travelling periodic component as in the TR-crash case, however it is now consisting of an oblique roll. In this region the (17,18) and the (18,16) modes dominate with the former shrinking and the latter growing, as can be seen in Figure 2. Above $\lambda = 25$ the patterns become increasingly complex with many modes with non-trivial magnitudes. For PD*, the V-stripe pattern was stable past $\lambda = 37$ and the $|W|$ solution showed a spatially and temporally periodic wave in the Y direction leading to the X-oscillations developing an undulation. For PD* at $\lambda = 37$ the Fourier spectrum is noticeably variable in time with the constant mode oscillating between zero and 180 and smaller oscillations noticed in other modes. The maximum peaks, averaged over $7 \leq \tau \leq 8$, occurring in the (17,16) mode with a magnitude of 1400, and the (17,18) mode with a magnitude of 1300, then the (17,14), (18,16), (18,18), (17,20) modes are all over 200.

For the next set of parameters considered in this thesis, referred to as CAW, chaotic

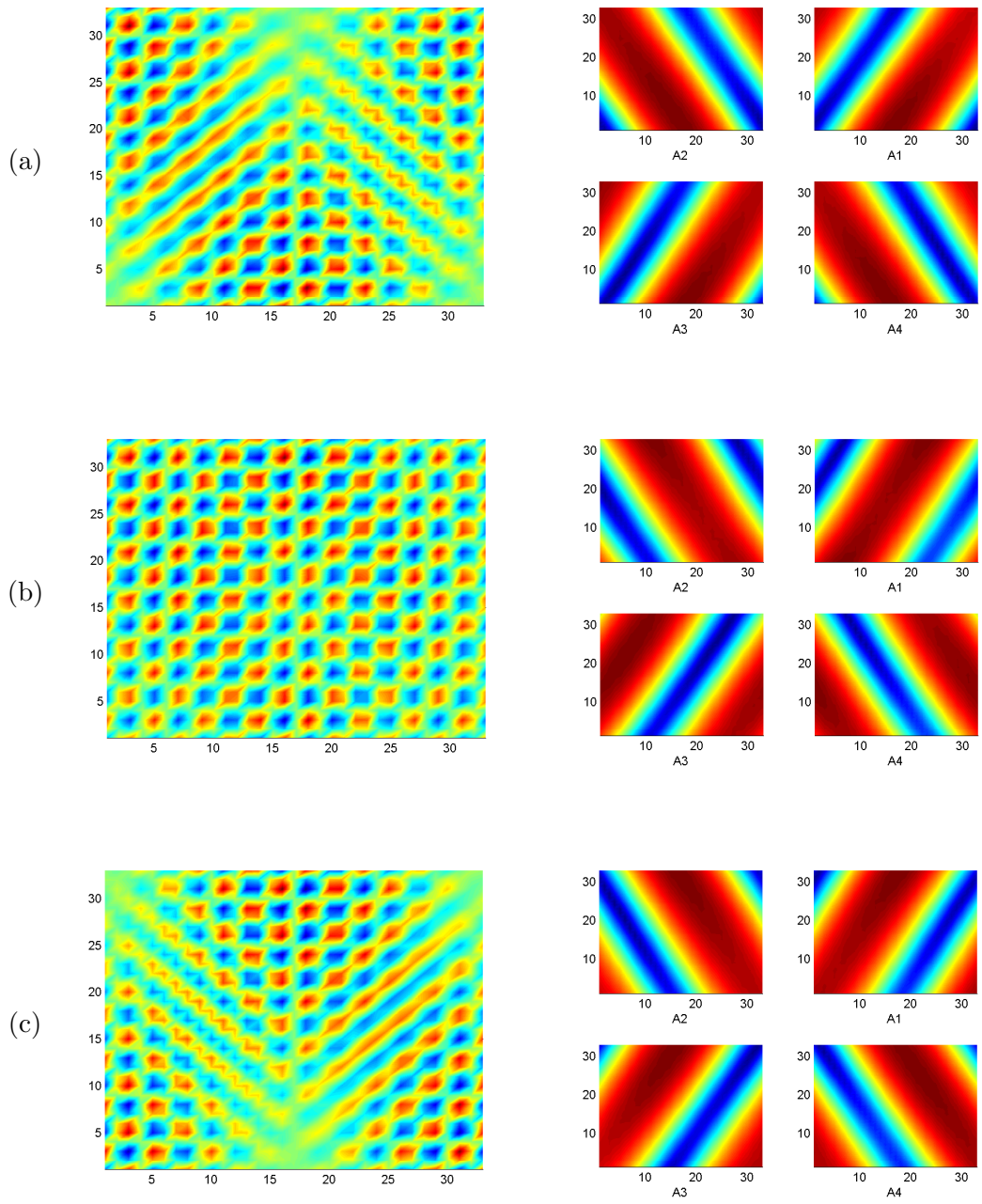

Figure 5: V-stripe pattern (left) and $|A_j|$ (right) for PD* at $\lambda = 37$ for (a) $\tau = 3.8454$, (b) $\tau = 3.8563$, (c) $\tau = 3.8618$.

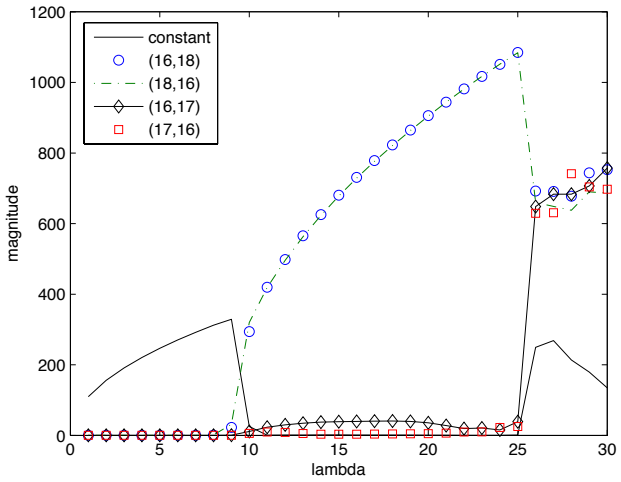

Figure 6: Plot of main modes of CAW (averaged over $7 \leq \tau \leq 8$) for $1 \leq \lambda \leq 30$

alternating waves are observed in the unbounded systems [47]. The parameters are

$$(e_1, e_2, e_3, e_4, e_5) =$$

$$(-1 - 0.7048i, -1.1805 - 1.2256i, -1.0579 - 1.9018i, 1.1001 - 1.4069i, -1.9091 - 1.4926i),$$

$$(d_{pp}, d_{pq}, d_{qq}, v_r) = (0.9347 - 1.1142i, 0.2071 - 0.4659i, 0.3437 - 0.1956i, 1.13).$$

One interesting aspect of this set is that e_4 has a positive real part making it a destabilizing parameter. For this set of parameters the solution shows a mirror symmetry across the two axes where a minimum rotates in each quadrant of the main state giving rise to alternating diamond and 'X' patterns (DX) as in Figure 7. The dominant modes of the Fourier spectrum of CAW over $1 \leq \lambda \leq 30$ are displayed in Figure 6. The figure shows that the constant mode is dominant through $\lambda = 9$ and for $10 \leq \lambda \leq 25$ the (16,18) and (18,16) modes are dominant leading to stationary oblique rolls with two periods in the $|W|$ solution over this range. For $\lambda \geq 26$, the patterns are highly complex and difficult to categorize while the Fourier spectrum shows several significant peaks indicating a complex pattern for W.

The composition of the DX pattern through the amplitudes is similar to that of the V-

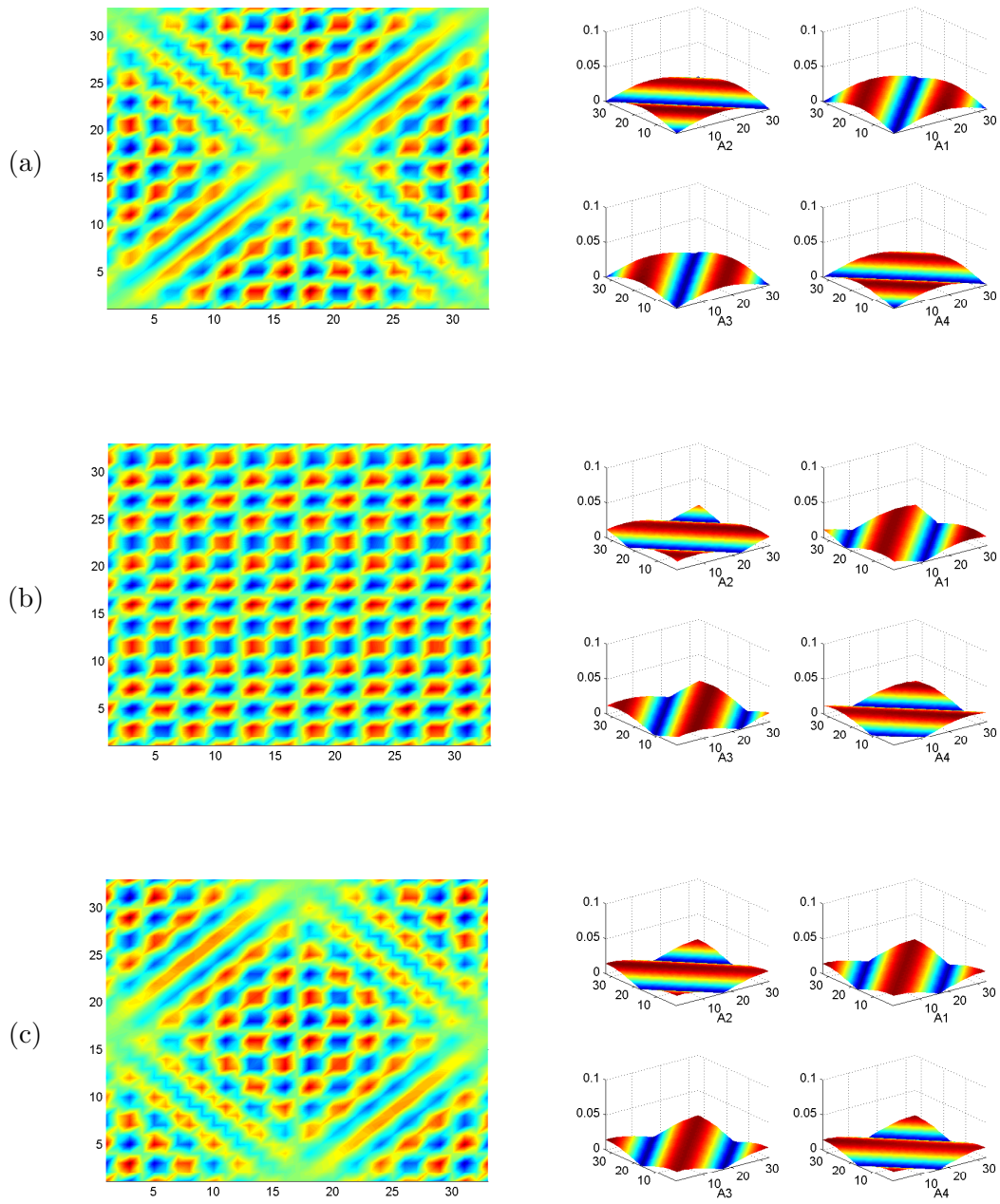

Figure 7: DX pattern (left) and $|A_j|$ (right) for CAW at $\lambda = 11$ for (a) $\tau = 3.2895$, (b) $\tau = 3.3936$, (c) $\tau = 3.4539$.

	E	I	E_t	EU
e_1	-1+i	-1+0.54i	-1+i	-1+i
e_2	-2.5-1.1i	-2.5-1.1i	-1.1-1.1i	-2.5-1.1i
e_3	-3.4-2i	-3.4-2i	-2.4-2i	-3.4-2i
e_4	-5.7-i	-5.7-i	-5-i	-5.7-i
e_5	-3.5-0.5i	-3.5-0.5i	-3.5-0.5i	-3.5-0.5i
d_{pp}	1+0.2i	0.9-4i	1-0.2i	0.9-i
d_{pq}	0.2+0.03i	0.6-3i	0.8-0.3i	0.2-0.02i
d_{qq}	0.15+0.03i	1.6-7i	0.9-0.3i	1.2+2i

Table 3: Parameter sets from [21]

stripe pattern in that there are regions with alternating maxima and minima of (A_1, A_3) and (A_2, A_4) leading to standing waves. The primary difference between the V-stripe pattern and the DX pattern is the presence of four regions of standing waves in the main cell instead of two.

Lastly we study four parameter sets considered in [21]. For all four parameter sets, travelling waves are stable normal form solutions, but in the setting of the infinite extent amplitude equations they show different types of instabilities. The parameter values are given in Table 3 and are referred to as E, I, E_t and EU corresponding to the instabilities observed in [21]. The parameters d_{ppr} and d_{qqr} are here not rescaled to 1 which then implies that the rescaled group velocities simplify to $v_r = v_q/v_p$. For these simulations, $v_p = 1.16$ and $v_q = 0.87$.

For I and EU we see similar behavior, although at different values of λ. As λ is increased, the initial instability in both cases is the V-stripe pattern which then degrades to spatially and temporally complex patterns.

For E and E_t the initial, categorizable, instability shows the DX pattern. For set E, the SR pattern is stable until $\lambda = 9$ where the pattern is highly complex. The DX pattern then emerges and is stable over $10 \leq \lambda \leq 38$. The $|W|$ solution is similar to CAW over its DX λ regime.

While we did not see stable travelling waves in any of the simulations described in this subsection, we did observe phases of travelling rectangles in parts of the domain for certain

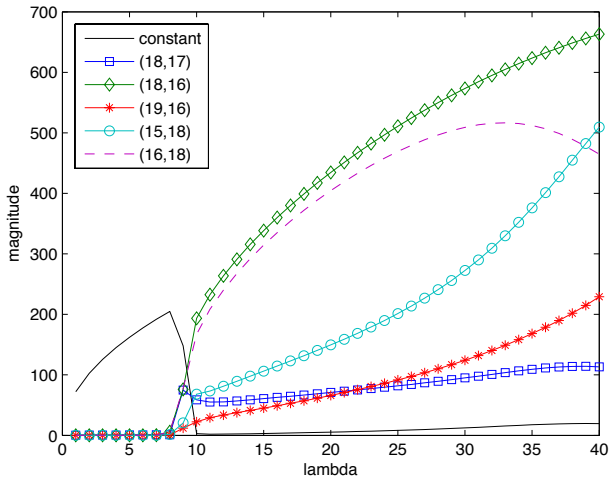

Figure 8: Plot of main modes of E (averaged over $7 \leq \tau \leq 8$) for $1 \leq \lambda \leq 40$

values of the parameters. To see what happens to travelling waves, an initial condition in the form of a travelling wave was entered for the parameter set above, but in the long run the persistent pattern was unaffected. This can be explained by the perfect reflections at the boundaries translating, for example, an A_1 wave into an A_4 wave at the $y = -L_q/2$ boundary. Since these travelling waves have wavefronts in oblique directions the pattern resulting from this interaction is a travelling rectangle in the $-x$ direction. Consequently, any travelling wave pattern is likely to decay to travelling rectangles which, for small driving, turn into the predominant standing rectangles. The Fourier spectra show a preference for the constant mode for small λ confirming that the standing rectangles are stable for small driving. The modes that appear as λ increases depend upon the specific parameters of the system leading to different behaviors once the standing rectangles become unstable. Increasing λ activates more Fourier modes and causes time varying spectra leading to more complex wave patterns.

5.2 Effects of the Bounded Domain: $\rho_p, \rho_q \neq 1$

In this subsection we explore the role of the parameters ρ_p and ρ_q. We consider the case of $\rho_p = \rho_q = \rho_k$ and study two parameter sets that show distinct patterns in the perfectly

reflecting case. First, the PD set for the wobble-TR state at $\lambda = 11$, then for a random matrix that shows the V-stripe state at $\lambda = 37$. Secondly, the E set for the DX state at $\lambda = 15$. In each case we vary ρ_k over the range of $0.1 \leq \rho_k \leq 2$ in increments of 0.1.

The action of the boundary parameters ρ_p and ρ_q affect the solution of the W equation by scaling the averages. If $\rho_k < 1$ the averages become smaller, thus, when $\mathrm{Re}(e_j) < 0$ the averaged terms become less stabilizing and for $\rho_k > 1$ the averaged terms become more stabilizing. For the same value of λ, this effect means that $|W|$ will, on average, be larger for $\rho_k < 1$ and smaller for $\rho_k > 1$. It must be noted that changing ρ_p and ρ_q will have an effect on μ_c as seen in equation (3.28), increasing μ_c when the boundary parameters are less than one and decreasing μ_c when they are both greater than one. Note that since λ is relative to μ_c, changes in μ_c are adjusted for automatically in this method, thus simulations at the same value of λ are at different levels of driving for different values of ρ_k.

The boundary parameters also affect the A_j when they are constructed from the $\mathcal{O}(1)$ Y_j amplitudes due to the (x, y) powers occurring as multiplicative factors which act like "envelopes" on the A_j. For example, if $a = \alpha_p = \alpha_q = 0$, at $x = L_p/2$, $y = L_q/2$ we have $A_1 = \epsilon\rho_p\rho_q Y_1$ and at $x = -L_p/2$, $y = -L_q/2$ we have $A_1 = \epsilon Y_1$. Moreover, when $\rho_k < 1$ $|A_1|$ will, on average, have a minimum in the upper right hand corner of the cell and the related oblique travelling waves will be relatively small in that region. As $|A_1|$ becomes larger due to the "envelope" the oblique travelling wave will also grow in magnitude as it travels to the lower left corner where it is then reflected at a lower magnitude. This can be seen as energy absorption at the boundary taking an incident wave and reflecting it at a lower energy. For $\rho_k < 1$ the driving over the bulk is larger than R_c which grows the reflected waves as they travel across the cell until it interacts with the opposing edge. When $\rho_k > 1$ is sufficiently large, indicating a large energy input at the boundary, μ_c can be negative meaning that the driving for the system may be below R_c and still lead to persistent nontrivial patterns. This can be described as small perturbations being amplified at the reflecting boundary and then slowly decaying under a driving smaller than R_c until they become incident with the opposing boundary.

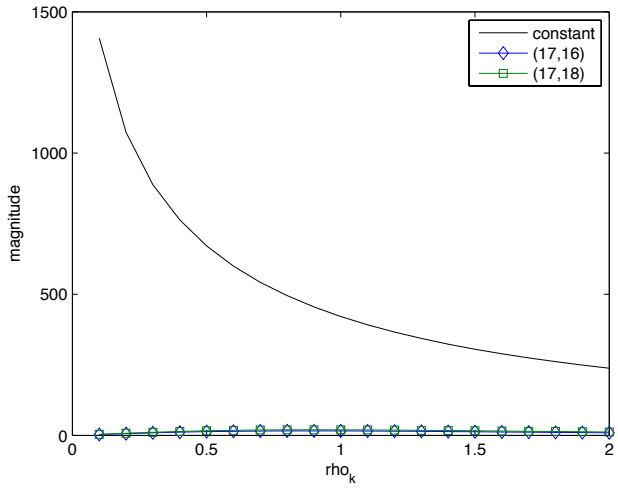

Figure 9: Plot of main modes of PD (averaged over $7 \leq \tau \leq 8$) at $\lambda = 11$ showing wobble-TR pattern at $\rho_k = 1$ for $0.1 \leq \rho_k \leq 2$.

We first consider the wobble-TR pattern of PD at $\lambda = 11$. At $\rho_k = 0.9$ the modification of the pattern is an off-center diamond pattern that alternates sides during the TR phase of the cycle as seen in Figure 10. As ρ_k decreases to 0.1, the periods of standing rectangles became shorter and the diamonds become more centered eventually becoming stationary, centered in the center of the cell, as the bounding 'ρ envelope' dominates the A_j's. As ρ_k increases above one, the behavior is similar to that of $\rho_k < 1$ with a diamond pattern alternating sides with waves emerging from the corners and moving towards the center. The centers of the alternating diamonds converge to the center of the cell as ρ_k increases to two. The $|W|$ solution maintains the behavior of the perfectly reflecting case for all values of ρ_k evaluated for this thesis. The Fourier spectrum of the $|W|$ solution is qualitatively similar to the spectrum for the $\rho_k = 1$ case in the previous section where the constant mode carries nearly all of the energy in the spectrum. However, the magnitude decreases as ρ_k increases, from 1405 at $\rho_k = 0.1$ to 237 at $\rho_k = 2$ as can be seen in Figure 9. The small values for (17,16) and (17,18) are largest around $\rho_k = 1$ and decrease for both smaller and larger ρ_k indicating that they could be the cause of the off-center minima for the diamond pattern.

For the V-stripe pattern we use the same random matrix for simulations at all values

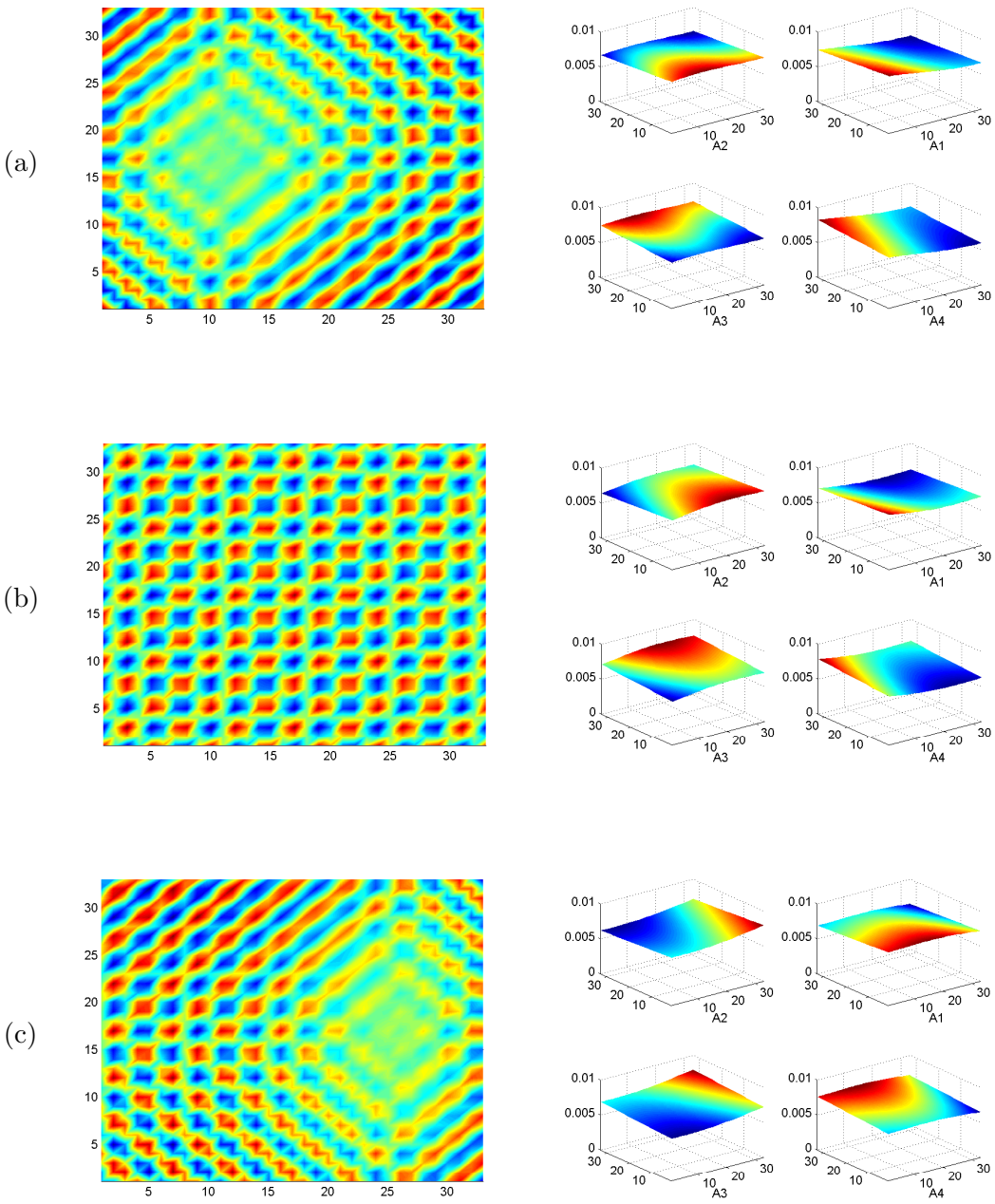

Figure 10: wobble-TR pattern (left) showing off-center diamonds and $|A_j|$ (right) with $\rho_k = 0.9$ for PD at $\lambda = 12$ for (a) $\tau = 5.5584$, (b) $\tau = 5.5603$, (c) $\tau = 5.6107$.

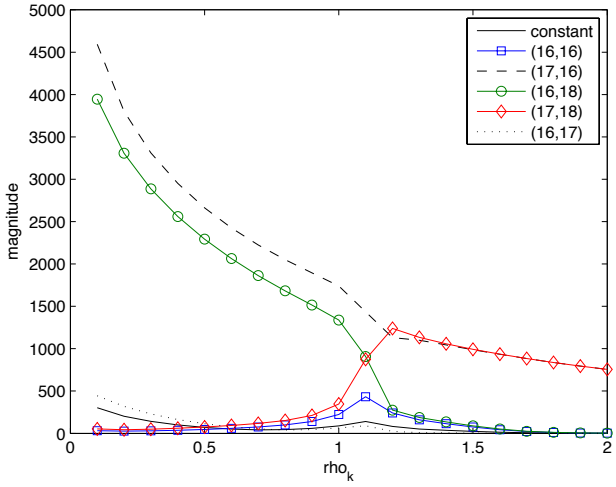

Figure 11: Plot of main modes of PD (averaged over $7 \leq \tau \leq 8$) at $\lambda = 37$ showing V-stripe pattern at $\rho_k = 1$ for $0.1 \leq \rho_k \leq 2$.

of ρ_k of PD such that the V-stripe pattern is stable at $\lambda = 37$ when $\rho_k = 1$. For this set of parameters we find the spatial average of $|A_j|$ an order of magnitude larger than the previous patterns. Consequently, the smaller variations for ρ_k less than one induce no observable change to the pattern as these are dominated by the driving term. The first discernible change as ρ_k decreases occurs at $\rho_k = 0.6$ as a slight tendency of the rectangles near the corners to move towards the corners with no noticeable change near the center. The corners eventually have phases of waves moving towards the corners while the V-stripe pattern persists in the middle of the cell for small $\rho_k = 0.1$ as seen in Figure 12. The $|W|$ solutions at $\rho_k = 1$ for this initial random matrix show the oblique rolls with two periods in the domain and show small spatial and temporal variations along the directions of the rolls. The Fourier spectrum of the $|W|$ solution at $\rho_k = 1$ (averaged over $7 \leq \tau \leq 8$) has dominant peaks at (17,16) and (16,18) as seen in Figure 11, with temporal variation in several neighboring peaks. As ρ_k decreases, the size and frequency of the spatial variations increase and the frequency of the temporal changes increase in magnitude. However, the size of the oblique rolls also increases, with $|W|$ showing larger maxima as ρ_k decreases. This keeps the ridges of the oblique rolls the dominant feature of the $|A_j|$, which causes the

observed pattern to remain unchanged in the bulk.

Above $\rho_k = 1$ the behavior changes more fundamentally. At $\rho_k = 1.2$ the pattern shows a TR-crash behavior with no hint of stationary oblique waves as can be seen in Figure 13. The $|W|$ solution fundamentally changes behavior with rolls in the X-direction replacing the oblique rolls with two periods in the X direction and a slow temporal undulation of the rolls in the Y direction. As can be seen in Figure 11 the dominant modes are transitioning at $\rho_k = 1.1$ and at $\rho_k = 1.2$ the (17,16) and (17,18) modes are dominant and nearly identical in magnitude while the (16,18) mode is significantly diminished. The (17,16) and (17,18) modes are dominant in the $\rho_k = 1$ case indicating X-periodicity with two rolls in that direction and, at most, only slight Y variation, which is what we see for $\rho_k \geq 1.2$ indicating the TR-crash behavior. As ρ_k approaches 2 the TR-crash pattern continues with center-moving oblique waves beginning to become more apparent at the corners. The V-stripe behavior does not reappear for $\rho_k > 1$. The Fourier spectra for $\lambda = 37$, using this specific initial random matrix, show time dependence for all ρ_k and shows significant variation in dominant modes as ρ_k changes.

The last set of parameters we consider is E which shows a DX pattern at $\lambda = 15$ when $\rho_k = 1$. Once again, the first variation of the pattern is a tendency for the waves to move towards the corners as ρ_k becomes smaller than one. This becomes more pronounced and becomes persistent as ρ_k decreases to 0.1 as can be seen in Figure 15. For increasing ρ_k above one, the DX pattern is robust against small increases and shows the tendency to have some motion of the rectangles from the corners towards the center during the shifts between the diamond and X patterns. This tendency for center moving waves simply becomes stronger as ρ_k increases without eliminating the DX pattern up to $\rho_k = 2$. The $|W|$ solutions for all values of ρ_k studied show temporally constant oblique rolls with two periods in the domain. This set of parameters shows a Fourier spectrum for W where the primary peaks are at the (16,18) and (18,16) modes, and the energy decreases in magnitude as ρ_k increases as seen in Figure 14. The magnitudes decrease consistently as ρ_k increases with no other modes showing increases which reinforces the persistence of the DX pattern throughout the full

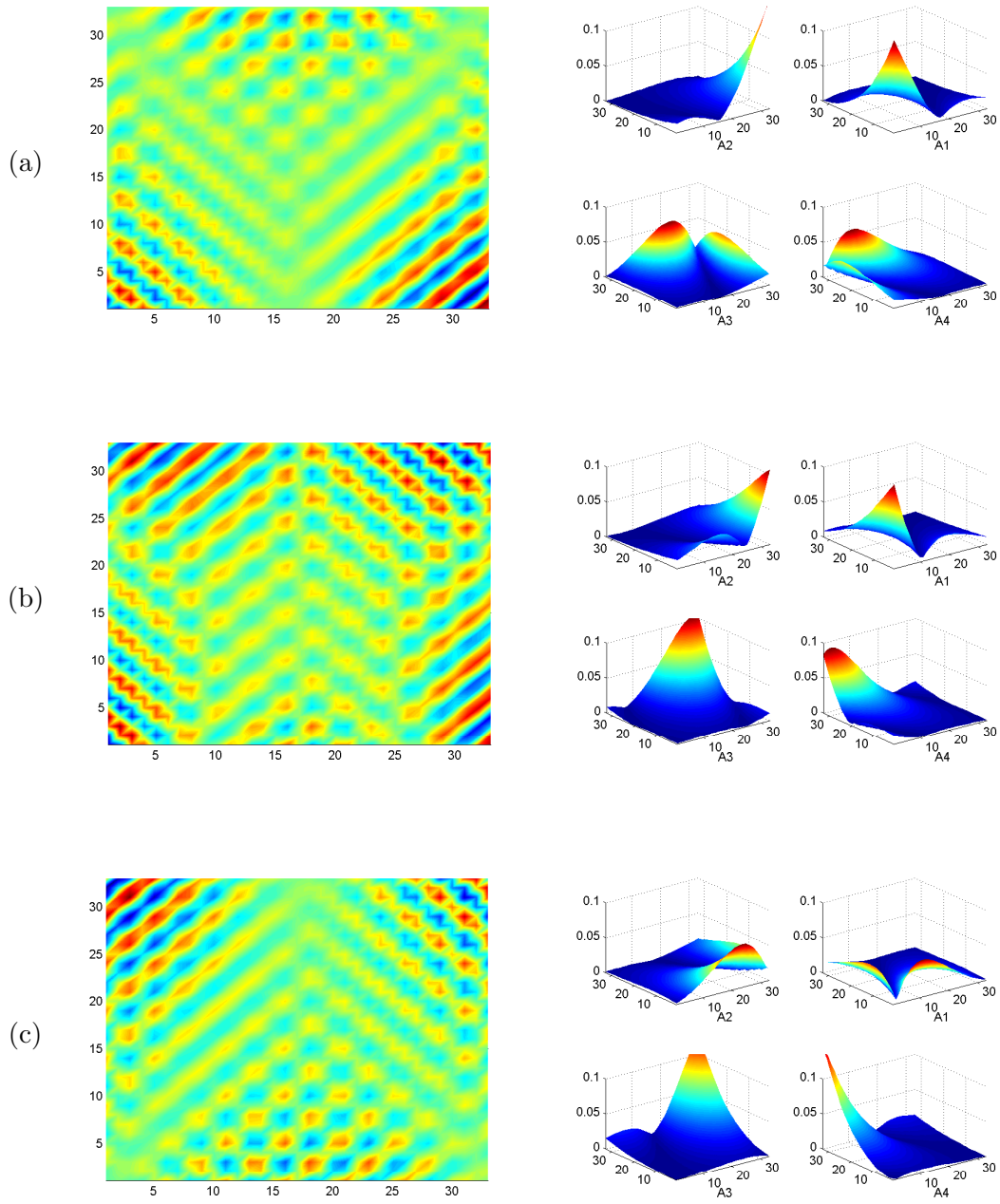

Figure 12: V-stripe pattern (left) showing travelling waves moving towards the corners and $|A_j|$ (right) at $\rho_k = 0.1$ for PD at $\lambda = 37$ for (a) $\tau = 6.6371$, (b) $\tau = 6.6458$, (c) $\tau = 6.6557$.

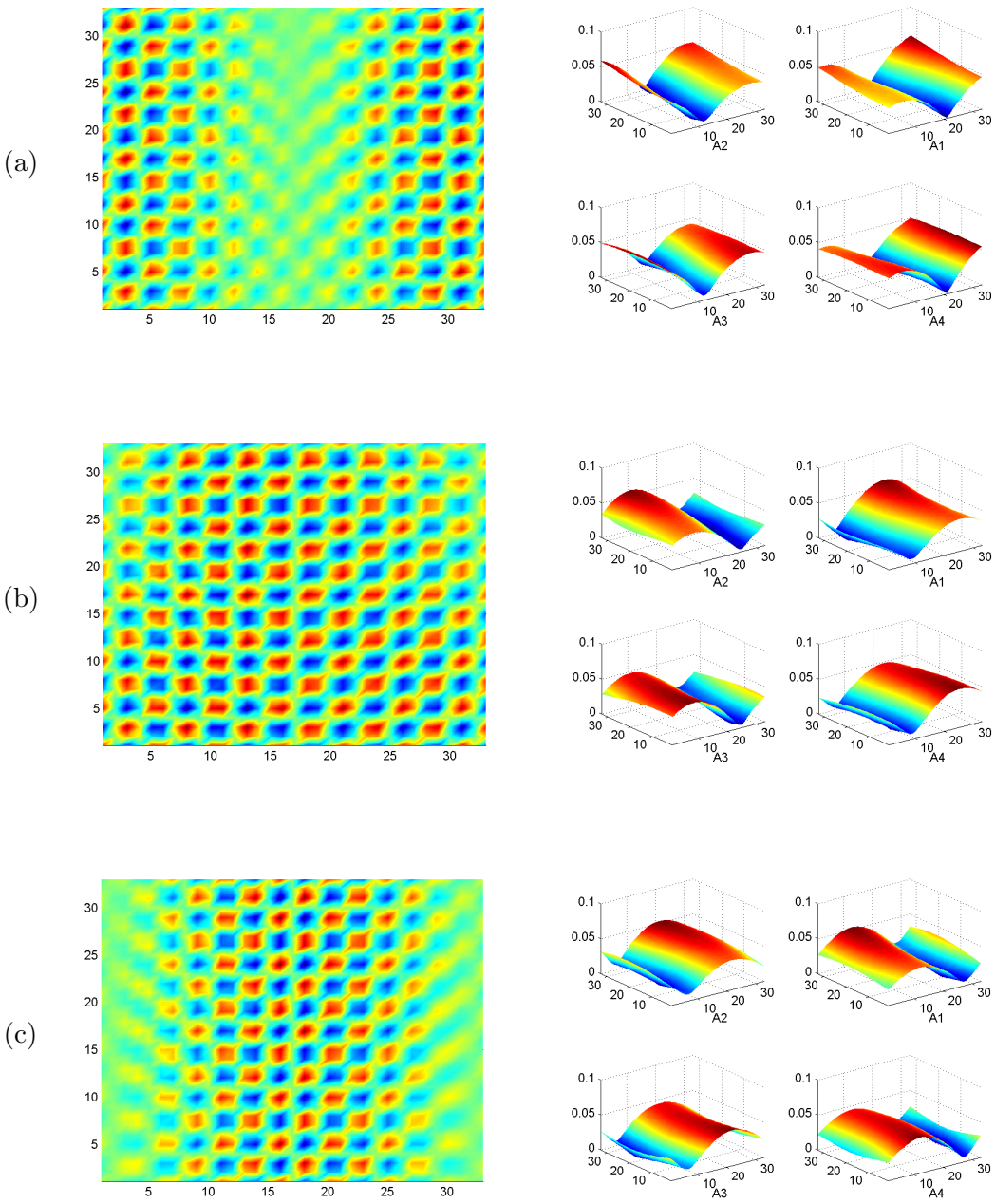

Figure 13: V-stripe pattern (left) showing TR-crash pattern and $|A_j|$ (right) at $\rho_k = 1.2$ for PD at $\lambda = 37$ for (a) $\tau = 6.5833$, (b) $\tau = 6.5899$, (c) $\tau = 6.5965$.

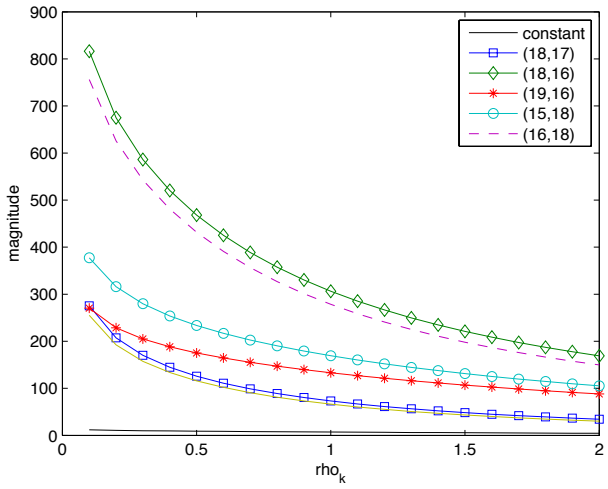

Figure 14: Plot of main modes of E (averaged over $7 \leq \tau \leq 8$) at $\lambda = 15$ showing DX pattern at $\rho_k = 1$ for $0.1 \leq \rho_k \leq 2$.

range of the boundary parameter.

Varying the boundary parameter ρ_k has an effect on the overall pattern. For patterns where $|W|$ is spatially and temporally slowly varying and small this is most evident in the behavior of the patterns near the edges while the behavior in the center of the cell is nearly unchanged. For patterns where $|W|$ is relatively large with relatively dynamic spatial and temporal behavior, such as the V-stripe pattern, a change in ρ_k can change the nature of the $|W|$ solution leading to a change of the pattern in the bulk as well as causing travelling oblique waves in the corners.

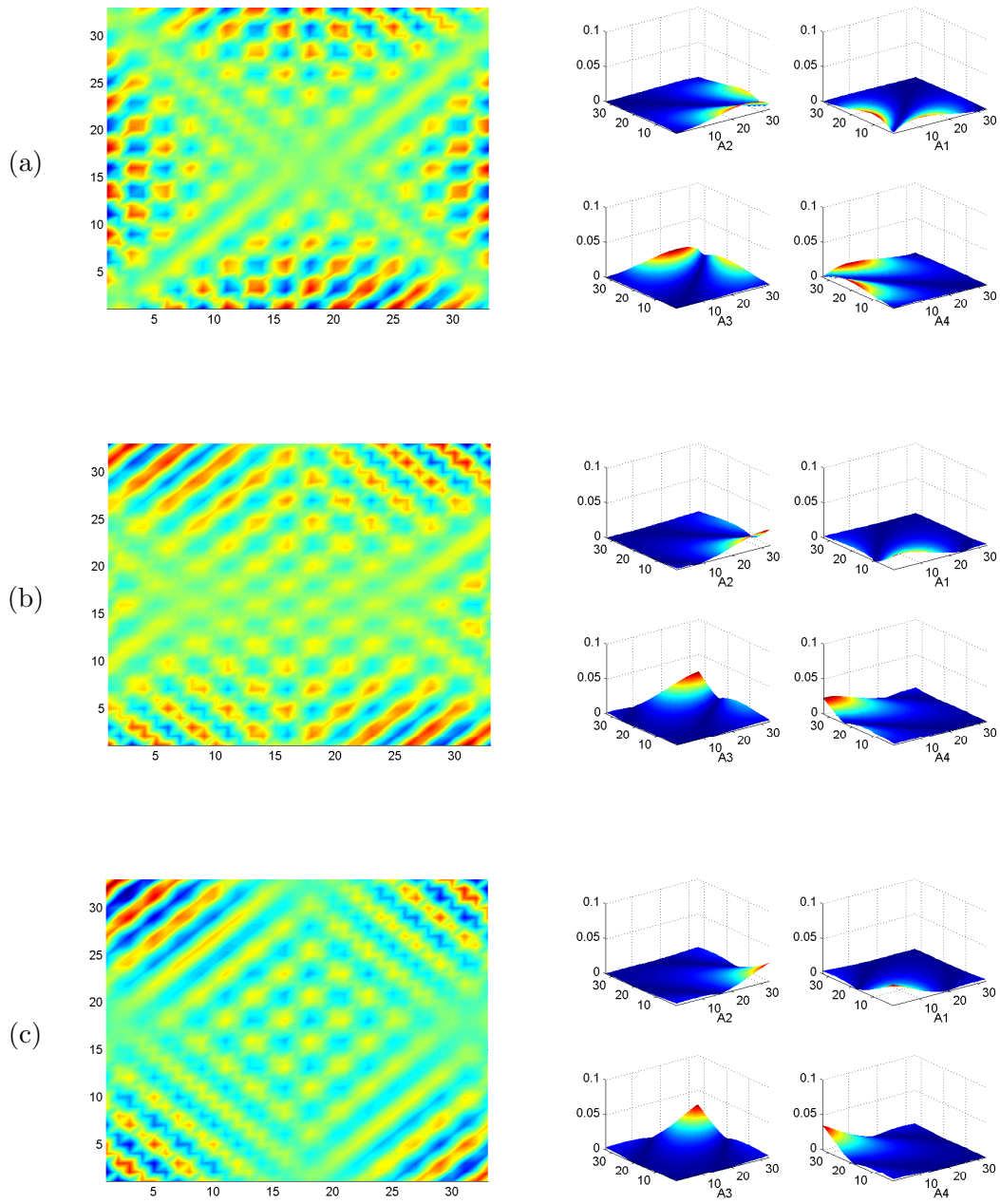

Figure 15: DX pattern (left) and $|A_j|$ (right) with $\rho_k = 0.1$ for E at $\lambda = 15$ for (a) $\tau = 6.5768$, (b) $\tau = 6.5899$, (c) $\tau = 6.6009$.

6 Conclusions

In this thesis we constructed a globally coupled Ginzburg-Landau equation from a set of coupled reaction diffusion equations posed in a large, but finite domain. We have shown that boundary conditions have an effect on the coupling of the equations and developed a method for finding solutions for the four main envelopes via a single, doubly periodic function $W(X, Y, \tau)$ obtained from the envelopes by applying a reflection principle. The resultant patterns of the original system can then be determined via a simplified system for W. Therefore the specific patterns observed, and over which intervals of external driving these patterns are stable, can be found by studying the W-solutions. This is much easier to pursue than computing the complex wave patterns of the original system.

Beyond this computational advantage, the importance ('added value') of our work lies in the fact that the equation for W is canonical, and is valid for any anisotropic PDE-system with two reflection symmetries that is posed in a large rectangle and encounters a Hopf bifurcation with four oblique travelling waves. The derivation in this thesis was done specifically for reaction diffusion systems with second order diffusion terms, however, the same procedure is applicable to other system as well, including the weak electrolyte model for electroconvection in nematic liquid crystals. A first step towards more general equations has been made by including higher order diffusion terms in the Activator-Inhibitor system.

Due to the boundary conditions, which allowed us to reduce the four coupled evolution equations to a single equation, the simulation of the amplitudes could be simplified to simulating the single equation for W in the doubly periodic domain for the characteristic wave variables using a Fourier-Galerkin approximation. The envelopes modulating the initial unstable modes could then be extracted from W by performing a computationally straightforward spatial transformation. In comparison to simulations of the unbounded case, we have seen that the boundary interactions have changed the behaviors of solutions in various parameter regimes. This exploration is by no means exhaustive and further simulations need to be done to see whether the behaviors of the infinite extent case are simply shifted to other parameter values, or precluded by the finite boundaries altogether.

The W-equation derived for the finite size system contains a rescaled bifurcation parameter, λ, and an aspect ratio, l. These parameters are not present in the four globally coupled Ginzburg Landau equations resulting for the unbounded domain, the parameter $\mathrm{Re}(a_0)$ in (2.23) can be rescaled to unity (which was done in [21]). In particular the variation of λ had a strong effect on the observed solutions in that their complexity increased when λ was increased. The reason is that the eigenvalues of the linearized W-system are discrete, and more and more modes get excited (non-decaying in the linearized W-equation) when λ increases. On the other hand, for small λ we always observed standing rectangles governed by a single mode. Since for any finite λ the number of excited modes is finite, it is tempting to assume that the W-dynamics resides in an attracting invariant manifold ('inertial manifold,' see [8]), whose dimension increases when λ crosses certain discrete values. On the other hand, an inertial manifold for the W-system would correspond to an inertial manifold for the original reaction diffusion system, and $O(1)$-variations of λ correspond to $O(\epsilon^2)$-variations of the original bifurcation parameter. This sensitivity of solutions of a 'finite size Ginzburg Landau system' on a rescaled bifurcation parameter can be expected for any type of instability, and could provide a new approach for computing and characterizing inertial manifolds in evolution equations posed in large domains under variation of a parameter.

Further extensions of this work include a numerical representation of the boundary layer solution that can be added to the bulk solution to improve the simulation of patterns in the entire domain. Another exploration is to pursue the derivation of the amplitude equations for more general evolution equations. A more challenging extension is to consider more general domains with curved boundaries. The bulk expansion is then still valid, but the boundary layer expansion and the matching become more difficult. In particular, curved boundaries will eliminate the ability to utilize a doubly periodic domain.

A Details of the Expansions in Section 3

A.1 Bulk Expansion

The complete expansion considered in the representation of the bulk solution as described in Section 3.2 is given by,

$$\begin{aligned}
u &= \{[(A_1U_0+V_1)e^{ip_cx+iq_cy}+(A_2U_0+V_2)e^{-ip_cx+iq_cy} \\
&\quad +(A_3U_0+V_3)e^{-ip_cx-iq_cy}+(A_4U_0+V_4)e^{+ip_cx-iq_cy}]e^{i\omega t}+cc\} \\
&\quad +\{[(A_1)^2e^{i2p_cx+i2q_cy}+(A_2)^2e^{-i2p_cx+i2q_cy)}+(A_3)^2e^{-i2p_cx-i2q_cy} \\
&\quad +(A_4)^2e^{i2p_cx-i2q_cy)}]e^{i2\omega t}U_6 \\
&\quad +[(A_1A_3+A_2A_4)W_{11}+(A_1A_2e^{i2q_cy}+A_3A_4e^{-i2q_cy})W_{12} \\
&\quad +(A_1A_4e^{i2p_cx}+A_2A_3e^{-i2p_cx})W_{13}]e^{i2\omega t} \\
&\quad +(A_1\bar{A}_3e^{i2p_cx+i2q_cy}+A_2\bar{A}_4e^{-i2p_cx+i2q_cy})W_{21} \\
&\quad +(A_1\bar{A}_2+\bar{A}_3A_4)e^{i2p_cx}W_{22}+(A_1\bar{A}_4+A_2\bar{A}_3)e^{i2q_cy}W_{23}+cc\} \\
&\quad +[|A_1|^2+|A_2|^2+|A_3|^2+|A_4|^2]U_7+HONRT,
\end{aligned} \tag{A.1}$$

where $HONRT$ denotes higher order non-resonant terms. The resonant term V_1 is expanded as,

$$\begin{aligned}
V_1 &= -iA_{1x}(U_{1p}+\mu U_{4p})-iA_{1y}(U_{1q}+\mu U_{4q})-A_{1xx}U_{2pp}-2A_{1xy}U_{2pq}-A_{1yy}U_{2qq} \\
&\quad +\mu A_1(U_3+\mu U_5)+A_1(|A_1|^2U_8+|A_2|^2U_9+|A_3|^2U_{10}+|A_4|^2U_{11}) \\
&\quad +A_2\bar{A}_3A_4U_{12}+HORT,
\end{aligned}$$

with $HORT$ denoting resonant terms of higher order. The other resonant terms V_2, V_3, V_4 follow by applying to V_1 the symmetry operations,

$$\begin{aligned}
(x, y, A_1, A_2, A_3, A_4) &\rightarrow (-x, y, A_2, A_1, A_4, A_3), \\
(x, y, A_1, A_2, A_3, A_4) &\rightarrow (-x, -y, A_3, A_4, A_1, A_2), \\
(x, y, A_1, A_2, A_3, A_4) &\rightarrow (x, -y, A_4, A_3, A_2, A_1),
\end{aligned} \tag{A.2}$$

respectively, leading to

$$\begin{aligned}
V_2 &= iA_{2x}(U_{1p} + \mu U_{4p}) - iA_{2y}(U_{1q} + \mu U_{4q}) - A_{2xx}U_{2pp} + 2A_{2xy}U_{2pq} - A_{2yy}U_{2qq} \\
&\quad +\mu A_2(U_3 + \mu U_5) + A_2(|A_2|^2U_8 + |A_1|^2U_9 + |A_4|^2U_{10} + |A_3|^2U_{11}) \\
&\quad +A_3\bar{A}_4A_1U_{12} + HORT
\end{aligned}$$

$$\begin{aligned}
V_3 &= iA_{3x}(U_{1p} + \mu U_{4p}) + iA_{3y}(U_{1q} + \mu U_{4q}) - A_{3xx}U_{2pp} - 2A_{3xy}U_{2pq} - A_{3yy}U_{2qq} \\
&\quad +\mu A_3(U_3 + \mu U_5) + A_3(|A_3|^2U_8 + |A_4|^2U_9 + |A_1|^2U_{10} + |A_2|^2U_{11}) \\
&\quad +A_4\bar{A}_1A_2U_{12} + HORT
\end{aligned}$$

$$\begin{aligned}
V_4 &= -iA_{4x}(U_{1p} + \mu U_{4p}) + iA_{4y}(U_{1q} + \mu U_{4q}) - A_{4xx}U_{2pp} + 2A_{4xy}U_{2pq} - A_{4yy}U_{2qq} \\
&\quad +\mu A_4(U_3 + \mu U_5) + A_4(|A_4|^2U_8 + |A_3|^2U_9 + |A_2|^2U_{10} + |A_1|^2U_{11}) \\
&\quad +A_1\bar{A}_2A_3U_{12} + HORT
\end{aligned}$$

The evolution equations for A_2, A_3, A_4 follow from (3.8) also by the operations (A.2),

$$\begin{aligned}
A_{2t} &= -(v_p + \mu b_{1p})A_{2x} + (v_q + \mu b_{1q})A_{2y} + d_{pp}A_{2xx} - 2d_{pq}A_{2xy} + d_{qq}A_{2yy} \\
&\quad +A_2(\mu a_0 + \mu^2 a_1 + e_1|A_2|^2 + e_2|A_1|^2 + e_3|A_4|^2 + e_4|A_3|^2) + e_5A_3\bar{A}_4A_1 + HOT
\end{aligned} \tag{A.3}$$

$$
\begin{aligned}
A_{3t} \;=\; & -(v_p+\mu b_{1p})A_{3x}-(v_q+\mu b_{1q})A_{3y}+d_{pp}A_{3xx}+2d_{pq}A_{3xy}+d_{qq}A_{3yy} \\
& +A_3(\mu a_0+\mu^2 a_1+e_1|A_3|^2+e_2|A_4|^2+e_3|A_1|^2+e_4|A_2|^2)+e_5A_4\bar{A}_1A_2+HOT
\end{aligned}
\tag{A.4}
$$

$$
\begin{aligned}
A_{4t} \;=\; & (v_p+\mu b_{1p})A_{4x}-(v_q+\mu b_{1q})A_{4y}+d_{pp}A_{4xx}-2d_{pq}A_{4xy}+d_{qq}A_{4yy} \\
& +A_4(\mu a_0+\mu^2 a_1+e_1|A_4|^2+e_2|A_3|^2+e_3|A_2|^2+e_4|A_1|^2)+e_5A_1\bar{A}_2A_3+HOT
\end{aligned}
\tag{A.5}
$$

Proceeding as explained in Section 3.2, shows that the non-resonant expansion vectors are the unique solutions of the equations,

$$
\begin{aligned}
&(A_1)^2\text{-terms:} && T(4p_c^2,4q_c^2,2\omega)U_6 &&= -\mathcal{B}(U_0,U_0),\\
&|A_1|^2\text{-terms:} && T(0,0,0)U_7 &&= -2\mathcal{B}(U_0,\overline{U}_0),\\
&A_1A_3 \text{ and } A_2A_4\text{-terms:} && T(0,0,2\omega)W_{11} &&= -2\mathcal{B}(U_0,U_0),\\
&A_1A_2 \text{ and } A_3A_4\text{-terms:} && T(0,4q_c^2,2\omega)W_{12} &&= -2\mathcal{B}(U_0,U_0),\\
&A_1A_4 \text{ and } A_2A_3\text{-terms:} && T(4p_c^2,0,2\omega)W_{13} &&= -2\mathcal{B}(U_0,U_0),\\
&A_1\overline{A}_3 \text{ and } A_2\overline{A}_4\text{-terms:} && T(4p_c^2,4q_c^2,0)W_{21} &&= -2\mathcal{B}(U_0,\overline{U}_0),\\
&A_1\overline{A}_2 \text{ and } A_4\overline{A}_3\text{-terms:} && T(4p_c^2,0,0)W_{22} &&= -2\mathcal{B}(U_0,\overline{U}_0),\\
&A_1\overline{A}_4 \text{ and } A_2\overline{A}_3\text{-terms:} && T(0,4q_c^2,0)W_{23} &&= -2\mathcal{B}(U_0,\overline{U}_0),
\end{aligned}
\tag{A.6}
$$

where $T(p^2,q^2,\Omega)=F_1-p^2D_p-q^2D_q-i\Omega I$. The resonant expansion vectors satisfy,

$$
\begin{aligned}
&A_1|A_1|^2\text{-terms:}\;\; T(p_c^2,q_c^2,\omega)U_8=e_1U_0-2\mathcal{B}(U_0,U_7)-2\mathcal{B}(\bar{U}_0,U_6)-3\mathcal{C}(U_0,U_0,\overline{U}_0),\\
&A_1|A_2|^2\text{-terms:}\;\; T(p_c^2,q_c^2,\omega)U_9=e_2U_0-2[\mathcal{B}(U_0,U_7+W_{22})+\mathcal{B}(\overline{U}_0,W_{12})+3\mathcal{C}(U_0,U_0,\overline{U}_0)],\\
&A_1|A_3|^2\text{-terms:}\; T(p_c^2,q_c^2,\omega)U_{10}=e_3U_0-2[\mathcal{B}(U_0,U_7+W_{21})+\mathcal{B}(\overline{U}_0,W_{11})+3\mathcal{C}(U_0,U_0,\overline{U}_0)],\\
&A_1|A_4|^2\text{-terms:}\; T(p_c^2,q_c^2,\omega)U_{11}=e_4U_0-2[\mathcal{B}(U_0,U_7+W_{23})+\mathcal{B}(\overline{U}_0,W_{13})+3\mathcal{C}(U_0,U_0,\overline{U}_0)],\\
&A_2\overline{A}_3A_4\text{-terms:}\, T(p_c^2,q_c^2,\omega)U_{12}=e_5U_0-2[\mathcal{B}(U_0,W_{22}+W_{23})+\mathcal{B}(\overline{U}_0,W_{11})+3\mathcal{C}(U_0,U_0,\overline{U}_0)],
\end{aligned}
\tag{A.7}
$$

and the solvability conditions yield the nonlinear coefficients in the envelope equations,

$$\begin{aligned}
e_1 &= \overline{U}_0^{*T}(2\mathcal{B}(U_0,U_7)+2\mathcal{B}(\overline{U}_0,U_6)+3\mathcal{C}(U_0,U_0,\overline{U}_0)),\\
e_2 &= 2\overline{U}_0^{*T}(\mathcal{B}(U_0,U_7+W_{22})+\mathcal{B}(\overline{U}_0,W_{12})+3\mathcal{C}(U_0,U_0,\overline{U}_0)),\\
e_3 &= 2\overline{U}_0^{*T}(\mathcal{B}(U_0,U_7+W_{21})+\mathcal{B}(\overline{U}_0,W_{11})+3\mathcal{C}(U_0,U_0,\overline{U}_0)),\\
e_4 &= 2\overline{U}_0^{*T}(\mathcal{B}(U_0,U_7+W_{23})+\mathcal{B}(\overline{U}_0,W_{13})+3\mathcal{C}(U_0,U_0,\overline{U}_0)),\\
e_5 &= 2\overline{U}_0^{*T}(\mathcal{B}(U_0,W_{22}+W_{23})+\mathcal{B}(\overline{U}_0,W_{11})+3\mathcal{C}(U_0,U_0,\overline{U}_0)).
\end{aligned} \tag{A.8}$$

A.2 Expansion at the Edge $y \sim -L_q/2$

The solution in the edge layer $y \sim -L_q/2$ is expanded in terms of slowly varying envelopes $M(x,t)$ and $N(x,t)$ similarly as the bulk solution in [43] in the form,

$$\begin{aligned}
u &= [(M\mathcal{U}^0 - iM_x(\mathcal{U}^1+\mu\mathcal{U}^4) - M_{xx}\mathcal{U}^2+\mu M(\mathcal{U}^3+\mu\mathcal{U}^5)\\
&\quad +M|M|^2\mathcal{U}^8+M|N|^2\mathcal{U}^9+M_t\mathcal{U}^{10}+HORT)e^{ip_cx+i\omega t}+cc]\\
&\quad +[(N\mathcal{U}^0+iN_x(\mathcal{U}^1+\mu\mathcal{U}^4)-N_{xx}\mathcal{U}^2+\mu N(\mathcal{U}^3+\mu\mathcal{U}^5)+N|N|^2\mathcal{U}^8\\
&\quad +N|M|^2\mathcal{U}^9+N_t\mathcal{U}^{10}+HORT)e^{-ip_cx+i\omega t}+cc]\\
&\quad +[(M^2e^{i2p_cx}+N^2e^{-i2p_cx})\mathcal{U}^6e^{i2\omega t}+MN\mathcal{W}^1e^{i2\omega t}+M\overline{N}\mathcal{W}^2e^{i2p_cx}\\
&\quad +cc]+(|M|^2+|N|^2)\mathcal{U}^7+HONRT,
\end{aligned} \tag{A.9}$$

where the expansion functions $\mathcal{U}^j(\tilde{y})$ depend on the edge variable $\tilde{y} = y+L_q/2$, and $HORT$ and $HONRT$ stand again for higher order resonant non-resonant terms, respectively. The

nonhomogeneous differential equations for the coefficient functions in (A.9) are,

$$
\begin{aligned}
M_x: \quad & D_q\mathcal{U}^1_{\tilde{y}\tilde{y}} + (-p_c^2 D_p + F_1 - i\omega I)\mathcal{U}^1 &&= 2p_c D_p \mathcal{U}^0,\\
M_{xx}: \quad & D_q\mathcal{U}^2_{\tilde{y}\tilde{y}} + (-p_c^2 D_p + F_1 - i\omega I)\mathcal{U}^2 &&= 2p_c D_p \mathcal{U}^1 + D_p\mathcal{U}^0,\\
\mu M: \quad & D_q\mathcal{U}^3_{\tilde{y}\tilde{y}} + (-p_c^2 D_p + F_1 - i\omega I)\mathcal{U}^3 &&= -f_2\mathcal{U}^0 - 2\mathcal{B}_1(u^1,\mathcal{U}^0),\\
\mu M_x: \quad & D_q\mathcal{U}^4_{\tilde{y}\tilde{y}} + (-p_c^2 D_p + F_1 - i\omega I)\mathcal{U}^4 &&= -f_2\mathcal{U}^1 + 2p_c D_p\mathcal{U}^3 - 2\mathcal{B}_1(u^1,\mathcal{U}^1),\\
\mu^2 M: \quad & D_q\mathcal{U}^5_{\tilde{y}\tilde{y}} + (-p_c^2 D_p + F_1 - i\omega I)\mathcal{U}^5 &&= -f_3\mathcal{U}^0 - f_2\mathcal{U}^3 - 2\mathcal{B}_1(u^1,\mathcal{U}^3),\\
M^2: \quad & D_q\mathcal{U}^6_{\tilde{y}\tilde{y}} + (-4p_c D_p + F_1 - i2\omega I)\mathcal{U}^6 &&= -2\mathcal{B}(\mathcal{U}^0,\mathcal{U}^0),\\
|M|^2: \quad & D_q\mathcal{U}^7_{\tilde{y}\tilde{y}} + F_1\mathcal{U}^7 &&= -2\mathcal{B}(\mathcal{U}^0,\bar{\mathcal{U}}^0),\\
MN: \quad & D_q\mathcal{W}^1_{\tilde{y}\tilde{y}} + (F_1 - i2\omega I)\mathcal{W}^1 &&= -2\mathcal{B}(\mathcal{U}^0,\mathcal{U}^0),\\
M\bar{N}: \quad & D_q\mathcal{W}^2_{\tilde{y}\tilde{y}} + (-4p_c^2 D_p + F_1)\mathcal{W}^2 &&= -2\mathcal{B}(\mathcal{U}^0,\bar{\mathcal{U}}^0),\\
M|M|^2: \quad & D_q\mathcal{U}^8_{\tilde{y}\tilde{y}} + (F_1 - p_c^2 D_p - i\omega I)\mathcal{U}^8 &&= -2\mathcal{B}_1(\mathcal{U}^7,\mathcal{U}^0) - 2\mathcal{B}_1(\mathcal{U}^6,\bar{\mathcal{U}}^0)\\
& && \quad -3\mathcal{C}_1(\mathcal{U}^0,\mathcal{U}^0,\bar{\mathcal{U}}^0),\\
M|N|^2: \quad & D_q\mathcal{U}^9_{\tilde{y}\tilde{y}} + (F_1 - p_c^2 D_p - i\omega I)\mathcal{U}^9 &&= -2\mathcal{B}_1(\mathcal{U}^7 + \mathcal{W}^2,\mathcal{U}^0) - 2\mathcal{B}_1(\mathcal{W}^1,\bar{\mathcal{U}}^0)\\
& && \quad -6\mathcal{C}_1(\mathcal{U}^0,\mathcal{U}^0,\bar{\mathcal{U}}^0),\\
M_t: \quad & D_q\mathcal{U}^{10}_{\tilde{y}\tilde{y}} + (F_1 - p_c^2 D_p - i\omega I)\mathcal{U}^{10} &&= \mathcal{U}^0.
\end{aligned}
\tag{A.10}
$$

The leading order coefficient function $\mathcal{U}^0(\tilde{y})$ is determined as described in Section 3.3. The higher order functions $\mathcal{U}^j(\tilde{y})$ have to satisfy the same boundary conditions at $\tilde{y} = 0$ and for $\tilde{y} \to \infty$ (remain bounded) as $\mathcal{U}^0(\tilde{y})$.

For matching purposes we only need to consider the asymptotic behavior of the $\mathcal{U}^j(\tilde{y})$,

and using (3.13) we determine the asymptotic behavior of the $\mathcal{U}^j(\tilde{y})$ as follows,

$$\begin{aligned}
\mathcal{U}^1 &= [-\tfrac{v_p}{v_q}(i\tilde{y}U_0 + U_{1q}) + U_{1p}]e^{iq_c\tilde{y}} + r_q[-\tfrac{v_p}{v_q}(-i\tilde{y}U_0 + U_{1q}) + U_{1p}]e^{-iq_c\tilde{y}} + EST,\\
\mathcal{U}^3 &= [\tfrac{ia_0}{v_q}(i\tilde{y}U_0 + U_{1q}) + U_3]e^{iq_0\tilde{y}} + r_q[\tfrac{ia_0}{v_q}(-i\tilde{y}U_0 + U_{1q}) + U_3]e^{-iq_0\tilde{y}} + EST,\\
\mathcal{U}^6 &= (e^{2iq_0\tilde{y}} + r_q^2e^{-2iq_0\tilde{y}})U_6 + r_qW_{13} + EST,\\
\mathcal{U}^7 &= (1+|r_q|^2)U_7 + (\bar{r}_qe^{2iq_0\tilde{y}} + r_qe^{-2iq_0\tilde{y}})W_{23} + EST,\\
\mathcal{W}^1 &= 2r_qW_{11} + (e^{2iq_0\tilde{y}} + r_q^2e^{-2iq_0\tilde{y}})W_{12} + EST,\\
\mathcal{W}^2 &= (1+|r_q|^2)W_{22} + (\bar{r}_qe^{2iq_0\tilde{y}} + r_qe^{-2iq_0\tilde{y}})W_{21} + EST,\\
\mathcal{U}^8 &= [i\tfrac{e_1+|r_q|^2e_4}{v_q}(i\tilde{y}U_0 + U_{1q}) + U_8 + |r_q|^2U_{11}]e^{iq_0\tilde{y}}\\
&\quad + r_q[i\tfrac{|r_q|^2e_1+e_4}{v_q}(-i\tilde{y}U_0 + U_{1q}) + |r_q|^2U_8 + U_{11}]e^{-iq_0\tilde{y}} + EST,\\
\mathcal{U}^9 &= [i\tfrac{e_2+|r_q|^2(e_3+e_5)}{v_q}(i\tilde{y}U_0 + U_{1q}) + U_9 + |r_q|^2(U_{10}+U_{12})]e^{iq_0\tilde{y}}\\
&\quad + r_q[i\tfrac{|r_q|^2e_2+e_3+e_5}{v_q}(-i\tilde{y}U_0 + U_{1q}) + |r_q|^2U_9 + U_{10} + U_{12}]e^{-iq_0\tilde{y}} + EST,\\
\mathcal{U}^{10} &= \tfrac{-i}{v_q}(i\tilde{y}U_0 + U_{1q})e^{iq_0\tilde{y}} + \tfrac{-ir_q}{v_q}(-i\tilde{y}U_0 + U_{1q})e^{-iq_0\tilde{y}} + EST,
\end{aligned} \tag{A.11}$$

where EST denotes exponentially decaying terms. The functions in (A.11) evolve asymptotically towards expressions involving the vectors from the bulk solution. However, looking at the equation for $\mathcal{U}^2$,

$$(D_q\partial_{\tilde{y}\tilde{y}} - p_c^2D_p + F_1 - i\omega I)\mathcal{U}^2 = 2p_cD_p\mathcal{U}^1 + D_p\mathcal{U}^0 \tag{A.12}$$

the right hand side of this equation depends on $\mathcal{U}^1$ which, asymptotically, contains $\tilde{y}$ linearly. The explicit form of the equation for $\mathcal{U}^2$ is given by,

$$\begin{aligned}
(D_q\partial_{\tilde{y}\tilde{y}} - p_c^2D_p + F_1 - i\omega)\mathcal{U}^2 &= [(1 - 2p_c\frac{v_p}{v_q}\tilde{y})D_pU_0 - \frac{v_p}{v_q}2p_cD_pU_{1q} + 2p_cD_pU_{1p}]e^{iq_c\tilde{y}}\\
&\quad + r_q[(1 + 2p_c\frac{v_p}{v_q}\tilde{y})D_pU_0 - \frac{v_p}{v_q}2p_cD_pU_{1q} + 2p_cD_pU_{1p}]e^{-iq_c\tilde{y}}.
\end{aligned}$$

To solve for $\mathcal{U}^2$, we use the ansatz $\mathcal{U}^2 = [H_+^2 + \tilde{y}K_+^2 + \tilde{y}^2s_+^2U_0]e^{iq_c\tilde{y}} + r_q[H_-^2 - \tilde{y}K_-^2 +$

$\tilde{y}^2 s_-^2 U_0]e^{-iq_c\tilde{y}}$, and find that $s_+^2 = s_-^2 = iv_p^2/(2v_q^2)$, where $K_+^2 = K_-^2 = (v_p/v_q)[(v_p/v_q)U_{1q} - U_{1p}]$, which implies $H_+^2 = H_-^2$. This is sufficient to show that these terms don't contribute to the boundary conditions. Since we concentrate on the U_{1q} terms for the second boundary conditions at $\tilde{y} = 0$, the important finding is that, with $K_+^2 = K_-^2$, we necessarily find that the U_{1q} terms in each must be equal, ie $H_+^2 = H_-^2 = \nu^2 U_{1q}+$ other terms. Similar arguments lead to equivalent forms for $\mathcal{U}^4$ and $\mathcal{U}^5$.

Consequently, up to U_0 and U_{1q} terms, the edge expansion becomes,

$$
\begin{aligned}
u \;=\; & \{U_0 e^{iq_c\tilde{y}}\Big(M - \tilde{y}\Big[(\frac{v_p}{v_q} + i\mu s_4)M_x + s_2 M_{xx} + (\mu\frac{a_0}{v_q} - \mu^2 s_5)M \\
& \qquad + \frac{e_1 + |r_q|^2 e_4}{v_q} M|M|^2 + \frac{e_2 + |r_q|^2(e_3+e_5)}{v_q} M|N|^2\Big]\Big) \\
& + r_q U_0 e^{-iq_c\tilde{y}}\Big(M + \tilde{y}\Big[(\frac{v_p}{v_q} + i\mu s_4)M_x + s_2 M_{xx} + (\mu\frac{a_0}{v_q} - \mu^2 s_5)M \\
& \qquad + \frac{|r_q|^2 e_1 + e_4}{v_q} M|M|^2 + \frac{|r_q|^2 e_2 + e_3 + e_5}{v_q} M|N|^2\Big]\Big) \\
& + U_{1q} e^{iq_c\tilde{y}}\Big((\frac{iv_p}{v_q} - i\mu\nu_4)M_x - \nu_2 M_{xx} + (\mu\frac{ia_0}{v_q} + \mu^2\nu_5)M \\
& \qquad + i\frac{e_1 + |r_q|^2 e_4}{v_q} M|M|^2 + i\frac{e_2 + |r_q|^2(e_3+e_5)}{v_q} M|N|^2\Big) \\
& + r_q U_{1q} e^{-iq_c\tilde{y}}\Big((\frac{iv_p}{v_q} - i\mu\nu_4)M_x - \nu_2 M_{xx} + (\mu\frac{ia_0}{v_q} + \mu^2\nu_5)M \\
& \qquad + i\frac{|r_q|^2 e_1 + e_4}{v_q} M|M|^2 + i\frac{|r_q|^2 e_2 + e_3 + e_5}{v_q} M|N|^2\Big) \\
& + HORT\} e^{ip_c x + i\omega t} \\
& + \{U_0 e^{iq_c\tilde{y}}\Big(N - \tilde{y}\Big[-(\frac{v_p}{v_q} + i\mu s_4)N_x + s_2 N_{xx} + (\mu\frac{a_0}{v_q} - \mu^2 s_5)N \\
& \qquad + \frac{e_1 + |r_q|^2 e_4}{v_q} N|N|^2 + \frac{e_2 + |r_q|^2(e_3+e_5)}{v_q} N|M|^2\Big]\Big) \\
& + r_q U_0 e^{-iq_c\tilde{y}}\Big(N + \tilde{y}\Big[-(\frac{v_p}{v_q} + i\mu s_4)N_x + s_2 N_{xx} + (\mu\frac{a_0}{v_q} - \mu^2 s_5)N \\
& \qquad + \frac{|r_q|^2 e_1 + e_4}{v_q} N|N|^2 + \frac{|r_q|^2 e_2 + e_3 + e_5}{v_q} N|M|^2\Big]\Big) \\
& + U_{1q} e^{iq_c\tilde{y}}\Big(-(\frac{iv_p}{v_q} - i\mu\nu_4)N_x - \nu_2 N_{xx} + (\mu\frac{ia_0}{v_q} + \mu^2\nu_5)N \\
& \qquad + i\frac{e_1 + |r_q|^2 e_4}{v_q} N|N|^2 + i\frac{e_2 + |r_q|^2(e_3+e_5)}{v_q} N|M|^2\Big)
\end{aligned}
$$

$$
\begin{aligned}
&+r_q U_{1q} e^{-iq_c\tilde{y}}\Big(-(\frac{iv_p}{v_q} - i\mu\nu_4)N_x - \nu_2 N_{xx} + (\mu\frac{ia_0}{v_q} + \mu^2\nu_5)N \\
&\qquad + i\frac{|r_q|^2 e_1 + e_4}{v_q} N|N|^2 + i\frac{|r_q|^2 e_2 + e_3 + e_5}{v_q} N|M|^2\Big) \\
&+HORT\}e^{-ip_c x + i\omega t} \\
&+cc + HONRT
\end{aligned} \tag{A.13}
$$

A.3 Matching and Boundary Conditions

Comparing (A.13) to (A.1) as explained in Section 3.4 leads to the the following matching conditions,

$$
\begin{aligned}
A_1 e^{-iq_c L_q/2} &= M + HOT, \\
A_4 e^{iq_c L_q/2} &= r_q M + HOT, \\
A_2 e^{-iq_c L_q/2} &= N + HOT, \\
A_3 e^{iq_c L_q/2} &= r_q N + HOT,
\end{aligned} \tag{A.14}
$$

and

$$
\begin{aligned}
-iA_{1y} e^{-iq_0 L_q/2} &= -i\frac{v_p}{v_q} M_x + \nu_2 M_{xx} + \mu\frac{ia_0}{v_q} M - i\nu_4\mu M_x + \nu_5\mu^2 M \\
&\quad + i\frac{e_1 + |r_q|^2 e_4}{v_q} M|M|^2 + i\frac{e_2 + |r_q|^2(e_3 + e_5)}{v_q} M|N|^2 - \frac{i}{v_q} M_t + HOT \\
iA_{4y} e^{iq_0 L_q/2} &= r_q[-i\frac{v_p}{v_q} M_x + \nu_2 M_{xx} + \mu\frac{ia_0}{v_q} M - i\nu_4\mu M_x + \nu_5\mu^2 M \\
&\quad + i\frac{|r_q|^2 e_1 + e_4}{v_q} M|M|^2 + i\frac{|r_q|^2 e_2 + e_3 + e_5}{v_q} M|N|^2 - \frac{i}{v_q} M_t] + HOT \\
-iA_{2y} e^{-iq_0 L_q/2} &= i\frac{v_p}{v_q} N_x + \nu_2 N_{xx} + \mu\frac{ia_0}{v_q} N + i\nu_4\mu N_x + \nu_5\mu^2 N \\
&\quad + i\frac{e_1 + |r_q|^2 e_4}{v_q} N|N|^2 + i\frac{e_2 + |r_q|^2(e_3 + e_5)}{v_q} N|M|^2 - \frac{i}{v_q} N_t + HOT \\
iA_{3y} e^{iq_0 L_q/2} &= r_q[i\frac{v_p}{v_q} N_x + \nu_2 N_{xx} + \mu\frac{ia_0}{v_q} N + i\nu_4\mu N_x + \nu_5\mu^2 N \\
&\quad + i\frac{|r_q|^2 e_1 + e_4}{v_q} N|N|^2 + i\frac{|r_q|^2 e_2 + e_3 + e_5}{v_q} N|M|^2 - \frac{i}{v_q} N_t] + HOT
\end{aligned}
$$

Equations (A.14) and (A.15) combine to give two pairs of boundary conditions for the bulk amplitudes,

$$\begin{aligned}
e^{iq_cL_q}A_4 &= r_qA_1 + HOT,\\
v_q(e^{iq_cL_q}A_{4y} + r_qA_{1y}) &= r_q(|r_q|^2-1)[(e_1-e_4)A_1|A_1|^2 + (e_2-e_3-e_5)A_1|A_2|^2] + HOT,\\
e^{iq_cL_q}A_3 &= r_qA_2 + HOT,\\
v_q(e^{iq_cL_q}A_{3y} + r_qA_{2y}) &= r_q(|r_q|^2-1)[(e_1-e_4)A_2|A_2|^2 + (e_2-e_3-e_5)A_2|A_1|^2] + HOT.
\end{aligned} \tag{A.15}$$

Analogously the set of boundary conditions at the edge $x = -L_p/2$ is obtained,

$$\begin{aligned}
e^{ip_cL_p}A_2 &= r_pA_1 + HOT,\\
v_p(e^{ip_cL_p}A_{2x} + r_pA_{1x}) &= r_p(|r_p|^2-1)[(e_1-e_2)A_1|A_1|^2 + (e_4-e_3-e_5)A_1|A_4|^2] + HOT,\\
e^{ip_cL_p}A_3 &= r_pA_4 + HOT,\\
v_p(e^{ip_cL_p}A_{3x} + r_pA_{4x}) &= r_p(|r_p|^2-1)[(e_1-e_2)A_4|A_4|^2 + (e_4-e_3-e_5)A_4|A_1|^2] + HOT,
\end{aligned} \tag{A.16}$$

and the boundary conditions at $y = L_q/2$ and $x = L_p/2$ follow from symmetry considerations,

$$\begin{aligned}
e^{iq_cL_q}A_1 &= r_qA_4 + HOT,\\
v_q(e^{iq_cL_q}A_{1y} + r_qA_{4y}) &= r_q(|r_q|^2-1)[(-e_1+e_4)A_4|A_4|^2 + (-e_2+e_3+e_5)A_4|A_3|^2] + HOT,\\
e^{iq_cL_q}A_2 &= r_qA_3 + HOT,\\
v_q(e^{iq_cL_q}A_{2y} + r_qA_{3y}) &= r_q(|r_q|^2-1)[(-e_1+e_4)A_3|A_3|^2 + (-e_2+e_3+e_5)A_3|A_4|^2] + HOT,
\end{aligned} \tag{A.17}$$

and

$$
\begin{aligned}
e^{ip_c L_p} A_1 &= r_p A_2 + HOT, \\
v_p(e^{ip_c L_p} A_{1x} + r_p A_{2x}) &= r_p(|r_p|^2 - 1)[(-e_1 + e_2)A_2|A_2|^2 + (-e_4 + e_3 + e_5)A_2|A_3|^2] + HOT, \\
e^{ip_c L_p} A_4 &= r_p A_3 + HOT, \\
v_p(e^{ip_c L_p} A_{4x} + r_p A_{3x}) &= r_p(|r_p|^2 - 1)[(-e_1 + e_2)A_3|A_3|^2 + (-e_4 + e_3 + e_5)A_3|A_2|^2] + HOT.
\end{aligned}
\tag{A.18}
$$

References

[1] I. S. Aranson and L. Kramer. The world of the complex Ginzburg-Landau equation. *Rev. Modern Phys.*, 74(1):99–143, 2002.

[2] V. I. Arnold. *Geometric Methods in the Theory of Ordinary Differential Equations.* Springer, 1983.

[3] B. P. Belusov. Oscillation reaction and its mechanism (in Russian). In *Sbornik Referatov po Radiacioni Medicine*, page 145. 1958 Meeting, 1959.

[4] D. Bensimon, P. Kolodner, C. M. Surko, H. Williams, and V. Croquette. Competing and coexisting dynamical states of travelling wave convection in an annulus. *J. Fluid Mech.*, 217:441–67, 1990.

[5] E. F. Carr. Influence of electric fields on the molecular alignment in the liquid crystal p-(anisalamino)-phenil acetate. *Mol.Cryst. Liqu. Cryst.*, 7:253, 1969.

[6] H. Chaté and P. Manneville. Spatiotemporal intermittency in coupled map lattices. *Physica D*, 32:409, 1988.

[7] P. Chossat and R. Lauterbach. *Methods in Equivariant Bifurcations and Dynamical Systems.* World Scientific, 2000.

[8] P. Constantin, C. Foias, B. Nicolaenko, and R. Temam. *Integral manifolds and Inertial Manifolds for Dissipative Partial Differential Equations.* Springer, 1989.

[9] J. D. Crawford and E. Knobloch. Symmetry and symmetry-breaking bifurcations in fluid mechanics. *Ann. Rev. Fluid Mech.*, 23:341–87, 1991.

[10] M. C. Cross. Traveling and standing waves in binary fluid convection. *Phys. Rev. Lett.*, 57:2935, 1986.

[11] M. C. Cross. Structure of nonlinear traveling wave-states in finite geometries. *Phys. Rev. A*, 38:3593, 1988.

[12] M. C. Cross, P. G. Daniels, P. C. Hohenberg, and E. D. Sigga. Effect of distant sidewalls on wave-number selection in Rayleigh-Bènard convection. *Phys. Rev. Letters*, 45(11):898–901, 1980.

[13] M. C. Cross, P. G. Daniels, P. C. Hohenberg, and E. D. Sigga. Phase-winding solutions in a finite container above the conservative threshold. *J. Fluid Mech.*, 127:155–183, 1983.

[14] M. C. Cross and P. C. Hohenberg. Pattern formation outside of equilibrium. *Rev. Mod. Phys.*, 65:851, 1993.

[15] G. Dangelmayr, G. Acharya, J. T. Gleeson, I. Oprea, and J. Ladd. Diagnosis of spatiotemporal chaos in wave envelopes of a nematic electroconvection pattern. *Phys. Rev. E*, 79:1, 2009.

[16] G. Dangelmayr, B. Fiedler, K. Kirchgässner, and A. Mielke. *Dynamics of Waves in Dissipative Systems: Reduction, Bifurcation and Stability.* Addison Wesley Longman Limited, 1996.

[17] G. Dangelmayr and E. Knobloch. Hopf bifurcation with broken circular symmetry. *Nonlinearity*, 4:399–427, 1991.

[18] G. Dangelmayr, E. Knobloch, and M. Wegelin. Dynamics of traveling waves in finite container. *Europhys. Lett.*, 16(8):723–729, 1991.

[19] G. Dangelmayr and L. Kramer. Mathematical tools for pattern formation. In F. H. Busse and S. C. Müller, editors, *Evolution of Spontaneous Structures in Dissipative Continuous Systems*, pages 1–85. Springer, 1998.

[20] G. Dangelmayr and I. Oprea. A bifurcation study of wave patterns for electroconvection in nematic liquid crystals. *Mol. Cryst. Liqu. Cryst*, 413:2441, 2004.

[21] G. Dangelmayr and I. Oprea. Modulational stability of travelling waves in 2d anisotropic systems. *J. Nonlin. Sci.*, 18(1):1, 2008.

[22] G. Dangelmayr, J. D. Rodriguea, and W. Güttinger. Dynamics of waves in extended systems. *Lectures in Applied Mathematics, AMS*, 29:145–161, 1993.

[23] G. Dangelmayr and M. Wegelin. Hopf bifurcations in anisotropic systems. In M. Golubitsky, D. Luss, and S. Strogatz, editors, *Pattern Formation in Continuous and Coupled Systems*, pages 33–42. Springer, IMA Vol. Math. Appl. 115, 1999.

[24] P. G. Daniels. Effect of distant sidewalls on the transition to finite amplitude Bènard convection. *Proc. R. Soc. Lond. A.*, 358:173–197, 1977.

[25] P. G. Daniels. The effect of distant side-walls on the evolution and stability of finite-amplitude Bènard convection. *Proc. R. Soc. Lond. A.*, 378:539–566, 1981.

[26] M. Dennin. *A study in pattern formation: Electroconvection in nematic liquid crystals.* PhD thesis, Department of Physics, University of California, Santa Barbara, 1995.

[27] M. Dennin, G. Ahlers, and D. S. Cannell. Chaotic localized states near the onset of electroconvection. *Phys. Rev. Lett.*, 77(12):2475, 1996.

[28] M. Dennin, D. S. Cannell, and G. Ahlers. Patterns of electroconvection in a nematic liquid crystal. *Phys. Rev. E*, 57:638, 1998.

[29] P. G. Drazin. On the effect of sidewalls on Bènard convection. *ZAMP*, 26:239–243, 1975.

[30] V. L. Ginzburg and I. D. Landau. (in Russian). *JETP*, 20:1064, 1950.

[31] M. Golubitsky and I. Stewart. Hopf bifurcation in the presence of symmetry. *Archive for Rational Mech. and Anal.*, 87(2):107–165, 1985.

[32] M. Golubitsky, I. Stewart, and D. G. Schaeffer. *Singularities and Groups in Bifurcation Theory, Volume II.* Springer, 1988.

[33] W. Helfrich. Conduction-induced alignment of nematic liquid crystals: basic model and stability considerations. *J. Chem. Phys.*, 51:4092, 1969.

[34] R. B. Hoyle. *Pattern formation.* Cambridge University Press, Cambridge, 2006. An introduction to methods.

[35] E. Kaplan and V. Steinberg. Measurement of reflection of travelling waves near the onset of binary fluid convection. *Phys. Rev. E*, 48:R661–4, 1993.

[36] J. P. Keener. *Principles of Applied Mathematics.* Perseus Books, 2000.

[37] J. Kevorkian and J. D. Cole. *Perturbation Methods in Applied Mathematics.* Springer, 1981.

[38] E. Knobloch and J. DeLuca. Amplitude equations for traveling wave convection. *Nonlinearity*, 3:975–980, 1990.

[39] E. Knobloch and M. R. E. Proctor. Nonlinear periodic convection in double diffusive convection. *J. Fluid Mech.*, 109:291–316, 1981.

[40] P. Kolodner. Repeated transients of weakly nonlinear travelling wave convection. *Phys. Rev. E*, 47:1938–48, 1993.

[41] J. Lega. Phase diffusion and weak turbulence. In G. Dangelmayr and I. Oprea, editors, *Dynamics and Bifurcation of Patterns in Dissipative Systems*, pages 143–157. World Scientific Series on Nonlinear Science, Vol. 12, 2004.

[42] P. Manneville. *Instabilities, chaos and turbulence.* Imperial College Press, London, 2004. An introduction to nonlinear dynamics and complex systems.

[43] C. Martel and J. M. Vega. Finite size effects near the onset of the oscillatory instability. *Nonlinearity*, 9:1129–1171, 1996.

[44] J. D. Murray. *Mathematical Biology.* Springer, 1993.

[45] A. C. Newell and J. A. Whitehead. Finite bandwith, finite amplitude convection. *J. Fluid Mech.*, 38:279, 1969.

[46] I. Oprea and G. Dangelmayr. Dynamics and bifurcations in the weak electrolyte model for electroconvection of nematic liquid crystals: a Ginzburg-Landau approach. *Eur. J. Mech. B/Fluids*, 27(6):726–749, 2008.

[47] I. Oprea, I. Triandaf, G. Dangelmayr, and I.B. Schwartz. Quantitative and qualitative characterization of zigzag spatiotemporal chaos in a system of amplitude equations for nematic electroconvection. *Chaos*, 17(1):1, 2007.

[48] R. D. Pierce and E. Knobloch. Evolution equations for counterpropagating edge waves. *J. Fluid Mech.*, 264:137, 1994.

[49] A. A. Predtechensky, W. D. McCormick, J. B. Swift, Z. Noszticzius, and H. L. Swinney. Onset of traveling waves in isothermal double diffusive convection. *Phys. Rev. Lett.*, 72:218–21, 1994.

[50] D. H. Sattinger. *Group Theoretic Methods in Bifurcation Theory.* Springer, 1979.

[51] L. A. Segel. Distant side-walls cause amplitude modulation of cellular convection. *J. Fluid Mech.*, 38:203, 1969.

[52] M. Silber, H. Riecke, and L. Kramer. Symmetry-breaking Hopf bifurcation in anisotropic systems. *Physica D*, 61:260–278, 1992.

[53] V. Steinberg, J. Fineberg, E. Moses, and I. Rehberg. Pattern selection and transition to turbulence in propagation waves. *Physica D*, 37:359–83, 1989.

[54] M. Tinkham. *Introduction to Superconductivity.* McGrawHill, 1996.

[55] M. Treiber. *On the theory of the electrohydrodynamic instability in nematic liquid crystals near onset.* PhD thesis, Department of Physics, University of Bayreuth, 1996.

[56] M. Treiber and L. Kramer. Bipolar electrodiffusion model for electroconvection in nematics. *Mol Cryst. Liqu. Cryst.*, 261:311, 1995.

[57] M. Treiber and L. Kramer. Coupled complex Ginzburg-Landau equations for the weak electrolyte model of electroconvection. *Phys. Rev. E*, 58:1973, 1998.

[58] A. Turing. The chemical basis of morphogenesis. *Proc. Roy. Soc. B*, 237:37–52, 1952.

[59] F. Verhulst. *Nonlinear Differential Equations and Dynamical Systems*. Springer, 2nd ed., 1996.

[60] M. Wegelin. *Nichtlineare Dynamik raumzeitlicher Muster in hierarchischen Systemen*. PhD thesis, Department of Physics, University of Tuebingen, 1993.

[61] G. B. Whitham. *Linear and Nonlinear Waves*. Wiley, 1999.

[62] A. N. Zaikin and A. M. Zhabotinsky. Concentration wave propagation in two-dimensional liquid-phase self-organizing systems. *Nature*, 225:535, 1970.